ISTANBUL TECHNICAL UNIVERSITY ★ GRADUATE SCHOOL

FABRICATION OF ENHANCED CORE-SHELL CO-ZIF-67@MOX (M = ZN, MN AND K) NANOCOMPOSITES VIA INTERMEDIATE PYROLYSIS AND PLASMA TREATMENT FOR FISCHER TROPSCH SYNTHESIS

M. Sc. THESIS

Yavuz AYDEMİR

Department of Chemical Engineering

Chemical Engineering Programme

Thesis Advisor: Assoc. Prof. Dr. Alper SARIOĞLAN

JUNE 2023

İSTANBUL TEKNİK ÜNİVERSİTESİ ★ LİSANSÜSTÜ EĞİTİM ENSTİTÜSÜ

FABRICATION OF ENHANCED CORE-SHELL CO-ZIF-67@MOX (M = ZN, MN AND K) NANOCOMPOSITES VIA INTERMEDIATE PYROLYSIS AND PLASMA TREATMENT FOR FISCHER TROPSCH SYNTHESIS

YÜKSEK LİSANS TEZİ

Yavuz AYDEMİR
(506211029)

Kimya Mühendisliği Anabilim Dalı

Kimya Mühendisliği Programı

Tez Danışmanı: Doç.Dr. Alper SARIOĞLAN

HAZİRAN 2023

Yavuz AYDEMİR, a M. Sc. student of ITU Graduate School, student ID 506211029, successfully defended the thesis entitled "FABRICATION OF ENHANCED CORE-SHELL CO-ZIF-67@MOX (M = ZN, MN AND K) NANOCOMPOSITES VIA INTERMEDIATE PYROLYSIS AND PLASMA TREATMENT FOR FISCHER TROPSCH SYNTHESIS", which he prepared after fulfilling the requirements specified in the associated legislations, before the jury whose signatures are below.

Thesis Advisor : **Doç. Dr. Alper SARIOĞLAN** ....
İstanbul Technical University

Jury Members : **Prof. Dr. Hasan Can OKUTAN** ....
İstanbul Technical University

Prof. Dr. Şahika Sena BAYAZİT ....
İstanbul University

Date of Submission : 22 May 2023

Date of Defense : 13 June 2023

To my love and family,

FOREWORD

My special thanks to Assoc. Prof. Dr. Alper SARIOĞLAN, my M.Sc. advisor, for his invaluable guidance and expertise. He has provided me with a unique engineer's perspective and supported me throughout my research journey.

I want to express my heartfelt thanks to Prof. Dr. Melek TÜTER, who has provided me with her support, guidance, and inspiration throughout my entire educational journey.

And also my special thanks to our esteemed mentor, Asst. Prof. Dr. Sogand AGHAMOHAMMA, who provided invaluable assistance during my research, equipment procurement, and material sourcing throughout my thesis work. I am sincerely grateful for her support and guidance.

I am grateful to Utku Burgun for their support and guidance during my experimental studies and thesis process. He has been both a mentor and a friend, and I deeply appreciate his patience and assistance. I would like to express my sincere gratitude to ITU SENTEK for granting me the opportunity to use the equipment in my research and for the my colleagues who have provided invaluable assistance during my research. My heartfelt thanks goes to Cansu YILDIRIM, Yasaman FALLAHİ, Müzeyyen DEMİRCİ, Pınar ŞAKOĞLU, Yusuf Tolunay KILIÇ, Berna TOPRAK, Deniz BİLGİN, Selin ERTUNAN, and Buket KELEŞOĞLU.

I am deeply grateful to my brother, Fatih AYDEMİR and dear friend Gözde AYDEMİR, who have never withheld their support from me. Their constant encouragement and assistance have been invaluable throughout my journey. Additionally, I would like to extend my heartfelt thanks to my father and mother for their support.

I would like thank to my dear friends Seltan, Canberk, Doruk, and Kaan, who have always been by my side. Their belief in me and their unconditional love have been the pillars of my strength.

Lastly, I would like to extend my sincerest wishes to Eylül DEMİRCİ, who has embraced me and provided unwavering love and support throughout the entire journey. Her presence and unwavering encouragement have meant the world to me.

June 2023 Yavuz AYDEMİR
(Chemical Engineer)

TABLE OF CONTENTS

Page

ABBREVIATIONS

AC	**:**	Alternative Current
ASF	**:**	Anderson-Schulz-Flory
BET	**:**	Brunauer–Emmett–Teller
DBD	**:**	Dielectric Barrier Discharge
FESEM	**:**	Field Emission Scanning Electron Microscope
FID	**:**	Flame Ionization Detector
FT	**:**	Fischer-Tropsch
FTS	**:**	Fischer-Tropsch Synthesis
HTFT	**:**	High Temperature Fischer Tropsch
LPG	**:**	Liquid Petroleum Gas
LTFT	**:**	Low Temperature Fischer Tropsch
MOF	**:**	Metal-Organic-Framework
TCD	**:**	Thermal Conductivity Detector
TGA	**:**	Thermo Gravimetric Analysis
TPR	**:**	Temperature Programmed Reaction
WGS	**:**	Water-Gas Shift
ZIF	**:**	Zeolitic Imidazolate Framework

LIST OF TABLES

Page

LIST OF FIGURES

Page

FABRICATION OF ENHANCED CORE-SHELL CO-ZIF-67@MOX (M = ZN, MN AND K) NANOCOMPOSITES VIA INTERMEDIATE PYROLYSIS AND PLASMA TREATMENT FOR FISCHER TROPSCH SYNTHESIS

SUMMARY

Shortage of crude oil and environmental pollution problems oblige humanity for the research on alternative processes of producing value added chemicals. Depletion of crude oil is major concern because of the energy needs. Fuels are the most common energy source all around the world and the best known fuels are gasoline, diesel and jet fuels which are composed of averagely %70 parrafins.

In this manner, Fischer Tropsch Synthesis (FTS), which produces valuable chemicals and clean liquid hydrocarbons by transforming the syngas (CO and H_2) derived from coal biomass such as carbon-containing wastes, is one of the best alternatives.

Factors such as temperature, pressure, feed gas composition, catalyst type, catalyst composition, presence of promoter, reactor technology affect the production of hydrocarbons via FTS. To use Fischer Tropsch Synthesis commercially, developing new FT catalysts with high selectivity in the desired target hydrocarbon range is a key factor for processes.

According to literature, the activity of Fischer Tropsch catalysts depends on the H_2 adsorption capacity and the ability for the dissociative adsorption of CO. Transition metals in groups III-VI of the periodic table have been reported to be ineffective for FTS. The elements of group VIII-X have been widely used for Fischer Tropsch Synthesis, the most common of these are ruthenium, nickel, iron and cobalt. While ruthenium is expensive, nickel have high methanation tendency and iron is more suitable for olefin production. Cobalt is known for its high FT activity, low tendecy for WGS, durability and high activity for heavy hydrocarbons. It is more proper to use cobalt based catalyst for the production parrafins.

As in the literature, zeolitic imidazolate frameworks (ZIFs) have crystalline structure, extremely high surface area and tunable pore aperture as well ZIFs consist of transition-metal cations. At ZIF-67, cobalt is the transition metal that has high FT activity, high selectivity to paraffins and low water-gas shift activity.The aim of the study was developing the most proper catalyst for the production of liquid paraffins with developing novel core–shell-structured Co-ZIF-67@MOx (M = Zn, Mn and K) nanocomposites via intermediate pyrolysis and plasma treatment. Cobalt nitrate hexahydrate and 2-methylimidazole were used for the production of ZIF-67. ZIF-67 have to be pretreated to become a catalyst so it has pretreatment steps as pyrolysis, calcination and plasma treatment. Thanks to pretreatments such as pyrolysis, it is expected that the number of the active metal sites has been increased, cobalt

distribution over carbon structure has been enhanced and the agglomeration problem has been prevented. Furthermore, calcination is applied to remove excess carbon via oxidizing them under high temperature without losing base material. Dispersion degree of cobalt active metal sites would be also well preserved and the removal of carbons from the structure was completed while they were replaced by cobalt oxides. Moreover, stability and activity of the catalyst were foreseen to be improved via plasma treatment. Therefore, Co-ZIF-67s was subjected to plasma technique prior to the corresponding pyrolysis and calcination steps. In this regard, ZIF-67 were synthesized and then 12 catalysts were produced as follows: 6 of them were pyrolyzed between 400-900°C without any plasma treatment and the rest of the samples pyrolyzed between 400-900°C were plasma treated later on. All 12 samples were finally calcined at 350°C. And then the most promising catalyst was coated with Na, Mn, K seperately. Pyrolyzed between 400-600°C catalysts were named as low temperature pyrolysis catalysts, group I, and 700-900°C ones were named as high temperature pyrolysis catalysts, group II.

In the manner of selectivity and activity, the prepared Co-ZIF-67 catalysts were evaluated for their FTS performance under the conditions of 230°C, 15 bar, H_2/CO = 2, and GHSV of 900 $mL.g^{-1}$ in a fixed bed reactor.

For the characterization of catalysts XRD, FTIR, FESEM, BET, EDAX-dot mapping, TGA and H_2-TPR were applied. Synthesized ZIF-67 was confirmed with XRD and FTIR analysis. And the BET surface area of the pure ZIF-67 is 1824 m^2/g and total pore volume of 0.6 cm^3/g. C, N and Co in ZIF-67 were confirmed by EDAX spectra with atomic ratios 63.52, 11.91 and 0.39%, respectively.

After characterization of pure ZIF-67, XRD and FTIR results indicated that pyrolysis and calcination were effective for the transformation of ZIF-67 precursor into pure Co_3O_4 phase. It is clear from FESEM images that, as the pyrolysis temperature increased, the particles began to become more sphere like and tend to loosely aggregate and plasma treatment partly helps to avoid agglomeration. N_2 sorption measurements have shown that BET surface area and pore volume of catalyst were sharply decreased from 1824 m^2/g to 10-40 m^2/g and 0.6 cc/g to 0.01-0.05 cc/g, respectively.

In this work, catalysts performance was evaluated with product selectivity, deactivation and CO conversion values. Among the low temperature pyrolysis catalysts, CoZ@600 showed the highest overall average CO conversion with a value of 31,3%. Plasma treated catalysts showed higher initial CO conversion but they were deactivated fast which means non-plasma treated catalysts were more stable than the plasma treated ones. For all group II catalysts, initially high CO conversions were observed. As in the case of group I catalysts, the highest CO conversions were achieved over plasma treated catalysts. Among the group II catalysts, P_CoZ@900 has shown the highest overall average CO conversion with 26,1% in 40h time on stream. Moreover, last but not least, a stepwise decrease in CO conversion was observed for P_CoZ@900. When the product selectivities were evaluated, whatever the pyrolysis temperature is, plasma treated samples have shown higher olefin selectivity. Among all the 12 catalysts, CoZ@500 and CoZ@600 showed the highest overall average C_2-C_4 paraffin and C_5^+ selectivities. After deductions from not only CO and H_2 conversions but also product selectivity, CoZ@600 gave the most promising results. Due to this outcome, coating with Zn, Mn and K were applied to CoZ@600. Among the coated catalysts, CoZ@600-ZnOx has shown promising results not only with 34,9% CO and 38,4% H_2 conversion but also with 21,4% C_2-C_4 paraffin and 30,3% C_5^+ selectivity on average.

Therefore, considering the aim of the study to contribute literature with the purpose of reducing dependence on crude oil and meeting the world's fuel requirements, CoZ@600-ZnOx has been evaluated as one of the most proper candidate catalyst for the production of long hydrocarbon chains.

FİSCHER TROPSCH SENTEZİ İÇİN PİROLİZ VE PLAZMA İŞLEMİ İLE GELİŞTİRİLMİŞ ÇEKİRDEK-KABUK YAPILI CO-ZIF-67@MOX (M = ZN, MN VE K) NANOKOMPOZİTLERİNİN ÜRETİMİ

ÖZET

Ham petrolün kıtlığı ve çevresel kirlilik sorunları, insanlığı, değerli kimyasalların alternatif üretim süreçleri üzerine araştırma yapmaya zorlamaktadır. Ham petrolün tükenmesi, enerji ihtiyaçlarından kaynaklanmaktadır. Yakıtlar dünya genelinde en yaygın enerji kaynağıdır ve en bilinen yakıtlar benzin, dizel ve jet yakıtlarıdır ki bunlar ortalama olarak %70 parafin içermektedirler.

Bu bağlamda, kömür, biyokütle gibi karbon içeren atıklardan elde edilen sentez gazının (CO ve H_2) Fischer-Tropsch Sentezi (FTS) ile değerli kimyasallar ve temiz sıvı hidrokarbonlar üretme süreci, en iyi alternatiflerden biridir.

Sıcaklık, basınç, besleme gazı bileşimi, katalizör türü, katalizör bileşimi, promotörün varlığı, reaktör teknolojisi gibi faktörler, FTS aracılığıyla hidrokarbon üretimini etkilemektedir. Fischer-Tropsch Sentezini ticari olarak kullanabilmek için, hedeflenen hidrokarbon aralığında ürün veren, yüksek seçiciliğe ve dönüşüme sahip yeni FTS katalizörlerinin geliştirilmesi önemli bir faktördür.

Literatüre göre, Fischer-Tropsch katalizörlerinin etkinliği, H_2 adsorpsiyon kapasitesine ve CO disosiyatif adsorpsiyon yeteneğine bağlıdır. Periyodik tablonun III-VI gruplarındaki geçiş metallerinin FTS için etkisiz olduğu araştırmalar ile görülmüştür. VIII-X grup elementleri Fischer-Tropsch Sentezi için yaygın olarak kullanılmış olup, bunların en yaygın olanları rutenyum, nikel, demir ve kobalttır. Rutenyum pahalıdır, nikel yüksek metanasyon eğilimine sahiptir ve demir, olefin üretimi için daha uygundur. Kobalt ise yüksek FTS etkinliği, düşük WGS eğilimi, dayanıklılık ve ağır hidrokarbonlar için yüksek aktiviteye sahip olmasıyla bilinmektedir. Parafin üretimi için kobalt bazlı katalizörlerin kullanılması daha uygundur.

Literatürde de belirtildiği gibi, zeolitik imidazolat çerçeveleri (ZİF'ler) kristal yapıya sahiptir, son derece yüksek yüzey alanına ve ayarlanabilir gözenek çapına sahiptir ve aynı zamanda ZIF'ler, geçiş metali katyonları içerir. ZIF-67'de bulunan katyon kobalttır. Böylece, yüksek FTS etkinliği, parafinlere yüksek seçicilik ve düşük su-gaz kaydırma aktivitesine sahiptir.

Bu çalışmanın amacı, ara piroliz ve plazma işlemi aracılığıyla yeni bir çekirdek-kabuk yapısına sahip Co-ZIF-67@MOx (M = Zn, Mn ve K) nanokompozitleri geliştirerek, sıvı parafinlerin üretimi için en uygun katalizörü geliştirmektir. ZIF-67'nin üretimi için kobalt nitrat hekzahidrat ve 2-metilimidazol kullanılmıştır. ZIF-67 bir katalizör haline gelmesi için ön hazırlık işlemine tabi tutulmalıdır, bu nedenle piroliz, kalsinasyon ve plazma işlemi gibi ön işlem adımları uygulanmaktadır. Piroliz gibi ön işlemler

sayesinde aktif metal bölgelerin sayısının artması, karbon yapı üzerinde kobalt dağılımının iyileşmesi ve topaklaşma sorununun önlenmesi beklenmektedir. Ayrıca, temel malzemeyi kaybetmeden yüksek sıcaklık altında fazla karbonun oksitlenerek yapıdan uzaklaştırılması için kalsinasyon uygulanmaktadır. Bu ön hazırlık aşamaları ile kobalt aktif metal bölgelerin yüzeyde dağılımının iyileştirilmesi ve yapıdaki karbonların yerini kobalt oksitler alması beklenmektedir. Ek olarak, katalizörün stabilitesi ve aktivitesinin plazma işlemiyle de iyileştirilebileceği öngörülmektedir. Bu nedenle Co-ZİF-67'ler piroliz ve kalsinasyon adımlarından önce plazma işlemine tabi tutulmuştur. Bu bağlamda, ZIF-67 sentezlenmiştir ve ardından 12 katalizör üretilmiştir: bunlardan 6 tanesi herhangi bir plazma işlemi olmaksızın 400-900°C arasında pirolize edilmiş, geri kalan örnekler 400-900°C'de piroliz işleminden sonra plazma ile muamele edilmiştir. Daha sonra 12 örnek sırayla 350°C'de kalsine edilmiştir. En umut verici katalizör ayrı ayrı Na, Mn, K ile kaplanmıştır. 400-600°C arasında pirolize edilen katalizörler düşük sıcaklık piroliz katalizörleri (grup I) olarak adlandırılmıştır Diğer katalizörler, yani yüksek sıcaklık piroliz katalizörleri (grup II) olarak adlandırılmıştır.

Hazırlanan Co-ZİF-67 katalizörleri, Fischer-Tropsch Sentezi (FTS) performansları için belirli koşullarda sabit yataklı bir reaktörde test edilmiştir. FTS deneyleri, 230°C sıcaklık, 15 bar basınç, H_2/CO mol oranı 2 ve gaz saati hacim hızı (GHSV) 900 $mL.g^{-1}$ koşullarında gerçekleştirilmiştir.

Katalizörlerin karakterizasyonunda XRD, FTIR, FESEM, BET, EDAX-dot haritalama, TGA ve H_2-TPR teknikleri uygulanmıştır. Sentezlenen ZİF-67 yapısı, XRD ve FTIR analizi sonuçları ile doğrulanmıştır. Saf ZİF-67'nin BET yüzey alanı 1824 m^2/g ve toplam gözenek hacmi 0.6 cm^3/g olarak ölçülmüştür. ZIF-67 içerisindeki C, N ve Co elementlerine ait EDAX spektrumlarıyla sırasıyla %63.52, %11.91 ve %0.39'dir.

Saf ZİF-67'nin karakterizasyonu yapıldıktan sonra, hazırlanan katalizörlerde XRD ve FTIR sonuçları, piroliz ve kalsinasyonun ZİF-67'nin Co_3O_4 fazına dönüşümünde etkili olduğunu göstermektedir. FESEM görüntülerinden açıkça görülmektedir ki, piroliz sıcaklığı arttıkça parçacıklar daha küresel bir yapıya dönüşmekte ve daha az düzeyde topaklanma eğilimindedir. Plazma işlemi, bu topaklanmayı önlemeye kısmen yardımcı olmaktadır. N_2 adsorpsiyon ölçümleri, katalizörün BET yüzey alanı ve gözenek hacminin sırasıyla 1824 m^2/g'den 10-40 m^2/g'ye ve 0.6 cc/g'den 0.01-0.05 cc/g'ye keskin bir şekilde azaldığını göstermektedir.

Bu çalışmada, katalizörlerin ürün seçiciliği, deaktivasyonu ve CO dönüşüm değerleriyle performansları değerlendirilmiştir. Düşük sıcaklık piroliz katalizörleri arasında, CoZ@600 en yüksek toplam ortalama CO dönüşümü değerine sahiptir ve bu değer %31,3 olarak hesaplanmıştır. Plazma işlemi gören katalizörler daha yüksek başlangıç CO dönüşümü göstermiştir, ancak hızlı bir şekilde deaktivasyona uğramışlardır, bu da plazma ile işlenmeyen katalizörlerin daha stabil olduğunu göstermektedir. Grup II katalizörlerinin tümünde başlangıçta yüksek CO dönüşümleri gözlenmiştir. Grup I katalizörleri durumunda olduğu gibi, daha yüksek başlangıç CO dönüşümleri, plazma işlemi uygulanmış katalizörlerle elde edilmiştir. Grup II katalizörleri arasında ise P_CoZ@900, 40 saat sürekli çalışma süresi boyunca %26,1'lik en yüksek toplam ortalama CO dönüşümüne sahiptir. Ayrıca, P_CoZ@900 katalizöründe adım adım Co dönüşüm yüzdesinde azalma gözlemlenmiştir.

Ürün seçicilikleri değerlendirildiğinde, piroliz sıcaklığı ne olursa olsun, plazma ile işlenmiş örnekler daha yüksek olefin seçiciliği göstermiştir. 12 katalizörün tamamı arasında, CoZ@500 ve CoZ@600 en yüksek toplam ortalama C_2-C_4 parafin ve C_5^+ seçiciliklerini göstermiştir. CO ve H_2 dönüşümlerinin yanı sıra ürün seçiciliğine de bakıldığında, CoZ@600 en umut vaadeden sonuçları vermiştir. Bu sonuç üzerine CoZ@600'ün üzerine Zn, Mn ve K kaplaması uygulanmıştır. Kaplanmış katalizörler arasında, CoZ@600-ZnOx sadece %34,9 CO ve %38,4 H_2 dönüşümüyle değil, aynı zamanda ortalama %21,4 C_2-C_4 parafin ve %30,3 C_5^+ seçiciliği ile umut vermiştir.

Bu nedenle, çalışmanın amacı olan ham petrol bağımlılığını azaltmak ve dünyadaki yakıt ihtiyaçlarını karşılamak için literatüre katkı sunma hedefi göz önüne alındığında, CoZ@600-ZnOx, uzun hidrokarbon zincirlerinin üretimi için uygun bir katalizör adayı olduğu değerlendirilmiştir.

1. INTRODUCTION

Petroleum is a fossil fuel feedstock mainly consisting of carbon and hydrogen with small amounts of oxygen, nitrogen and sulfur. Petroleum based feedstock can be found in gaseous, liquid or solid form. Gaseous oil is called as natural gas while unrefined liquid petroleum is called as crude oil. In solid forms, petroleum generally known as bitumen. These are also called "Hydrocarbons" because the main components of crude oil and natural gas are hydrogen and carbon (Dembicki, 2017). Petroleum consists of %98 hydrocarbons so it is not only used for fuels but also for feedstock in the production of chemicals. That’s why shortage of crude oil resources also affects chemical industries as well (Suaria et al., 2018). Hydrocarbons consist of olefins and paraffins. General formula of olefins is C_nH_{2n} and they are known as alkenes. Olefins are unsaturated hydrocarbons that contain at least one carbon-carbon (C=C) double bond in their structure (Dembicki, 2017). They are commonly used as raw materials for the production of polymers, drugs, plastics, cosmetics and cleaning products (Galvis et al., 2012). Paraffins are saturated hydrocarbons and have no double or triple bond in their structure with a general formula C_nH_{2n+2}. Paraffins which are known as alkanes, can be classified in three different groups as gaseous and liquid paraffins & paraffinic waxes whose have different usage areas like paper industry, household chemicals, cosmetics, drugs and mostly fuels (Eser, 2011.; Freund et al., 1982).

In general, main constituents of gaseous paraffins are natural gas and liquefied petroleum gas. Liquid paraffins are fuels like gasolines that can be used for aviation, kerosene for jet fuels, diesel fuels and lubricating oils. Solid paraffins are asphalt and bitumen. Up to date, conventional production way for paraffins is distillation of crude oil at different temperatures for each product (Speight, 2020). The conventional production routes based on fossil feedstocks makes paraffins crude oil dependent products. Turkey imports crude oil and its products every year, and also exports some of crude oil derivative products. In 2021, 31.5 million tons of crude oil imported and distilled for producing gasoline, diesel, fuel oil, aviation fuels, marine fuels and kerosene. After import-export operations, domestic consumption of paraffin based crude oil products was 26 million tons (Enerji Piyasası Düzenleme Kurumu, 2023).

The world has driven to a crisis because of dwindling crude oil resources and increasing environmental problems which have obliged humanity for the research on alternative processes of producing value added chemicals and sustainable energies (Yao et al., 2020). And also, paraffins that are fuels, are indispensable for our lives but its feedstock which is crude oil will be run out in 2050s (Kuo, 2019).

As a promising alternative to crude oil dependent fuel production, Fischer Tropsch Synthesis (FTS) has been used for a century. FTS is a catalytic process that uses syngas (CO, H_2) to produce hydrocarbons under certain conditions. In FTS, catalysts have crucial impact on activity and selectivity that is why catalyst design has a vital role. Agglomeration problem, stability, deactivation rate; surface area, activity and, selectivity are the significant features of the catalyst.

According to the literature research, the research direction was mainly on developing a suitable catalyst with a high CO conversion and C_5^+ selectivity whereas suppressing CH_4 and CO_2 selectivity for the production of synthetic fuels via FTS directly from syngas. Cobalt, iron, ruthenium and nickel are the common FTS catalyst but cobalt is the most used one for the production of liquid paraffin in fuel range hydrocarbons through FTS. However, it has some disadvantageous such as mass transfer limitations in pellet type cobalt catalysts and activity loss through its sintering and poor reducibility (Dry, 2004). In this sense, by eliminating the disadvantageous of cobalt and enhancing its properties, it was aimed to develop novel core−shell-structured Co-ZIF-67@MOx (M = Zn, Mn and K) nanocomposites via intermediate pyrolysis and plasma treatment. In the first step of this thesis, catalysts were synthesized and pyrolyzed at different temperatures, then tested under FTS conditions at ITU Catalyst Lab in high-pressure catalyst test system equipped with a fixed bed reactor. The effect of plasma treatment has also been investigated on pyrolyzed catalysts. In the second part, the candidate catalysts showing the promising results were chosen and metal oxide coating was applied on them and tested under the same conditions.

In developing the most proper catalyst for production of liquid paraffins; plasma treatment, pyrolysis temperature, metal oxide shell all were investigated with a motivation of finding a way out for Turkey from crude oil dependency.

2. LITERATURE REVIEW

2.1 The Fischer Tropsch Process: Historical and Current Situation

Fischer Tropsch Synthesis is a well-established technology used in producing diesel and gasoline from natural gas and coal base feedstocks. In 1913, Friedrich Bergius invented coal liquefaction in Germany. In 1926, Franz Fischer and Hans Tropsch were enlightened from Bergius and invented the process for synthesis of liquid hydrocarbons. Fischer Tropsch is a process in which hydrocarbons are produced by catalytic conversion of syngas, a mixture of H_2 and CO gases. The industrialization and commercialization of FT technology was first initiated by Ruhrchemie AG in 1936. The industrial capacity of the FT process in Germany was approximately 600 thousand tons in 1940 (Galvis, 2013; Mahmoudi et al., 2017).

Due to the rapidly increasing fuel consumption, depleting oil resources and high oil prices after the Second World War, FT process studies gained importance. Although the United States opened three FT facilities between 1940 and 1950, they closed at the end of 1950s. The reason behind that methane for the production of syngas became more expensive than crude oil economy. In the other side, The Sasol FT plant, Sasol 1, was established in 1952 in Sasolburg, South Africa to put use their rich coal reserves. Because of the energy crisis in 1970s, crude oil supply has been severely diminished. Fischer Tropsch technology came to the fore again and in 1976 the Sasol 2 facility was opened in Secunda. In the 1980s, Sasol opened its third FT facility, with a total annual capacity of 6 million tons. Later on, two new FT plants based on syngas derived from natural gas were commissioned in the 1990s, the Mossgas plant (PetroSA) in South Africa and the Shell plant in Bintulu. The capacities of these facilities were 1,000,000 and 500,000 tons per year, respectively. Increasing commercial developments in the Gas-to-Liquid fuel production process continued in the 2000s and ORYX (Sasol/Chevron/QP) and Pearl (Shell/QP) facilities in Qatar had annual capacities of 1.7 million and 7 million tons, respectively (Leckel, 2009; Mahmoudi et al., 2017).

Shell started their first commercial gas to liquid facility in Bintulu, Malaysia in 1993 with the technology of Shell Middle Distillate Synthesis (SMDS). However, during 1997, plant was destroyed by an explosion. After reconstruction, Shell developed its own technology, Low Temperature Fischer Tropsch (LTFT) based on SMDS in 2000. Cobalt was used as catalyst in these facilities to convert syngas into middle distillates and hydrocracked into products with desired boiling points (Leckel, 2009).

In 2006, The Sasol Oryx plant used similar LTFT technology, which was based on Sasol Slurry Phase Distillate (SPD). In this plant cobalt based special catalyst was operated at 25 bar, 250 °C. In the plant, upon production of waxes and condensates from syngas with LTFT, hydrocracking process took place just like in Pearl facilities (Leckel, 2009).

Recent years, studies focused on Fischer Tropsch process variables and catalysts that can affect the range of products rather than operation temperature and pressure. It is known that yield, selectivity and catalyst activity is interrelated with the active metal, support, promoters and pre-treatment conditions that's why recent studies has focused on these (Eliseev et al., 2018).

2.2 Fischer Tropsch Mechanism and Products

FTS reaction is a kind of surface polymerization where syngas is converted into a wide range of products such as paraffins, olefins, alcohols and aldehydes over a suitable catalyst. FTS is a highly exothermic reaction. The main reactions of FT are shown below as given in 2.1, 2.2 and 2.3.

Paraffins Production $$(2\mathrm{n}+1)\mathrm{H}_2 + \mathrm{nCO} \rightarrow \mathrm{C}_n\mathrm{H}_{2n+2} + \mathrm{nH}_2\mathrm{O} \qquad (2.1)$$

Olefins Production $$(2\mathrm{n})\mathrm{H}_2 + \mathrm{nCO} \rightarrow \mathrm{C}_n\mathrm{H}_{2n} + \mathrm{nH}_2\mathrm{O} \qquad (2.2)$$

Water Gas Shift (WGS) $$\mathrm{CO} + \mathrm{H}_2\mathrm{O} \rightarrow \mathrm{C}O_2 + \mathrm{H}_2 \qquad (2.3)$$

FTS reaction is a kind of surface polymerization where syngas is converted into a wide range of products such as paraffins, olefins, alcohols and aldehydes over a suitable catalyst. FTS is a highly exothermic reaction. The main reactions of FT are shown below, just like in 2.4 and 2.5.

Alcohol Production: $(2n)H_2 + nCO \rightarrow C_nH_{2n+2}O + (n-1)H_2O$ (2.4)

Boudouard Reaction: $2CO \rightarrow C + CO_2$ (2.5)

Generally, reaction proceeds by the polymerization mechanism as initiation, chain growth and termination. As a first step of FT, dissociative adsorption of CO on metal atoms (M) occurs and C-M and O-M bonds form. With dissociated surface hydrogen atoms and carbide species, initiation starts with active CH_x monomers as shown in Figure 2.1 (Jahangiri et al., 2014).

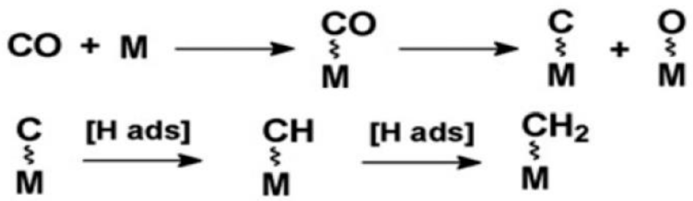

Figure 2.1: FTS reaction plan and carbide formation. (Jahangiri et al., 2014)

Upon chain initiation step, reaction proceeds with the chain growth together with continuous hydrogen and carbon monoxide adsorption to give CH_2 as shown in Figure 2.2. The growing alkyl chain can be terminated by hydrogenation to form paraffins or by β-scission to form olefins Figure 2.2 (Jahangiri et al., 2014).

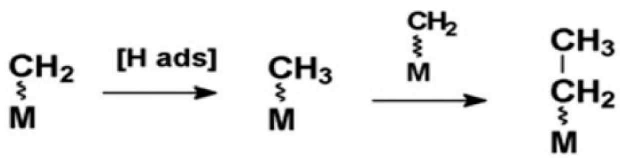

Figure 2.2: FTS reaction plan and chain growth mechanism. (Jahangiri et al., 2014)

The greatest challenge in FTS is the control of product selectivity. Generally, the products of FTS follow the Anderson-Schulz Flory (ASF) distribution. According to the ASF distribution, the molar fraction (M_n) of the n-number of hydrocarbon product depends only on the chain growth probability (α). This dependency and relation showed in the equations (2.6) and (2.7). Product selectivity is expressed as in mass fraction on carbon basis. The chain growth probability is given in equation (2.7) where rp and rt are the propagation rate constant and the termination rate constant, respectively (Gholami et al., 2017).

$$M_n = (1-a)^2 * (a)^{(n-1)} \tag{2.6}$$

$$a = rp/(rt + rt) \tag{2.7}$$

G Generally, the product distribution has a wide range of product over conventional FT catalysts. Light hydrocarbons (C_1-C_4) with high selectivity forms at low α values whereas high selectivity for heavy hydrocarbons (C_{21}^+) is achieved at high α values. For medium distillate products, for instance, the selectivity of hydrocarbons in the gasoline (C_5-C_{11}) and diesel (C_{12}-C_{20}) ranges has a maximum of 45% at around α=0.76 and 30% at α=0.89, respectively. , C_2-C_4 hydrocarbon selectivity reaches its maximum value of ~55% for α values to 0.5 according to the ASF model. Expected FT product distribution based on ASF model is shown in Figure 2.3 (Gholami et al., 2017; Yao et al., 2020; Cheng et al., 2017).

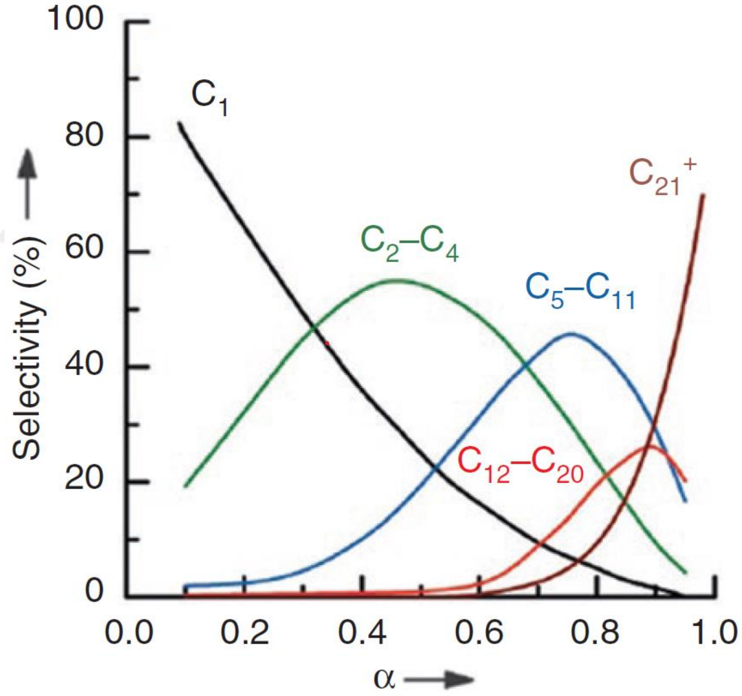

Figure 2.3: Product selectivity as a function of chain growth possibility. (Cheng et al., 2017)

Factors affecting the α value are: temperature, pressure, feed gas composition, catalyst type, catalyst composition, presence of promoter and reactor technology (slurry or fixed bed). For commercially viable Fischer-Tropsch Synthesis, developing new FT catalysts with tuned selectivity towards the desired hydrocarbon range is a key factor for industrial processeses (Cheng et al., 2017).

2.3 Importance of C_5^+ in Chemical Industries

Considering the last 10 years, annual usage of crude oil was about 14,7 billion liters. As it can be seen from Figure 2.4, consumption of crude oil had been increased at similar rates until 2020 but it decreased slightly in 2020 due to the impact of the Covid-19 pandemic. With the cure for the pandemic, trend of increase has started again. The provisions on reserves to production ratio states that globally ~47 years of oil has been left (Energy Institute, 2022).

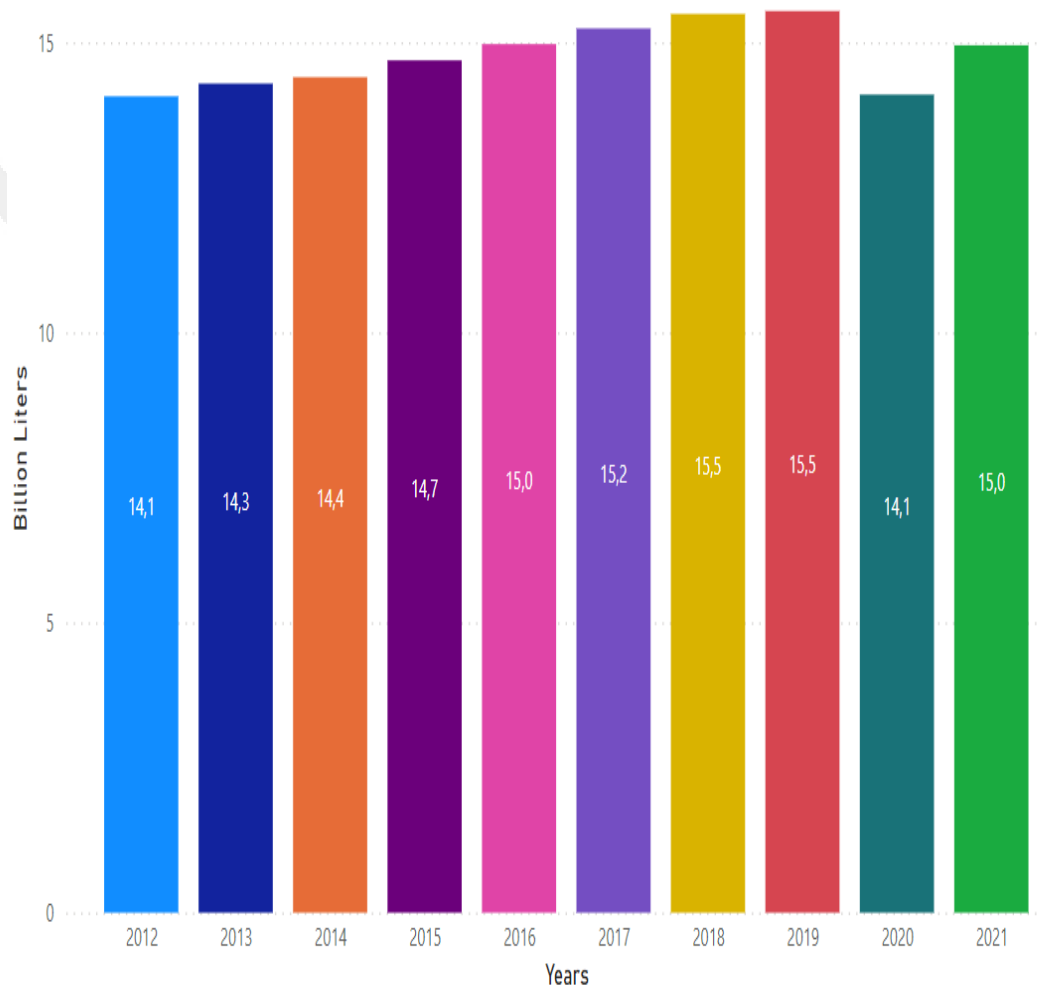

Figure 2.4: World Oil Consumption 2012-2021. (Energy Institute, 2022)

Crude oil has been used for the production of gasoline, diesel fuel, heating oil, kerosene, jet fuel, heavy fuel oil, LPG, petrochemical raw stocks, coke and asphalt. The refining products and their share changes based on the feedstock and the distillation processes. The USA refining products and its distribution have been shown in Figure 2.5.

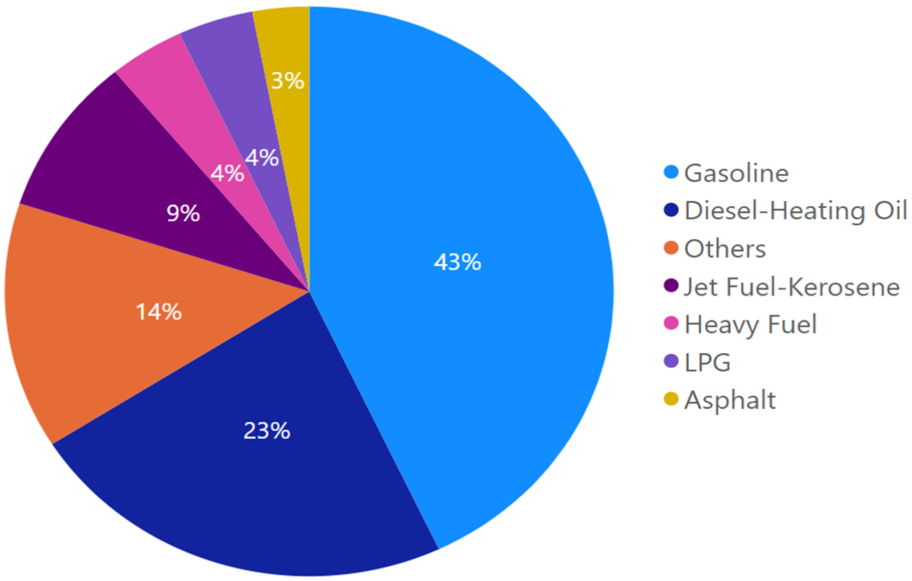

Figure 2.5: The USA refining products and its distribution. (U.S. Energy Information Administration, 2022)

Billion liters of crude oil are needed in order to meet the demand for hydrocarbon products that are used in different fields such as transportation, chemical industry, residential and commercial use and electricity production. In 2021, roughly 67% of crude oil refining products were used for transportation 27% in industry in USA as given below in Figure 2.6 (U.S. Energy Information Administration, 2022).

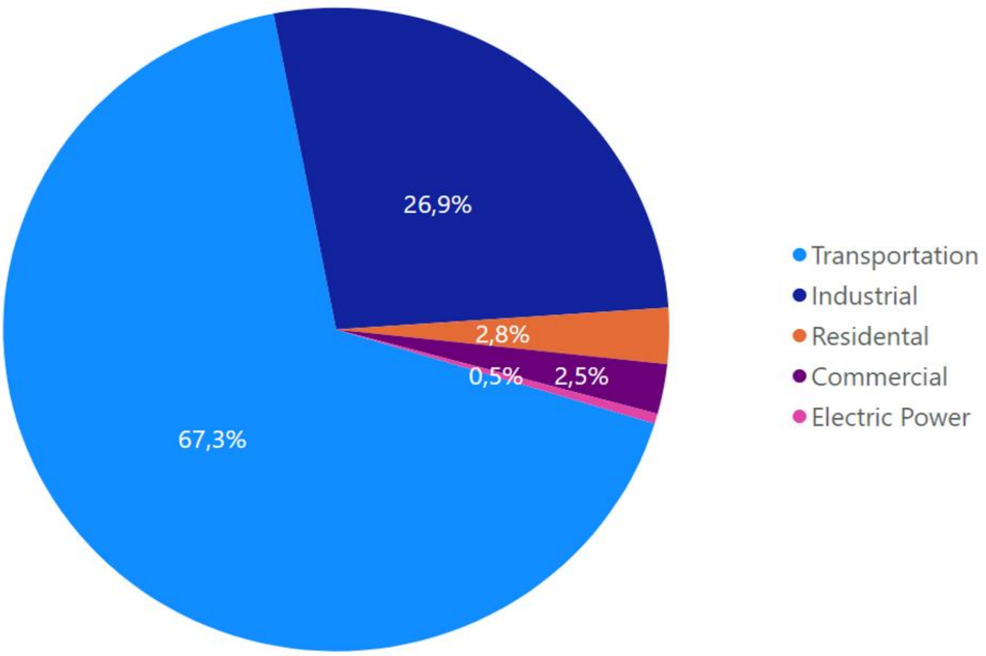

Figure 2.6: USA crude oil refining products shares per sector in 2021. (U.S. Energy Information Administration, 2022)

In the USA, gasoline, diesel, and jet fuels covered 90% of the whole energy need for transportation. (Davis & Boundy, 2021) Transportation is indispensable for humanity and besides that, chemical industry is a must for the continuation of life. These two sectors, which are vital for human beings, demands nearly 94% of crude oil . So, the exploration of the technological ways to sustainably supply alternative fuels chemicals is a requisite (U.S. Energy Information Administration, 2022).

Since the average paraffin contents of the main fuels, gasoline, diesel and jet fuel are 40-50%, 80%, 99%, respectively, alternative fuel technologies focus on synthetic paraffin production in the C_5^+ range (Gokulakrishnan et al., 2015; Ahmed, 1999; Stratiev & Bourgas, 2015).

2.4 Catalysts for Fischer Tropsch

One of the most well-known ways of producing synthetic paraffin is the Fischer-Tropsch Synthesis, and there is still a need to develop an efficient and effective catalyst. For producing hydrocarbons from syngas, the catalysts must be active for CO activation to initiate the reaction by forming surface CH_x species. Surface oxygen atoms left upon CO dissociation has been removed in the form of water vapor or carbon dioxide. The activity of FT catalysts depends on both H_2 adsorption capacity and the reducibility of metal oxide for an effective dissociative CO adsorption. Transition metals in groups III-VI of the periodic table have been reported to be ineffective for FTS. Transition metals Ir, Pt and Pd which are in XI and XII of the periodic table are prone to associative CO adsorption and are not effective for FTS. The elements of group VIII-X have been widely used for Fischer Tropsch Synthesis, the most common of these are ruthenium, nickel, iron and cobalt (Dry, 2004).

Ruthenium is the most active metal for FTS and suitable for the production of long chain hydrocarbons. Despite these properties, ruthenium has not been used commercially because its price is fifty thousand times higher than iron and it is scarce in the world's reserves (Gholami et al., 2017).

Nickel has the second highest activity between Ru, Ir, Co. However, Ni not only has a high methanation tendency but also causes metal loss with producing volatile carbonyl groups under process temperature and pressure. That’s why it is not suitable and advantageous for FTS (Jahangiri et al., 2014).

Iron catalysts exist in metallic iron, iron carbides and iron oxides during FT synthesis. The distribution of these phases depends on the reaction conditions and results in different catalytic performances. Iron oxide is not active in FT synthesis. Therefore, the oxidation of the catalyst leads to the loss of active surfaces. Iron based catalysts are poison-resistant and provide flexible product range. Iron catalyst has high WGS activity, making it for FTS suitable for syngas with a low H_2 to CO ratio as in coal gasification. Moreover, iron exhibits high selectivity to olefins. Fe has economically advantages over ruthenium and cobalt however, its poor selectivity to paraffin and fast deactivation are the main drawbacks for synthetic fuel production (Gholami et al., 2020).

Conventional cobalt catalysts have high CH_4 and C_{5+} but low olefin selectivity compared to iron catalysts. They possess low intrinsic WGS activity and therefore syngas is not wasted to CO_2 formation. Although cobalt is more expensive than iron, it is commercially in use thanks to its low deactivation rate and high FTS yield. High temperature FTS is not preferred over cobalt catalysts to avoid high methane selectivity at the expense of C_{5+} hydrocarbons (Gholami et al., 2020). Comparison of the cobalt and iron catalyst can be summarized as given in the Table 2.1.

Table 2.1 Comparison of Cobalt and Iron Catalysts.

Parameter	**Cobalt Catalyst**	**Iron Catalysts**
Cost	More expensive	Less expensive
Lifetime	Resistant to deactivation	Less resistant (coking, iron carbide, carbon deposit)
Activity/Productivity	Higher	Lower due to water effect
WGS Reaction	Less noticeable	Significant
H_2/CO ratio	~2.0	0.5-2.5
Attrition Resistance	Good	Not very resistant
Selectivity	Mostly Paraffins	Mostly Olefins

Iron and Cobalt are the most common commercialized catalysts for the Fischer Tropsch Synthesis. There are two different processes for FT (Fischer-Tropsch) technology. One is the high-temperature Fischer Tropsch (HTFT) process, in which syngas reacts in a fluidized bed reactor with an iron-based catalyst to produce hydrocarbons in a range from C_1 to C_{15}. This method is mostly used to make liquid fuels and added value chemicals such as olefins. The low-temperature Fischer Tropsch (LTFT) process can use either iron or cobalt as catalysts to produce linear long-chain hydrocarbon waxes and paraffins. These are high-quality C_{5+} hydrocarbons to be used as fuels. Most of the FT technologies developed in the last two decades are based on LTFT process (Khodakov et al., 2007). Schematic representation of LTFT and HTFT are shown in Figure 2.7 and 2.8.

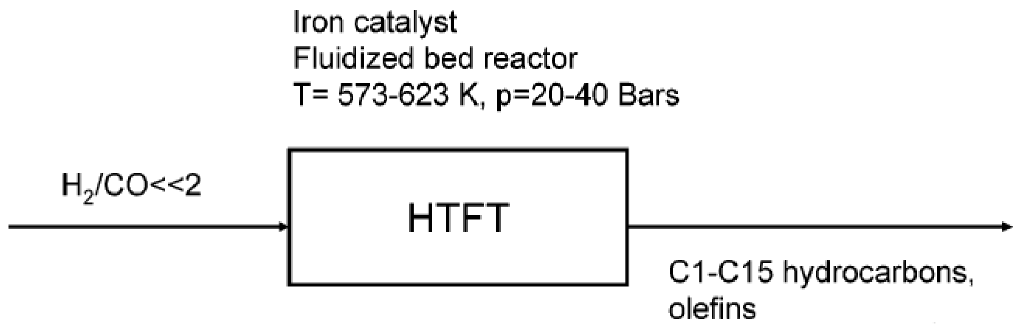

Figure 2.7: High Temperature Fischer Tropsch processes. (Khodakov et al., 2007)

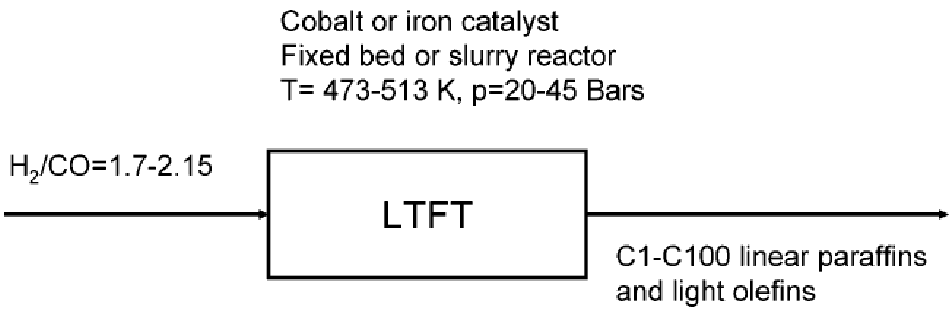

Figure 2.8: Low Temperature Fischer Tropsch processes. (Khodakov et al., 2007)

Main differences of LTFT and HTFT are operation temperature, reactor type and hydrogen to carbon monoxide ratio of the feed. The products in these LTFT and HTFT processes are long chain, saturated hydrocarbons and short chain, unsaturated hydrocarbons, respectively.

2.5 Catalyst design and treatments

For designing heterogeneous catalysts with the best possible performance for the Fischer Tropsch Synthesis process, it is necessary to take into account a range of physicochemical properties. These are pore volume and size, porosity, surface area & dispersion and composition. If a surface area and dispersion of catalyst is high, that means there are more active and available sites on the surface of the catalyst. Pore volume, pore size and porosity controls the inlet and outlet diffusion rates of the reactants and products, respectively. Higher pore size provides much interaction of the reactants with the surface of the catalyst. Catalysts have certain properties that determine their effectiveness in promoting chemical reactions. These properties include activity, selectivity, and stability. The activity of a catalyst refers to its ability to enhance the reaction rate, while its selectivity indicates how selective it is by promoting only certain reactions. The stability of a catalyst determines how well it maintains its performance over time (Bartholomew & Farrauto, 2006).

There are several pretreatments to improve chemical and catalytic properties of the catalysts for Fischer Tropsch Synthesis. These methods can be applied during catalyst synthesis or prior to the reaction. Physical properties of catalyst can be enhanced by supporting active cobalt metal with a substrate that have prominent physical properties. Some of the common pretreatment methods are pyrolysis and calcination.

2.5.1 Pyrolysis

Pyrolysis is a thermal decomposition process that happen under inert atmosphere such as nitrogen or argon. Generally, it is used for eliminating organic substances from structure and leaves carbonaceous solid. Pyrolysis temperature depends on the thermal stability of the material to be treated. Application of pyrolysis as a pretreatment is expected to enhance the dispersion of active metals and to suppress the agglomeration of Co-Co otherwise results in a decrease in activity through the loss of catalytic surface area (Jahangiri et al., 2014).

As an example of pyrolysis, Chen et al. (2021) has worked on M-MOF-74 which is a honeycomb-like material that is formed by the combination of divalent metal ions and

2,5-dihydroxyterephthalic acid. Cobalt was chosen for a divalent metal. Chemical formula of the Co-MOF-74 is $C_8H_4Co_2O_8$. Co-MOF-74 was pyrolyzed under Argon. Upon pyrolysis, carbon matrix of the material partly decomposed by leaving encapsulated cobalt behind it as shown in Figure 2.9 (Chen et al., 2021).

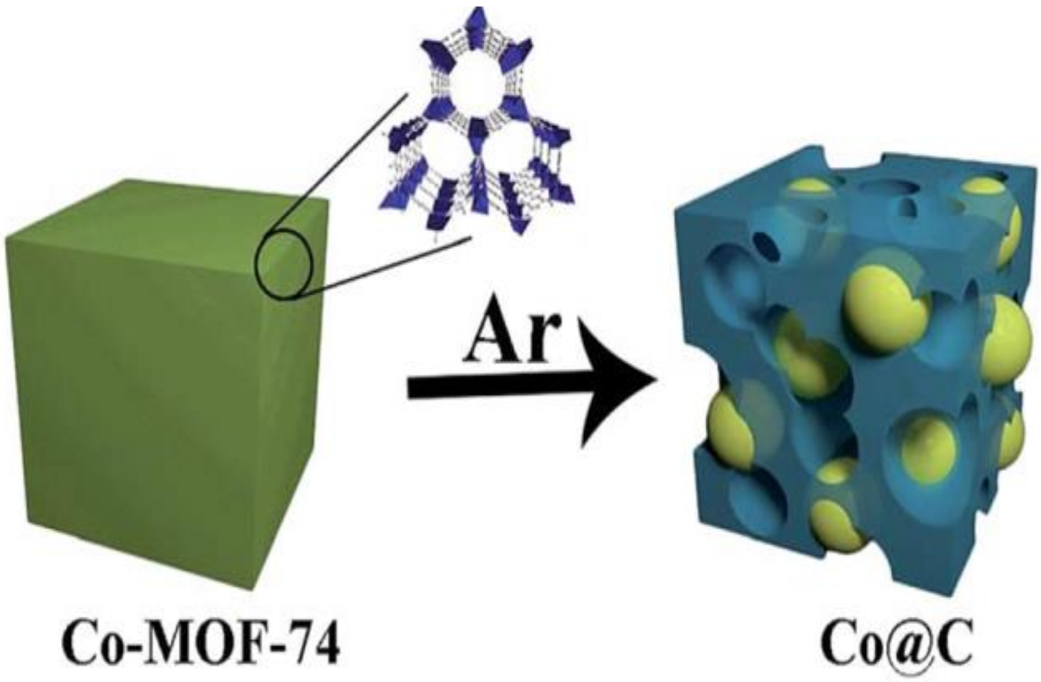

Figure 2.9: Pyrolysis of Co-MOF-74. (Chen et al., 2021)

It was seen that the number of the active metal sites have been increased by keeping cobalt dispersion as much as possible as given in Figure 2.9.

2.5.2 Calcination

Calcination is another thermal process that occurs under air or oxygen atmosphere. Generally, the aim of the calcination is to bring the catalyst precursor into its metal oxide form at high temperature. Application of calcination on catalysts helps to remove carbonaceous residues as well in order to reach high active metal content. This will lead to improve the catalytic surface much more available for the reaction and improve the overall activity (Gholami et al., 2020).

As an example of calcination, Sun and his colleagues investigated cobalt oxide shell formation during the calcination of cobalt carbide. Oxygen in air reacts with the surface carbon and leaves an amorphous cobalt oxide outer layer as represented in the Figure 2.10 (Sun et al., 2017).

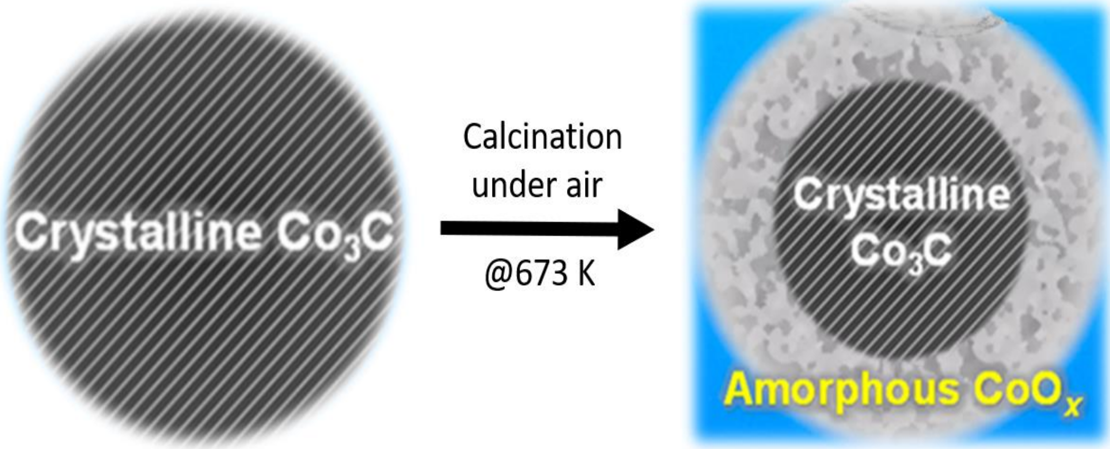

Figure 2.10: Calcination of Co_3C – after a while. (Sun et al., 2017)

In this work, calcination was applied for 2 hours at 673K. Oxygens attacked to carbons and then CoO_x compound took place at the outer surface of the catalyst. As the calcination has been continued to completion for oxidation in a well-controlled manner, whole cobalt carbide phase transforms into amorphous cobalt oxide. This phase transformation was illustrated in Figure 2.11.

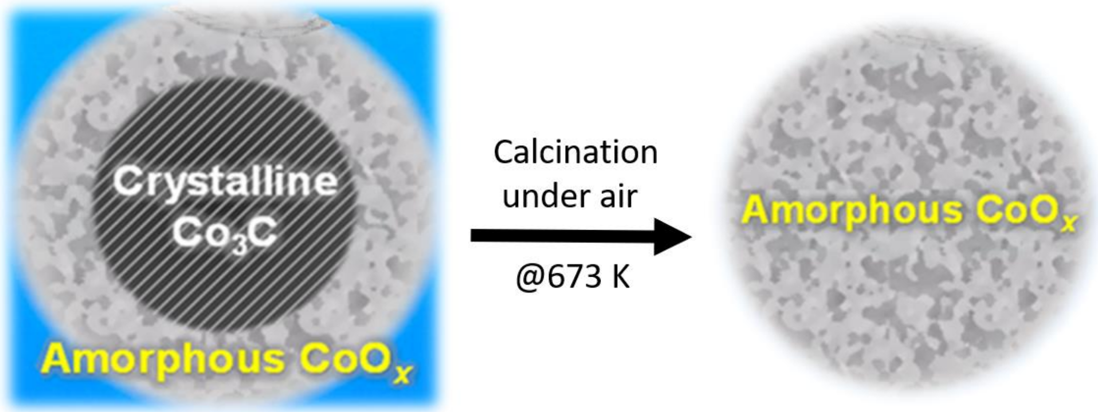

Figure 2.11: Calcination of Co_3C – at the end. (Wang et al., 2018)

Upon completion of calcination, all carbon in cobalt carbide have been removed with oxygenation. So, all structure has been changed from cobalt carbide to cobalt oxides.

2.5.3 Plasma treatment

While pyrolysis and calcination are two commonly used methods for treating traditional catalysts, plasma treatment is a promising technique that has been shown to improve catalytic properties. Plasma treatment is a process used to modify the surface of a catalyst in order to improve its activity and stability. In this process, the catalyst is exposed to plasma for ionization to produce positively and negatively charged particles. The energetic particles in the plasma can react with the surface of the catalyst, altering its chemical, physical and catalytic properties such as dispersion, stability and activity (Tao et al., 2019).

In 2019, Tao et.al (2019) studied on plasma treatments as an effective method for catalyst synthesis. Fe-MOFs have been prepared using plasma technology and it was shown that plasma treatment has significantly saved from the preparation time and improved the adsorption performance of the catalysts. Dielectric barrier discharge (DBD) has been suggested for the preparation of MOFs. With DBD reactor system, solution was pumped to discharge place to synthesize Fe-MOFs. Schematic diagram of DBD is represented in Figure 2.12 (Tao et al., 2019).

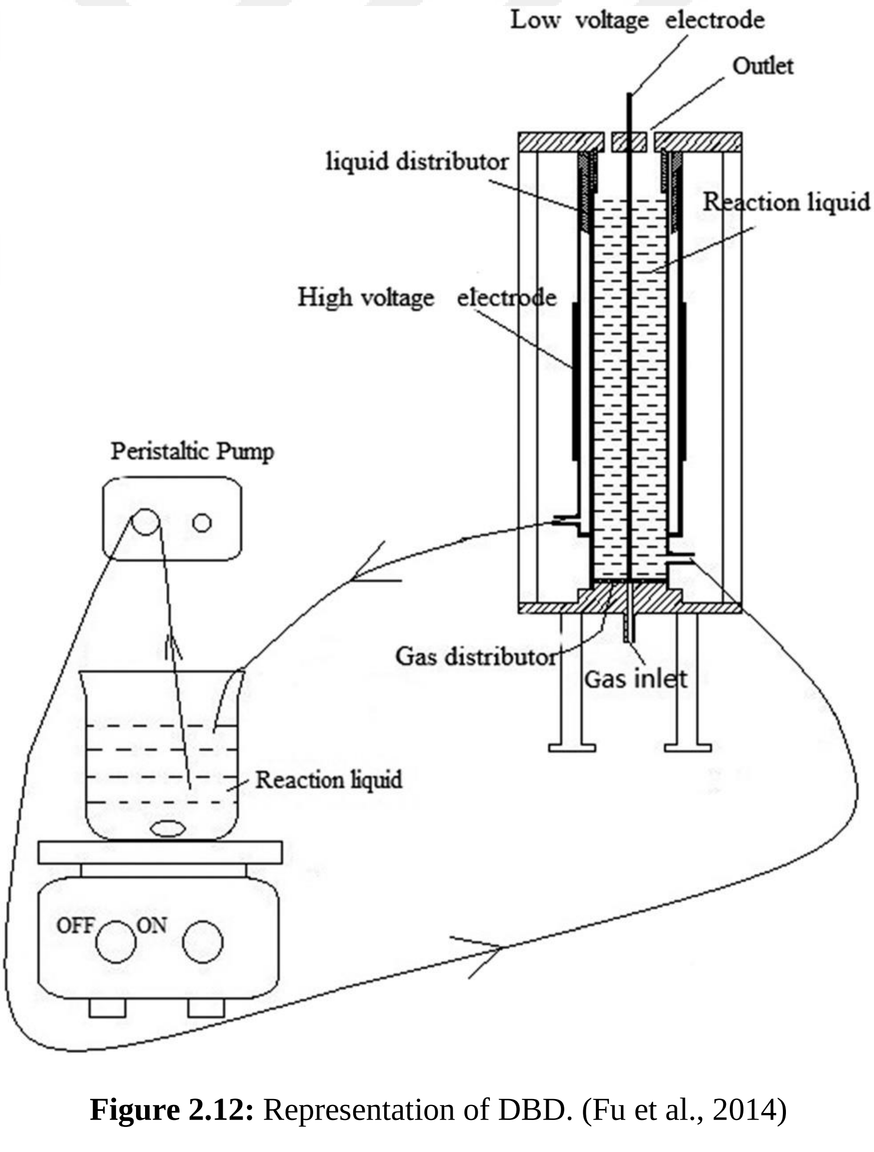

Figure 2.12: Representation of DBD. (Fu et al., 2014)

In the DBD reactor for the synthesis of Fe-MOFs, reaction liquid is prepared outside the reactor and pumped to the reactor. And when discharge is created between two electrodes, the temperature in the channels reaches several hundred degrees of Kelvin as a result of the strong electric field impact, and the energy of charged particles can be many electron volts. This is due to the strong impact of the electric field on the channels (Fu et al., 2014).

Fu and his co-workers (2014) have investigated the direct effect of plasma treatment on the catalysts. DBD reactor was used for the plasma treatment. A high-voltage AC generator was operated to initiate DBD plasma under a flow of argon gas at atmospheric pressure. The sample was subjected to DBD plasma treatment for 30 minutes. Schematic representation of their process was shown in Figure 2.13.

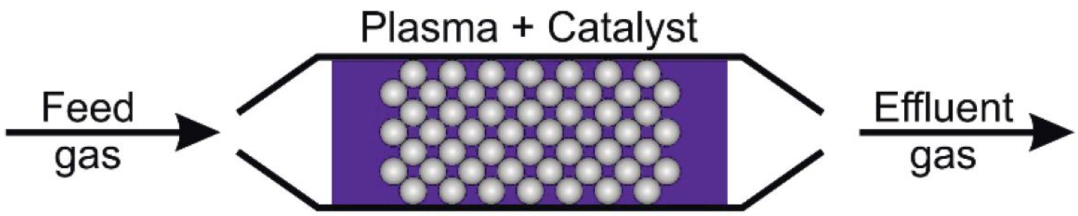

Figure 2.13: Schematic representation of plasma treatment. (Li et al., 2019)

As a result of their study, cobalt dispersion has been improved with plasma treatment. This method has several advantages for the preparation of catalysts. It allows for the decomposition of the precursor in a shorter period of time at a lower temperature with less energy input. This makes plasma an effective alternative approach for the preparation of cobalt-based catalysts for the synthesis of FT. The use of plasma treatment can greatly improve the efficiency and effectiveness of the catalyst preparation process (X. Li et al., 2019).

2.6 Cobalt as a Fischer Tropsch Catalyst

In 2019, Xu Li and a group of scientists, studied for understanding the behavior of the Fischer Tropsch cobalt catalysts. Four different cobalt precursors, $Co(NO_3)_2.6H_2O$, $Co(C_2H_3O_2)_2 \cdot 4H_2O$, $CoCl_2 \cdot 6H_2O$, $Co(OH)_2$, were used to prepare cobalt/SiO_2 catalyst. The catalysts were labelled as Co-Nit, Co-Ace, Co-Chl and Co-Hyd, respectively. The activity and selectivity of these catalysts were evaluated using a small stainless-steel tubular fixed-bed reactor. The reactor had a diameter of ½ inch and was typically filled with a mixture of 2 g of catalyst and 8 g of SiC. Before beginning the Fischer-Tropsch synthesis reaction, the optimal reduction temperature for each catalyst was determined through temperature programmed reduction (TPR) analysis and the catalysts were activated at these temperatures. The Co-Nit and Co-Hyd catalysts were reduced by a mixture of 100 cm^3/min hydrogen and 100 cm^3/min nitrogen at 1 bar for 12 hours at 350°C, while the Co-Ace and C-Chl catalysts were reduced in situ at 450°C under the same conditions. After the reduction process, the reactor temperature was set to 120°C under nitrogen flow. By flowing N_2/H_2/CO with a ratio of 2/2/1, inside pressure of the reactor was increased to 15 bars. Then, the temperature was gradually increased to 230°C at a rate of 1°C per minute to avoid hot spots caused by the highly exothermic Fischer-Tropsch synthesis reaction. The reaction was continued for 30 hours. In their study, they have calculated the conversion and selectivity by the equations (2.8) and (2.9) where F and Cn are the molar flow rates and carbon number of products, respectively (Xie et al., 2019).

$$CO\ conversion\ (\%) = \frac{F_{CO,in} - F_{CO,out}}{F_{CO,out}} \tag{2.8}$$

$$Selectivity\ (\%) = \frac{nF_{Cn,out}}{F_{CO,in} - F_{CO,out}} \tag{2.9}$$

The main results were that higher conversion rates over Co-Nit and Co-Hyd were observed in comparison to Co-Chl and Co-Ace. Not only the conversion rates but also selectivity has changed as well based on the cobalt precursor. Higher C_{5+} selectivity has obtained on Co-Nit and Co-Hyd at the expense of methane selectivity. Best results in terms of C_2-C_4 and C_{5+} hydrocarbon yield was achieved on conventionally prepared cobalt catalyst by cobalt nitrate. Co-Hyd was also seen to be the good candidate when C_5^+ demand is high (Xie et al., 2019).

Xie et al. (2019) studied the effect of promoter on the performance of cobalt catalysts. Seven different cobalt catalyst over manganese oxide support have been synthesized. Bimetallic Co_1Mn_3 and Co_3Mn_1 catalysts have been impregnated with $Na_2S_2O_3$, Na_2CO_3, Na_2S and $(NH_4)_2SO_4$. The effect of reaction conditions have been evaluated as well on Co_1Mn_3-Na_2S (Al, 2019). It was found that C_{5+} selectivity were decreasing when the reaction temperature were increased from 240 ° to 280°C. In the second set of reactions, the effect of pressure were investigated by keeping the temperature constant at 240 °C. It was shown that higher pressures improves C_5^+ selectivity further. So 240 °C and 10 bar seemed the best operating conditions when C_{5+} was the target product (Al, 2019).

In 2019, Jung and Ko studied the effects of cobalt metal loading on FTS activity over alumina supported cobalt catalysts. The performance of the catalysts have been compared regarding their textural properties, CO conversions and product selectivity. Four catalysts with different cobalt loadings on gamma alumina have been prepared, as in 5 wt% Co/γ-Al_2O_3, 10 wt% Co/γ-Al_2O_3, 15 wt% Co/γ-Al_2O_3, 20 wt% Co/γ-Al_2O_3.

When the cobalt load has been increased from 5 to 15%, the surface area and pore volume of the catalyst decreased in a linear fashion. This decrease has been attributed to the partial blocking of the pores of support by cobalt oxide clusters and/or the partial collapse of the porous structure due to the increased cobalt loading. However, when the cobalt loading was increased from 15 to 20%, pore volume, average pore diameter and the surface area remained unchanged. This was interpreted by the authors as the complete coverage of the alumina surface with cobalt oxide at 15% cobalt load and all the pores in the alumina support have been filled. Further increasing the cobalt loading to 20% seemed not to affect the interaction of cobalt oxide with the alumina surface, but it did increase the size of the cobalt oxide particles on alumina support (Al, 2019).

The catalytic activity tests of these four catalysts were evaluated under 20 bars and 210°C with a feed ratio of H_2/CO = 2 in a fixed bed reactor. Tests were conducted for 75 hours. The reaction temperature initially rose quickly to 236°C due to the exothermic heat generated by the FTS reaction, resulting in high CO conversion and high CH_4 selectivity. After 30 hours of reaction, the steady-state conditions have been established and much higher CO conversion close to 80% have been recorded over 15 wt% Co-Alumina catalyst (Lappas & Heracleous, 2016).

In terms of selectivity, all three catalysts with 10, 15 and 20 % Co loading have shown higher CO_2 and CH_4 but with a lower C_{5+} selectivity compared to 5% Co loading. This was attributed to the changing interaction of cobalt oxide with alumina upon loading amount which may induce the number of active cobalt sites and the available surface area (Lappas & Heracleous, 2016).

To sum up, the Fischer-Tropsch reaction is a surface polymerization reaction including initiation by CO activation into CHx monomers, hydrocarbon chain growth and termination of the growing chain to end up with linear paraffins or 1-olefins. Cobalt (Co) and iron (Fe) have been well proven catalysts for this reaction. Their choice depends on the target product since the selectivity of cobalt and iron catalysts differentiates. Cobalt catalysts have shown high CH_4 and C_5^+ but low olefin selectivity compared to iron catalysts. The activity of cobalt catalysts mainly depends on the reducibility and dispersion of cobalt oxides together with the particle size of the final metallic Co^o sites (Cheng et al., 2017). The main challenge in controlling cobalt crystal size is the cobalt-support interaction. In order to achieve high metal loading with reasonable dispersion and small metallic cobalt crystal size, the use of metal-organic frameworks (MOFs) is the main issue of this thesis. Metal organic frameworks (MOFs) are a class of micro porous crystalline materials made up of a metal and an organic ligand with high surface area and porosity. Carbon framework serves as a sacrificial template in the preparation of metal nanoparticles encapsulated by a carbon matrix under controlled pyrolysis-calcination-reduction conditions. The organic linker in the MOF structure partly decomposes to form both graphitic carbon and framework carbon hosting the metallic cobalt (Chen et al., 2020). Because of its low cost and easy preparation, MOF derived cobalt catalysts widely proceeds over ZIF67. Zeolitic imidazolate frameworks (ZIFs) is a kind of MOF but with a similar zeolite topology (Lv et al., 2013). Nitrogen content of the organic linker in ZIF-67 is considered to give N-doped carbon and Co-N moieties contributing to the catalytic performance. Nitrogen content of ZIF-67 may act as an electron donor and induce interaction between cobalt nanoparticles and N-doped carbon towards improving the final textural properties of the catalyst (Wang et al., 2018; Chen et al., 2019; Luo et al., 2019; Qiu et al., 2017).

Plasma techniques are commonly applied for the low temperature decomposition of the catalytic precursor. There are studies on glow discharge plasma for the decomposition of Ni, Fe and Co nitrates and improved metal dispersion with plasma treatment compared to the thermal calcination has been reported. Calcination by plasma was also seen effective in preventing the catalysts from sintering and aggregation. As a result of this, enhanced activity, C_{5+} selectivity and catalytic stability have been observed over them (Bai et al., 2012).

The defects in nanomaterials modifies the electronic and surface properties of materials. These defects can be point, line, plane or volume defects. The point defect are the vacancies, interstitial atoms, impurities and heteroatom doping. All these surface defects of the catalysts may have a positive effect on the activity of the catalysts. Plasma functions in surface cleaning, oxygen cavitation, and etching (Li et al., 2019).

By applying argon plasma etching as post treatment, surface defects and oxygen vacancies might be created to generate more active sites through lattice distortion and electronic compensation. Wang et al. (2018) used plasma etching to get a Co_3O_4 electrocatalyst with high surface area and more oxygen vacancies for oxygen evolution reaction (OER). They have reported an improved electrocatalytic performance of Co_3O_4 for OER induced by plasma-engraving due to the affected surface area and the oxygen vacancies (Xu et al., 2016).

As reported by Chu et al. (2008), an increase in Co dispersion has been achieved for alumina-supported Co catalysts prepared by the glow discharge plasma instead of thermal calcination. High catalytic activity in FT synthesis have been noticed on plasma-assisted catalysts with an improved cobalt dispersion and reducibility (Chu et al., 2008).

Although improved catalytic activity could be expected for nano-sized catalysts thanks to the increased number of actives sites such as edge and corner atoms, deteriorated stability would be another concern depending on reaction conditions. Nano-sized materials are more prone to sintering due to their high surface energy. In addition, selectivity to target product is the other important issue to be considered in the design of a catalyst. Various methods have been used to solve the above mentioned problems of nano-catalysts. These methods are embedding nanoparticles inside controlled cavities or channels of mesoporous materials or within the pores of graphitic spheres as applied in this thesis study; incorporating in the interstitial site of perovskite-like crystals and constructing core-shell nano-structures through layer by layer synthesis or surface-protected etching techniques (Gioria et al., 2021; Li & Tang, 2014; Li et al., 2016; Wang et al., 2018; Zhang et al., 2012).

The first two techniques cannot completely prevent sintering of nanoparticles through the Ostwald ripening (Gommes, 2019). The expected outcome of core-shell catalysts is enhanced catalytic activity and improved selectivity to alkenes and higher hydrocarbons which might be from the electronic effects induced by transition metal oxides such as manganese oxide.

To the best of our knowledge, there is no reported research on the effects of cold plasma (DBP) on the activity of MOF-derived cobalt catalysts for FTS. In this thesis, 12 sets of catalyst were prepared by pyrolysis, plasma and calcination treatments. Briefly, ZIF-67 was synthesized with a well-known route by using the reagents cobalt nitrate hexa-hydrate, 2-methylimidazole and methanol. Then the first 6 sets of catalysts were exposed to pyrolysis under N_2 stream at 400, 500, 600, 700, 800 and 900 °C. Then, all these were calcined mildly at 350 °C under air atmosphere. In the second sets of catalyst preparation, pyrolyzed samples were treated by dielectric barrier discharge plasma (DBD) as a non-thermal plasma technique for 30 min. as more and then mildly calcined. In the last part of the thesis, core-shell structures were studied. Regarding this, three sets of catalysts with Co/ZIF-67 core and a metal oxide shell have been prepared. Pyrolyzed cobalt particles were layered by K_2O, ZnO or MnO either.

Various characterizations were implemented for the prepared catalysts. In this regard, X-Ray Diffraction (XRD), Fourier Trasform-Infrared Spectroscopy (FTIR), Field Emission Scanning Electron Microscope (FESEM), Energy Dispersive X-Ray Spectroscopy (EDAX) Dot Mapping, Thermal Gravimetric Analysis (TGA) and Nitrogen Adsorption/Desoprtion Isotherms for BET Surface Area and Pore Volume and Elemental Analysis for CHN were applied.

Fischer-Tropsch reaction was conducted in a high pressure test system equipped with a fixed bed reactor (i.d.: 10 mm; length: 800 mm). Prior to the reaction, calcined catalyst was reduced with a gas mixture composed of 50v%H_2 -50v%N_2 at 400 ^{0}C for 16 hours at atmospheric pressure. Subsequently, the reactor was set to FT reaction conditions, namely 230°C and 15 bar. The product gas was quantitatively analyzed in every 30 minutes by online gas chromatography (Agilent, 7820A GC).

3. EXPERIMENTAL

In the experimental section, the materials and chemicals, catalyst synthesis and characterizations and catalytic test unit and calculations will be given and/or described.

3.1 Materials

In this part, materials/chemicals used for the catalyst synthesis and technical gases for the tests will be given.

3.1.1 Chemicals

Chemicals used for catalyst synthesis are given in Table 3.1. These chemicals were commercially supplied and used without further purification.

Table 3.1. Chemicals and properties.

Chemicals	Formula	Purity	Supplier
Cobalt Nitrate Hexahydrate	$Co(NO_3)_2 \cdot 6H_2O$	99%	Merck
2-methylimidazole	$C_4H_6N_2$	99%	Sigma Aldrich
Methanol	CH_3OH	≥99.7%	Sigma Aldrich
Ethanol	C_2H_5OH	≥99.7%	Merck
Zinc acetate	$Zn(CH_3CO_2)_2$	≥99%	Merck
Potassium acetate	$K(CH_3CO_2)$	≥99%	Merck
Manganese acetate	$Mn(CH_3CO_2)_2$	≥99%	Merck

3.1.2 Technical gases

Technical gases used in the catalyst preparation and experiments were listed in the Table 3.2.

Table 3.2. Technical Gases.

Gases	Purity	Supplier	Application
Air	High Purity	Linde	Oxidizing Gas
Nitrogen	≥99.99%	Linde	Inert Gas, Reactant Gas
Hydrogen	High Purity	Linde	Reactant Gas, Reducing Agent
Carbon Monoxide	95%	Linde	Reactant Gas

3.2 Catalyst Synthesis

In the synthesis of ZIF-67, 400 mL of methanol was used to dissolve 13.04 g of 2-methylimidazole and 400 mL of methanol was used to dissolve 5.85 g of $Co(NO_3)_2.6H_2O$ separately to create two homogeneous solutions. Solutions were stirred with magnetic stirrer until complete dissolution was reached. Cobalt nitrate hexahydrate solution was a reddish color and 2-methylimidazole solution was colorless. Reddish solution was added dropwise with separatory funnel on colorless solution at room temperature, as shown in Figure 3.1.

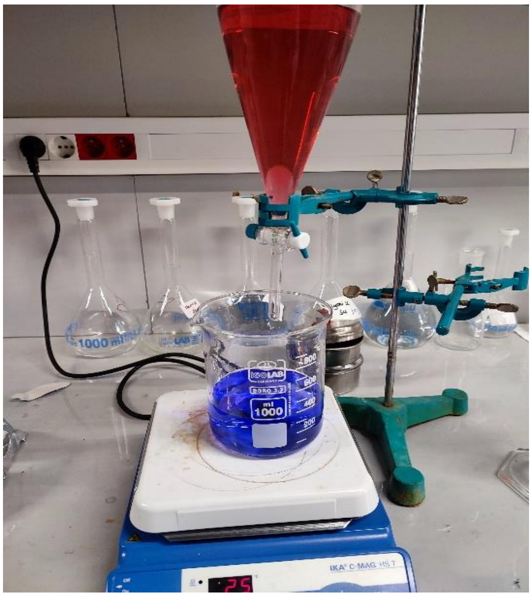

Figure 3.1: Mixing cobalt nitrate hexahydrate and 2-methyl imidazole.

As the reaction took place, the colorless solution began to turn bright purple. Cobalt nitrate hexahydrate was the metal salt and 2-methlyimidazole was the organic ligand. Upon completion of synthesis reaction, final solution reached bright purple color which was the original color of ZIF-67. The final mixture was stirred at room temperature for 24 hours to ensure the completeness of the reaction with a high yield. Final product were centrifuged at 10000 rpm for 10 minutes and washed with methanol for 5 times to get rid of unreacted substances. In Figure 3.2, it was seen the samples before (a) and after the centrifuge (b).

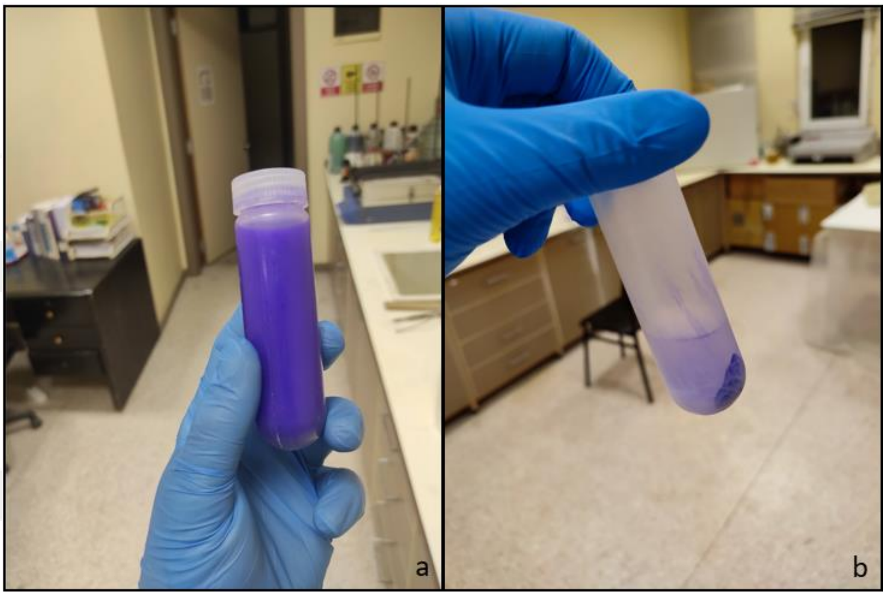

Figure 3.2: a) before centrifuge and **b)** after centrifuge.

After centrifugation, ZIF-67 was obtained in methanol. The, it was dried in a vacuum oven for 24 hours at 110°C to remove methanol from the ZIF-67. After drying, ZIF-67 powders were obtained as in Figure 3.3.

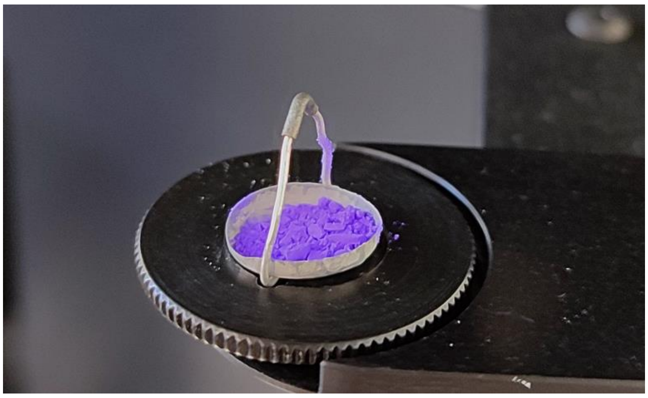

Figure 3.3: ZIF-67 powder.

For the first set of catalyst preparation, ZIF- 67 was transferred into a ceramic porcelain boat in a tube furnace. The heating procedure was as follows: the tube furnace was flushed with N_2 at 30 °C for 30 min, after which it was pyrolyzed for 4 hours at temperatures (T) being 400, 500, 600, 700, 800 and 900 °C with a heating rate of 2 °C per minute under N_2 flow (100 mL/min.gr). The pyrolyzed samples were calcined at 350 °C for 3 hours with a heating rate of 1 °C per minute under air flow (100 mL/min.gr). These catalysts were denoted as “CoZ@T” in which T represents the pyrolysis temperature. Applied synthesis procedure were given schematically as well in Figure 3.4.

In the second sets of catalyst preparation, pyrolyzed samples were exposed to argon plasma treatment before calcination. A dielectric barrier discharge was used to produce the argon plasma (DBD). The pyrolyzed catalyst samples were put into the DBD plasma reactor, which used a dynamic argon plasma as carrier gas. The applied voltage had a sinusoidal waveform with a frequency of around 10 kHz for 30 min. The plasma treated samples were calcined at 350 °C for 3 hours with a heating rate of 1 °C per minute under air flow (100 mL/min.gr). They were denoted as “P_CoZ@T” in which P in the beginning of the names represents the presence of plasma treatment.

For the fabrication of CoZ@ MOx (M = Zn, Mn and K) catalyst, 1.0 g of as-synthesized ZIF-67 and 3.0 g water were added into 300 mL of ethanol by stirring for 30 min, followed by sonication for 10 min and stirring for 30 min. The prepared solution is denoted as A. B solution consists of acetates of Zn, Mn and K (0.007 mole of each of them) and ethanol (23 mL). Then B solution was pumped into A solution at a rate of 0.5 mL.min-1 with continuous stirring. Subsequently, the mixture was heated in water bath at 80 °C for 90 min to promote hydrolysis. The ZIF-67@MOx was obtained by centrifugation, washing with ethanol, and drying at 100 °C for 12 h. Then the ZIF-67@MOx was pyrolyzed at 600 °C for 4 h in N_2. When the above sample was further calcinated at 350 °C for 3 h, the prepared product is denoted as CoZ@MOx being CoZ@K2O, CoZ@ZnO and CoZ@MnOx. Figure 3.5 shows the synthesis flowchart of the catalysts with core shell structure.

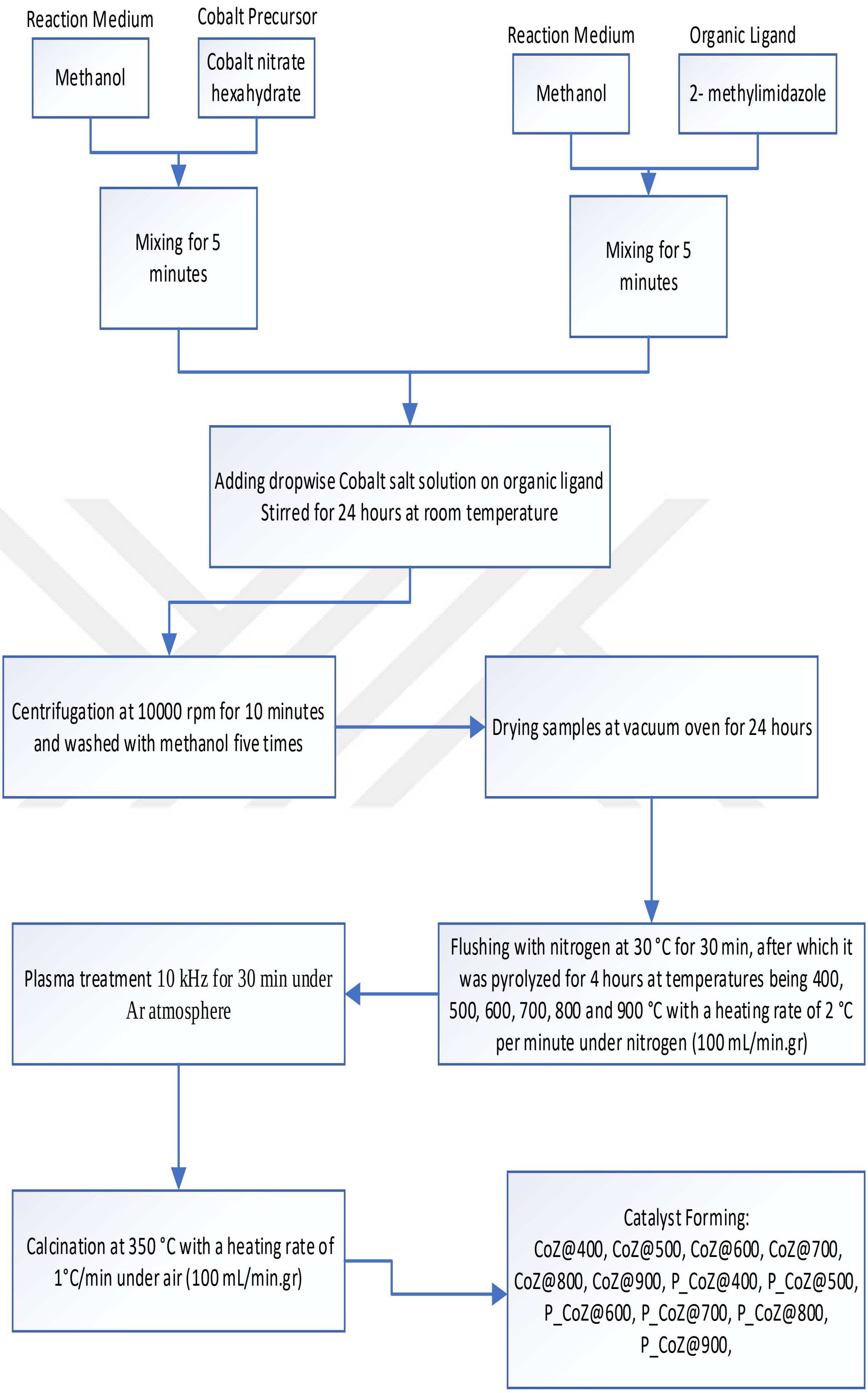

Figure 3.4: Synthesis flowchart of the catalysts with various carbonization temperatures and plasma treatment.

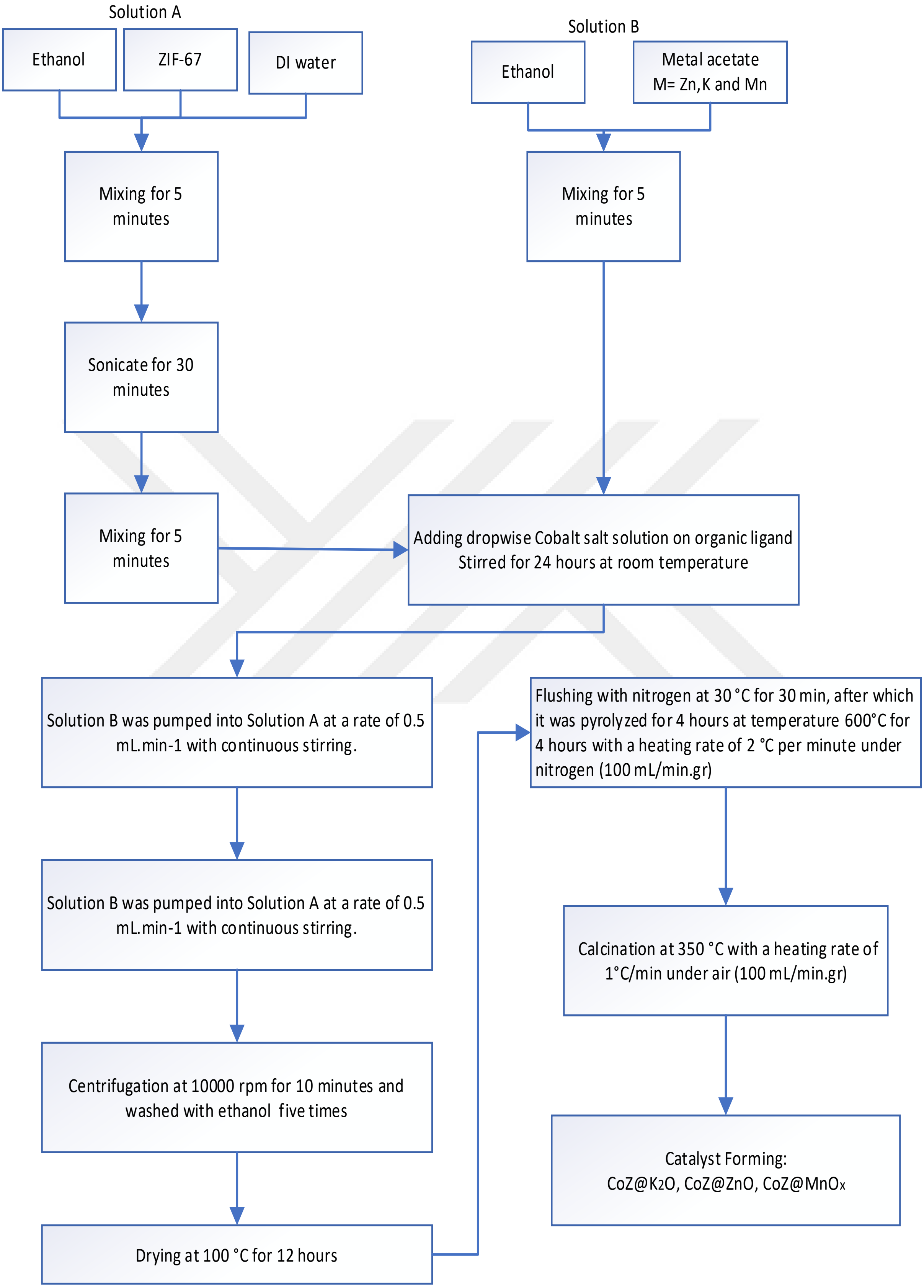

Figure 3.5: Synthesis flowchart of the catalysts with core shell structure.

Synthesized all 15 catalyst can be summarized as given in Table 3.3. While naming the samples, the denotation ‘’P’’ was used to indicate plasma treatment.

Table 3.3. Synthesized catalysts üand treatments.

Catalyst No	Sample	Treatment
1	CoZ@400	Pyrolysis at 400°C and calcination at 350°C
2	CoZ@500	Pyrolysis at 500°C and calcination at 350°C
3	CoZ@600	Pyrolysis at 600°C and calcination at 350°C
4	CoZ@700	Pyrolysis at 700°C and calcination at 350°C
5	CoZ@800	Pyrolysis at 800°C and calcination at 350°C
6	CoZ@900	Pyrolysis at 900°C and calcination at 350°C
7	P_CoZ@400	Pyrolysis at 400°C, arc plasma with a frequency of ~10 kHz and calcination at 350°C
8	P_CoZ@500	Pyrolysis at 500°C, arc plasma with a frequency of ~10 kHz and calcination at 350°C
9	P_CoZ@600	Pyrolysis at 600°C, arc plasma with a frequency of ~10 kHz and calcination at 350°C
10	P_CoZ@700	Pyrolysis at 700°C, arc plasma with a frequency of ~10 kHz and calcination at 350°C
11	P_CoZ@800	Pyrolysis at 800°C, arc plasma with a frequency of ~10 kHz and calcination at 350°C
12	P_CoZ@900	Pyrolysis at 900°C, arc plasma with a frequency of ~10 kHz and calcination at 350°C
13	CoZ@K_2O	Pyrolysis at 600°C and calcination at 350°C
14	CoZ@ZnO	Pyrolysis at 600°C and calcination at 350°C
15	CoZ@MnO_x	Pyrolysis at 600°C and calcination at 350°C

3.3 Catalyst Characterization

The catalysts were characterized with X-Ray Diffraction (XRD), Fourier Transform Infrared Spectroscopy (FTIR), Field Emission Infrared Scanning Electron Microscopy (FESEM) and Brunauer-Emmett-Teller (BET) Analysis, Thermogravimetric Analysis (TGA) and Temperature Programmed Reduction (H_2-TPR) for the investigation of surface composition, surface area, pore sizes, crystalline structure and reduction profile of catalysts. Details on the instruments used for characterizations were given in Table 3.4.

Table 3.4. Characterization methods, equipment and purposes.

Characterization Method	Equipment	The purpose of analysis
XRD	Siemens D5000	Phase analysis and crystal size
FTIR	Jasco-4000	Structure and surface functional group analysis
FESEM	Hitachi S-4160	Surface morphology
N_2 Sorption (BET)	Micrometrics 3 Flex	Textural properties such as surface area and pore volume
TGA	TA Instruments TGA 55 Model Analyser	Thermal decomposition profiles
TPR	Fixed Bed Reactor	Reducibility and dispersion of metal oxides

Crystal structure of ZIF-67 and the catalysts have been investigated through their x-ray diffraction (xrd) patterns in the range of 2θ=6-90˚.

FTIR transmittance spectra of ZIF-67 and catalysts were recorded at room temperature in the frequency range of 400–4000 cm^{-1}.

The surface images were taken for the morphology of ZIF-67 and elemental distribution has been determined with FESEM, EDAX and dot mapping. Microstructure images of the synthesized catalysts were taken by FESEM in two different magnifications (100 nm and 200 nm).

For the calculation of the surface area, the pore volume and pore size for ZIF-67 and synthesized catalysts, N_2 adsorption/desorption instrument has been used to drive the N_2 adsorption/desorption isotherms at 77,228 K. All samples have been degassed under vacuum at 200°C before taking the isotherms.

Thermal decomposition profiles of ZIF-67 has been driven by thermogravimetric analysis to evaluate the pyrolysis temperature. The heating profile for TGA was heating from ambient to 750°C and 900°C for fresh ZIF-67 and the pyrolyzed catalyst samples, respectively with a heating rate of 10°C/min under N_2 atmosphere. In each of TGA measurements, 20-25 mg of sample was used.

TPR measurements were carried out on thermal gravimetric analyzer with a heating rate of 15°C/min heating rate from ambient to 900°C. In the measurements, ~10 mg sample and a gas mixture of 20% H_2 and 80% N_2 were used.

3.4 Catalyst Test System and Procedure

Fischer-Tropsch reaction tests were carried out on a high-pressure fixed bed reactor set-up (i.d.: 10 mm; length: 800 mm). Figure 3.6 represents the FT catalyst test reactor setup. To prevent condensation, all product stream lines were heat traced. 0.5 g of each catalyst (50-150 μm) diluted with quartz particles with the same volume were charged to the reactor for FTS tests (0.6 ml catalyst bed diluent). Before FTS reaction, catalysts were reduced with a reducing gas mixture (50%H_2-50%N_2 volume based), at 400 °C for 16 hours at atmospheric pressure. FTS reactor conditions were as: 230°C and 15 bars, and 14.5 $mL.min^{-1}$ flow of 64v% H_2 / 29v% CO / 7v% N_2 (corresponding to a space velocity of 1.8 $L/g_{cat}.h$). Gaseous product compositions were analysed by online gas chromatography (7820A GC, Agilent). Thermal conductivity detector (TCD) with a Carboxen column was used to quantitatively determine the amounts of H_2, CO, CO_2, and N_2. Flame ionization detector (FID) with Alumina S column was implemented for C_1-C_{5+} hydrocarbons detection. Gas chromatography device was calibrated with known composition gas mixtures. Calibration allows for the establishment of a reference standard against which the unknown samples can be compared, enabling quantitative analysis. And also calibrations corrects any systematic errors or deviations in the instrument, such as baseline drift or retention time shifts, ensuring precise and consistent measurements.

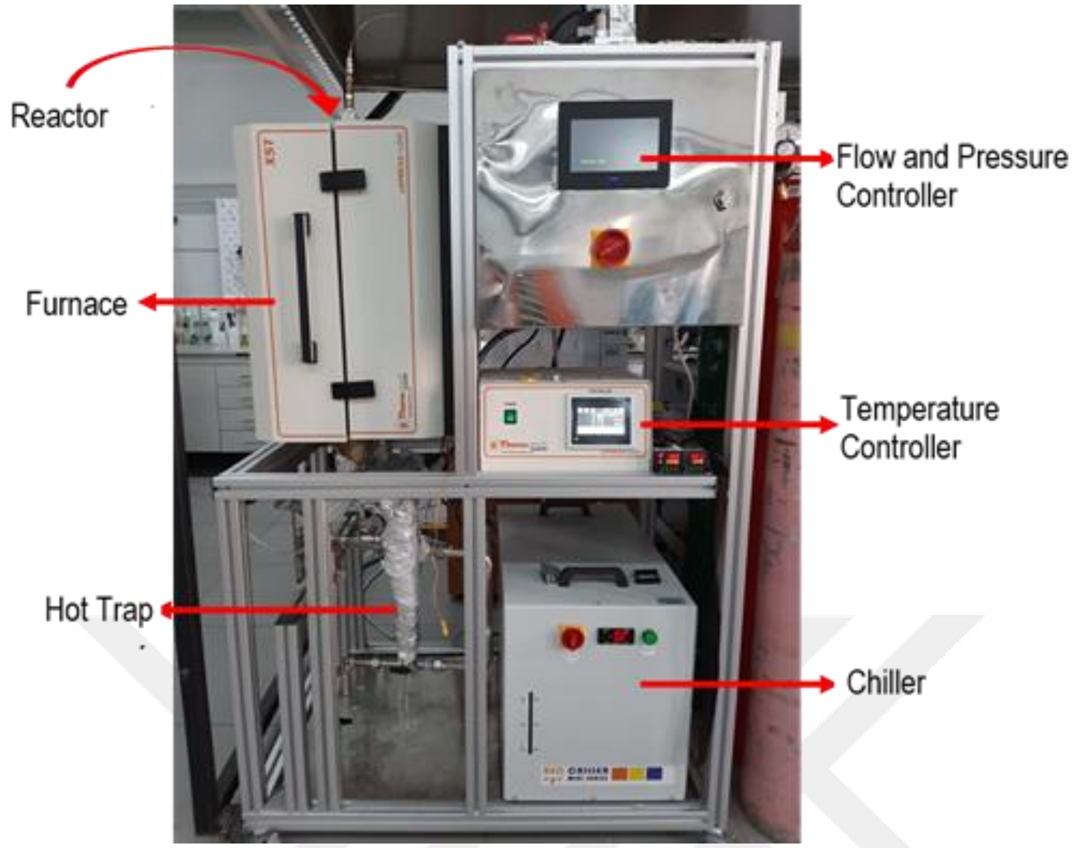

Figure 3.6: Catalytic test unit equipments.

Reduction temperature was chosen as 400°C based on H_2-TPR results as shown below in Figure 3.7.

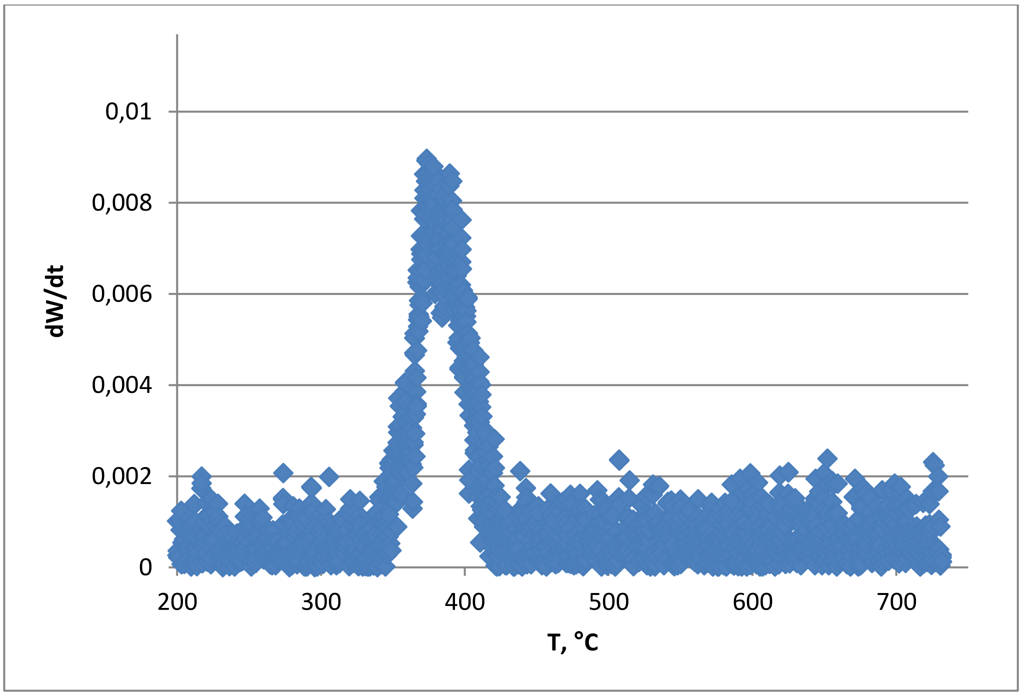

Figure 3.7: H_2-TPR result of CoZ@T.

Fischer-Tropsch reactions are divided into two operating temperature: High Temperature Fischer Tropsch (HTFT) and Low Temperature Fischer Tropsch (LTFT). HTFT operating mode that takes places in the 300-350°C temperature range and is used for the production of linear low-molecular weight olefins. LTFT operates in the 200-240°C range and produces high molecular weight linear paraffins which are known as synthetic fuels (Lappas & Heracleous, 2016).

Since the aim of the project was to produce synthetic fuels, FTS tests have been executed at LTFT conditions, namely at a temperature of 230°C and pressure of 15 bars. Catalytic test protocols are summarized as given in Table 3.5.

Table 3.5. Catalytic Tests procedure for FT reaction as decided by initial tests.

Parameter	**Value**
Amount of catalyst	0.5 gram
Amount of catalyst bed diluent	0.6 mL
Temperature	230°C
GHSV, L/g.cat.h	1.76
Pressure	15 bars
Feed gas composition	64v% H_2 / 29v% CO / 7v% N_2
Gas analysis method	Agilent, 7820A GC TCD Carboxen Column FID Alumina S Column
Duration of catalytic test	30-40 h
Liquid product sampling procedure	Hot trap at 150 °C / Cold trap at 0 °C
Liquid product analysis procedure	GC-MS

Once all the preparations have been completed and the trial test has been successfully completed without problems, catalyst samples, which were denoted as CoZ@400, CoZ@500, CoZ@600, CoZ@700, CoZ@800, CoZ@900, P_CoZ@400, P_CoZ@500, P_CoZ@600, P_CoZ@700, P_CoZ@800, P_CoZ@900, have been tested under the same reaction conditions.

3.5 Calculations

CO conversion (X_{CO}), hydrocarbon selectivity without CO_2 (S_{cn}) and CO_2 selectivity (X_{CO2}) were calculated as given in equations (3.1), (3.2) and (3.3) below:

Catalyst performance was determined based on the CO conversion (X_{CO}) in equation (3.1) and the CO_2 free hydrocarbon selectivity on carbon basis (S_{cn}) in equation (3.2), the CO_2 selectivity on carbon basis (X_{CO2}) in equation (3.3). In the following equations, “in” and “out” denote inlet and outlet of the reactor.

$$X_{CO} = \frac{(CO_{in} - CO_{out})}{(CO_{in})} \times 100 \tag{3.1}$$

$$S_{CN} = \frac{n_C \times F_{out} \times C_n(\text{ produced HC})}{(CO_{in} - CO_{out}) - {CO_2}_{\text{out}}} \tag{3.2}$$

$$X_{CO2} = \frac{{CO_2}_{out}}{(CO_{in} - CO_{out})} \times 100 \tag{3.3}$$

where CO_{in} and CO_{out} are the inlet and outlet molar flow rates (mol/h), respectively. X_n (HC) is the mole fraction of the hydrocarbon in the product stream and n_C is the carbon number of the hydrocarbon whose selectivity is calculated. CO_{2out} denotes the molar flow rate of CO_2 (mol/h) in the product stream.

4. RESULTS AND DISCUSSION

The aim of the thesis is to develop an active catalyst for syngas to synthetic fuels. Cobalt as an active metal has been chosen nano sized and carbon encapsulated cobalt catalysts have been prepared via the pyrolysis and plasma treatments of ZIF-67 structure. The effect of pyrolysis temperature and effect of cold plasma have been investigated. Moreover, cobalt oxide core have been layered with a metal oxide shell for stabilization and controlled diffusion of reactants and products. Then their FTS performance was measured by catalytic activity tests under HTFT conditions. Finally, catalytic activity-structure relationship has been investigated by applying catalyst characterizations.

4.1 Characterization and Structural Properties of ZIF-67

Zeolitic imidazolate framework 67 (ZIF-67) is considered the starting material in this study. Thus, its complete characterization was taken in account. In this section XRD, FTIR, FESEM, EDAX-dot mapping, TGA and BET characterizations for ZIF-67 will be explained.

The crystallite structure of ZIF-67 was analyzed by a wide-angle X-ray diffraction (XRD) in a range of $2\theta = 6\text{-}90^\circ$ as shown in Figure 4.1. The peaks of the synthesized ZIF-67 match well with the peaks of the simulated ZIF-67, which verifies the phase purity of the synthesized ZIF-67 (JCPDS No. 41-1487).

The pure phase ZIF-67 crystals showed a hierarchical structure with prominent reflections at 2θ=7.4°, 10.4°, 12.7˚, 14.8˚, 16.5˚, 18.0˚, 22.1˚, 24.5˚, 25.5˚, 26.7˚, 29.5˚, 30.6˚, 31.6˚ and 32.5˚ corresponding to (0 1 1), (0 0 2), (1 1 2), (0 2 2), (0 1 3), (2 2 2), (1 1 4), (2 3 3), (2 2 4), (1 3 4), (0 4 4), (3 3 4), (2 4 4) and (2 3 5) planes of ZIF- 67 single crystal.

FTIR analysis was applied for structure verification too as shown in Figure 4.1b. The characterization peaks at 697 and 760 cm-1 could be attributed to the out-of-plane bending of the imidazole ring, while the peaks between 600 and 1500 cm-1 could be assigned to in-plane bending. The apparent peaks in a range of 1350−1500 cm-1 were ascribed to the ring stretching, whereas the band at 1589 cm-1 could be addressed to the stretching mode of C=N bonds.

The peaks around 1580 and 1663 cm-1 have been related to the stretching and bending N−H vibrations in 2- MIM, respectively.

Additionally, two peaks at 2930 and 3140 cm-1 were assigned to the C−H bonds of aliphatic chain and the aromatic ring of the imidazole, respectively. The broad peaks that appeared at 3200−3700 cm-1 was indicative to the presence of bonded water in the samples.

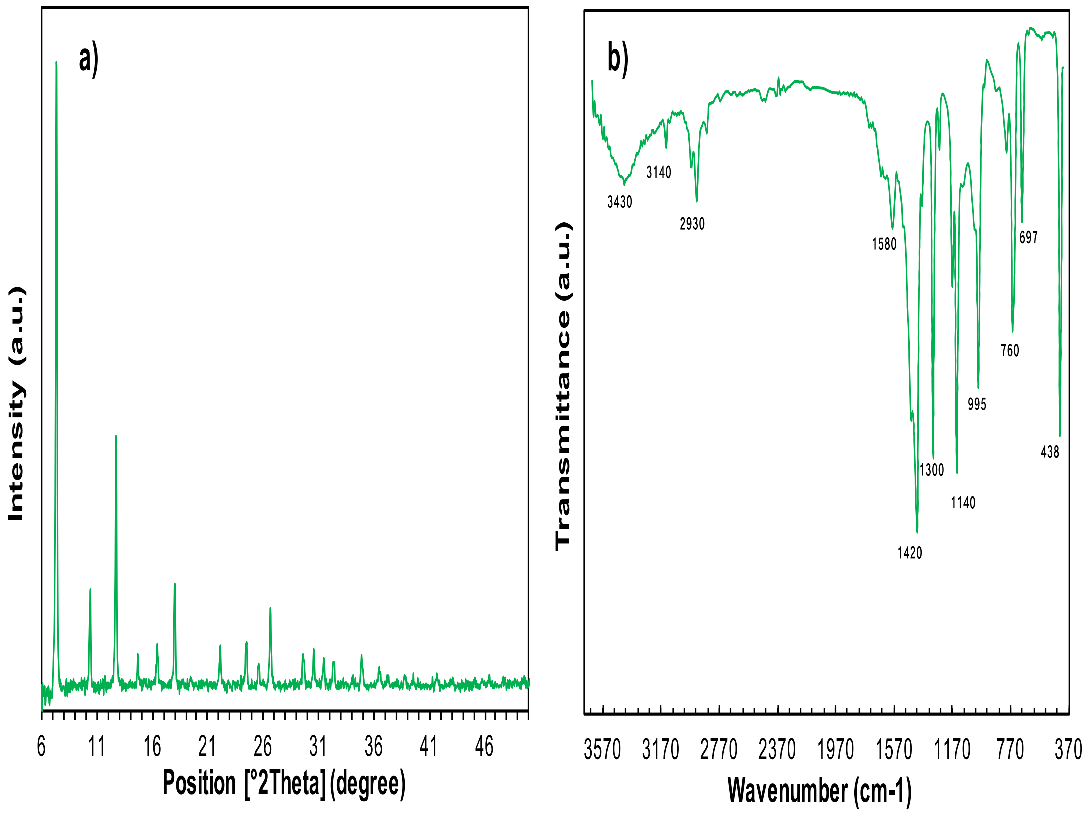

Figure 4.1: Textural characterization of ZIF-67: a) XRD, b) FTIR.

The N_2 adsorption-desorption isotherms of the pure ZIF-67 was Type-I suggesting the presence of permanent microporosity as seen in Figure 4.2. The BET surface area and total pore volume of the pure ZIF-67 were calculated as 1824 m^2/g and 0.6 cm^3/g, respectively which corresponds to the characteristic of a MOF structure with a large surface area. Finally, the average pore size of ZIF-67 was calculated as 1.36 nm.

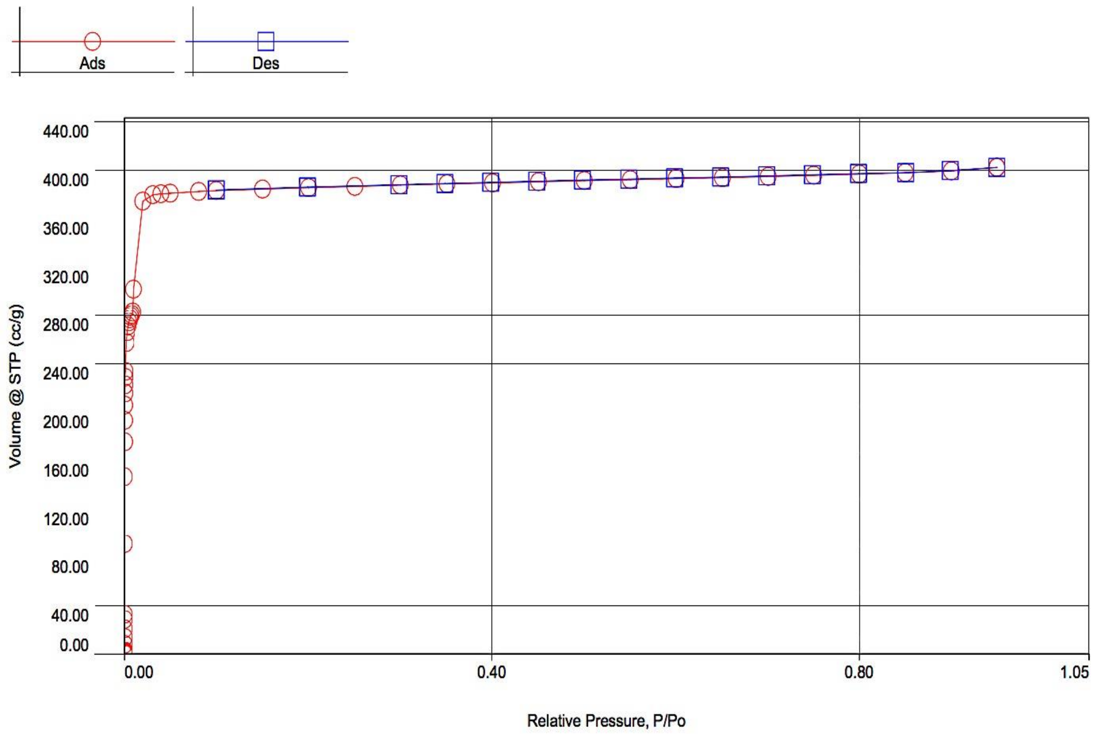

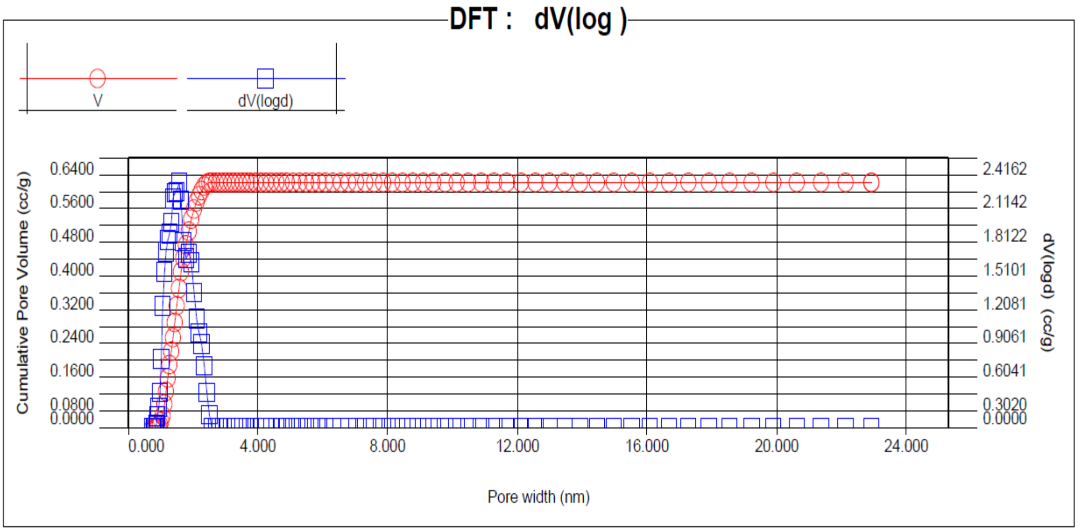

Figure 4.2: N_2 adsorption-desorption isotherms of the pure ZIF-67 with BJH pore size distribution.

The FESEM was applied to determine the morphology and the structure of the as-synthesized ZIF-67. As shown in the images of Figure 4.3, ZIF-67 crystals presented as polyhedrons with good facets, smooth surfaces, straight edges and symmetrical structures, with an average size of 500 nm.

The EDAX elemental map displayed the even distribution of C, N, Co and O in ZIF-67 which further confirmed the prior results. Based on EDAX analysis, C, N and Co in ZIF-67 were in atomic ratios of 63.52, 11.91 and 0.39%, respectively.

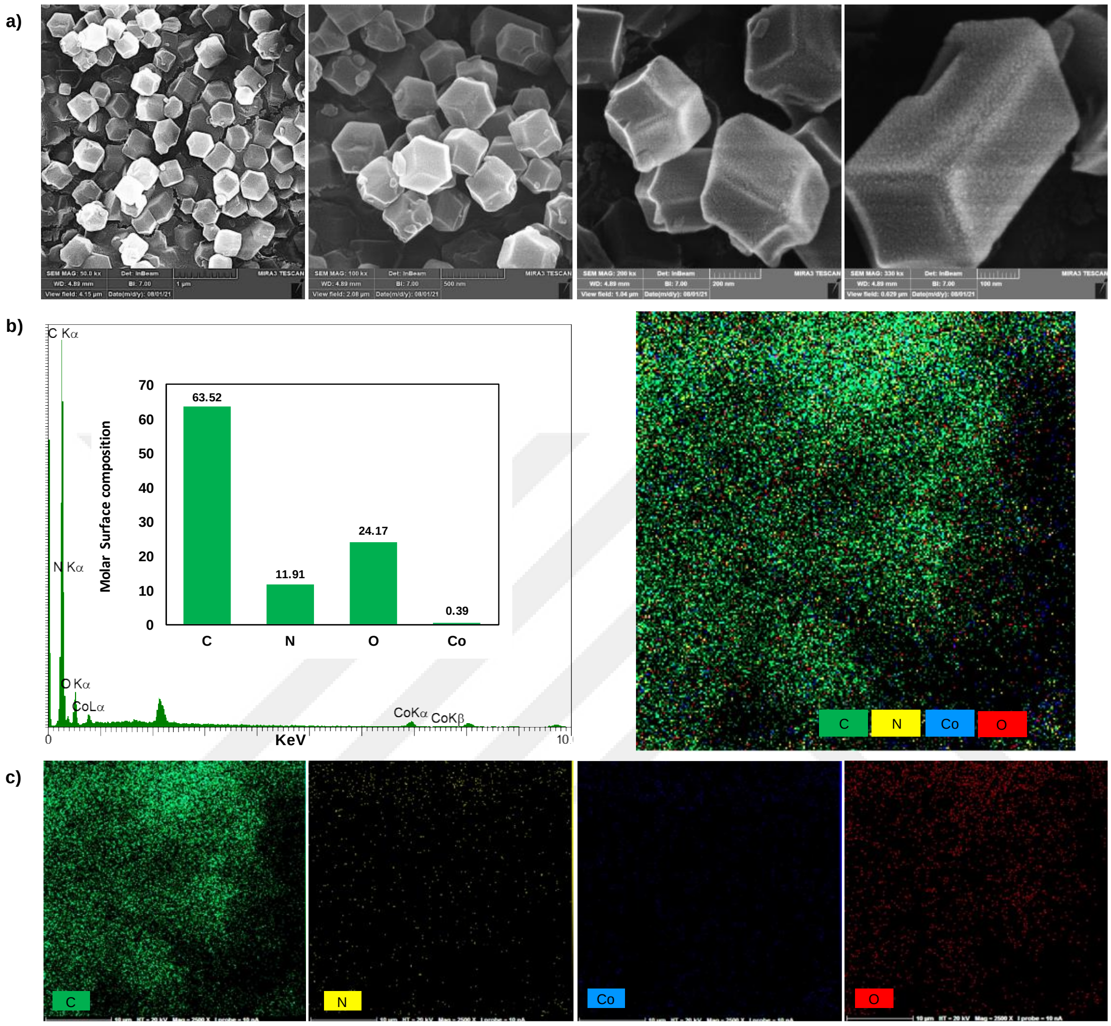

Figure 4.3: Morphological characterization of ZIF-67: a) FESEM and b) EDAX c) dot mapping images.

TGA analysis of the ZIF-67 has been shown in Figure 4.4 which was carried out either under Ar and N_2 atmospheres. A major weight loss of 75.22% have been occurred up to 700 °C under argon atmosphere owing to the structural collapse and decomposition of the organic compounds. The weight loss of ZIF-67 structure has been started from 400 °C and completed towards 680 °C. When N_2 atmosphere was applied as the carrier gas, the temperature range of weight loss was from 280 to 450 °C with a total weight loss of 73.22 %. It was seen that different decomposition profiles has been obtained under changing inert gas atmospheres.

As a plausible explanation, the shift in decomposition temperature might come from their different heat conductivity values and molecular sizes which may lead different temperature gradients in the sample.

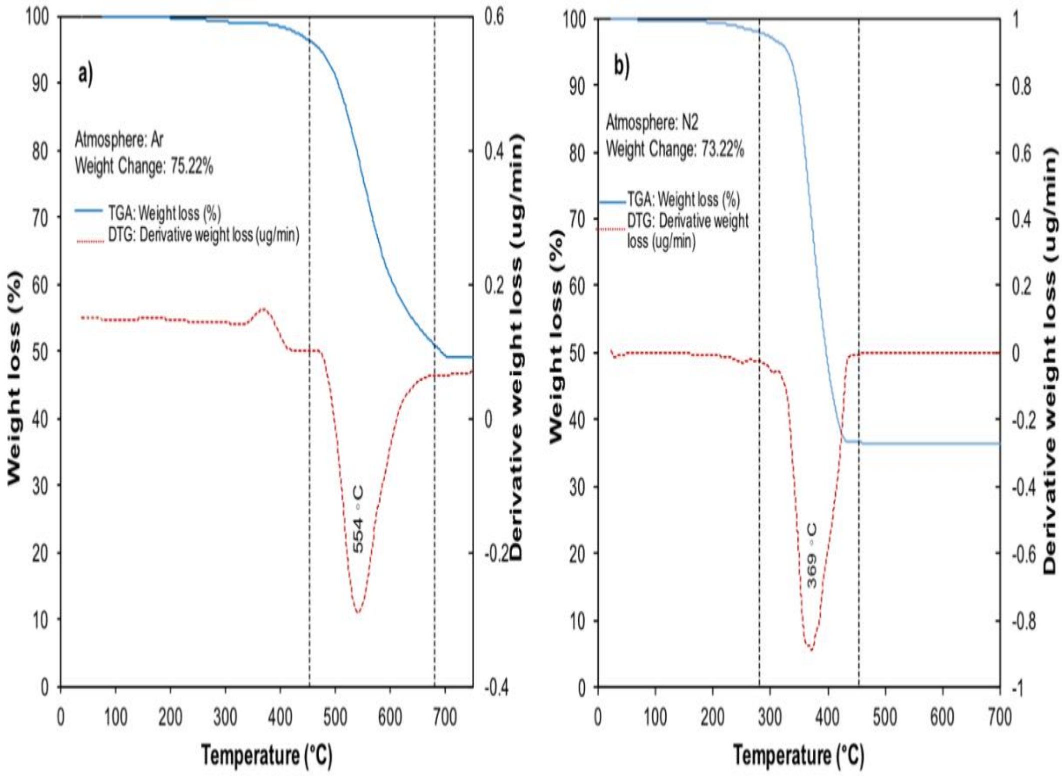

Figure 4.4: TGA analysis of ZIF-67 under: a) Ar and b) N_2 atmosphere.

4.2 Characterizations of Pyrolyzed and Calcined Catalyst Samples

As synthesized ZIF-67 has been pyrolyzed in an electrical tube furnace under N_2 atmosphere in a range of 400-900 °C. In this section, all 12 samples were divided in to 2 groups.

In group 1, low pyrolysis temperature (400, 500, 600 °C) alongside with plasma treatment was taken into account. Table 4.1 has shown the catalysts nomenclatures group 1 with low pyrolysis temperature. In the second group of the samples, high pyrolysis temperature being 700, 800 and 900 °C was selected to synthesize. Table 4.2 illustrates the catalysts nomenclatures group 2 with high pyrolysis temperature. In the following sections, various implemented characterization was done for each of these mentioned groups.

Table 4.1. Catalysts nomenclatures group 1 (Low Temperature Pyrolysis).

Sample	Pyrolysis Temperature	Plasma Treatment
CoZ@400	400 °C	--
P_CoZ@400	400 °C	√
CoZ@500	500 °C	--
P_CoZ@500	500 °C	√
CoZ@600	600 °C	--
P_CoZ@600	600 °C	√

Table 4.2. Catalysts nomenclatures group 2 (High Temperature Pyrolysis).

Sample	Pyrolysis Temperature	Plasma Treatment
CoZ@700	700 °C	--
P_CoZ@700	700 °C	√
CoZ@800	800 °C	--
P_CoZ@800	800 °C	√
CoZ@900	900 °C	--
P_CoZ@900	900 °C	√

4.2.1 XRD analysis

Figure 4.5 shows the XRD patterns of catalysts in group 1: (a) CoZ@400, (b) P_CoZ@400, (c) CoZ@500, (d) P_CoZ@500 (e) CoZ@600 and (f) P_CoZ@600 in $2\boldsymbol{\theta}$ range of 10-85 ˚. The crystal structure and phase purity of the catalysts in Group I were investigated by using XRD. The diffraction peaks at 19˚, 31.3˚, 37.1˚, 44.8˚, 55.65˚, 59.4˚, 65.2˚, 77.34˚ can be perfectly indexed to Co_3O_4 (111), (220), (311), (400), (442), (511), (440), (533) planes (JCPDS: 42-1467). For all six samples, no diffraction peaks related to CoO and other impurity phases have been observed, indicating the complete transformation of the ZIF-67 precursor into pure Co_3O_4 phase.

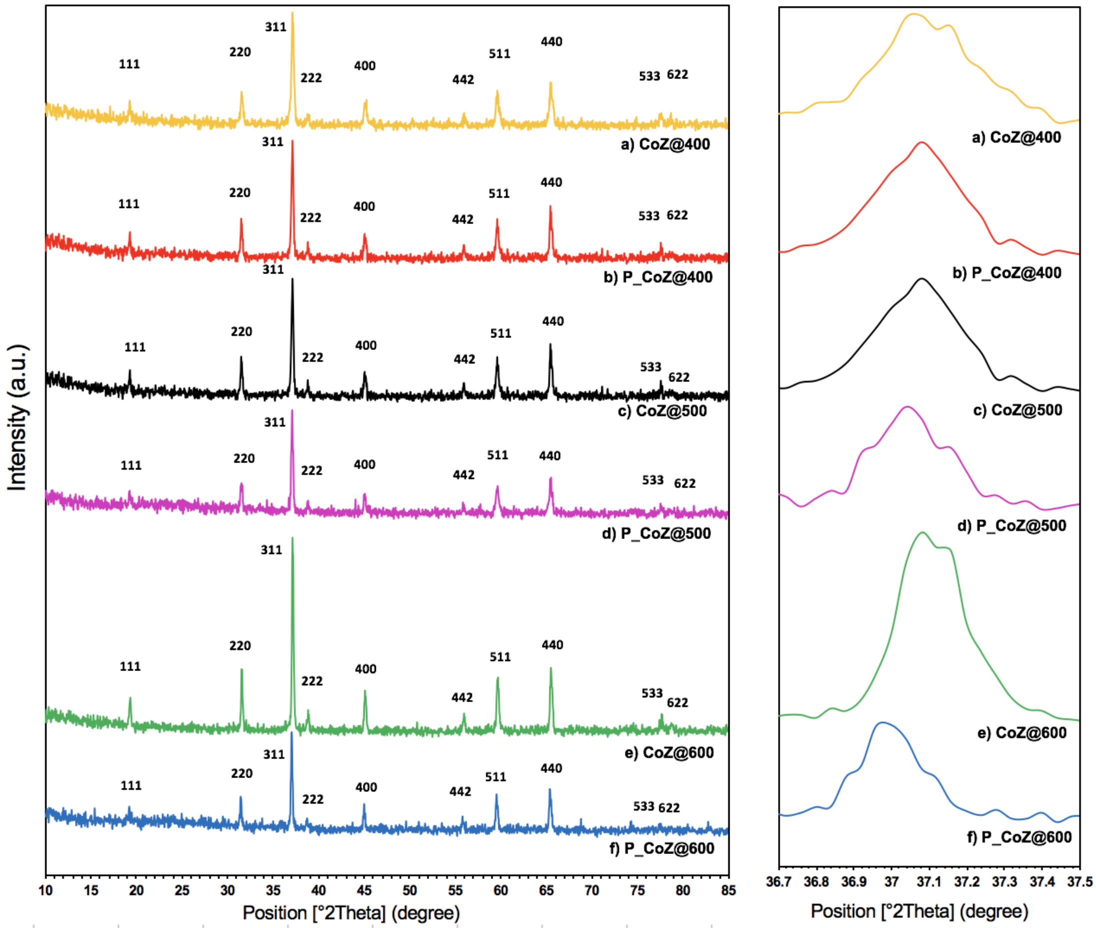

Figure 4.5: XRD patterns of catalysts: (a) CoZ@400, (b) P_CoZ@400, (c) CoZ@500, (d) P_CoZ@500 (e) CoZ@600 and (f) P_CoZ@600.

By comparing the XRD results of a) CoZ@400 c) CoZ@500 and e) CoZ@600, it can be implied that the intensity of the major Co_3O_4 peaks have been increased by increasing the carbonization temperature indicating Co_3O_4 crystallinity rise for CoZ@600. Table 4.3 gave the crystallite size of the catalysts by referencing the major plane of Co_3O_4 ($2\boldsymbol{\theta}$ =37˚). The crystallite size was estimated from the X-ray line broadening of the diffraction peaks using the Debye Scherrer equation "$D = 0.9\lambda/(\beta\cos\theta)$", where λ is the wavelength of Cu Kα radiation, β is the corrected full-width at half-maximum (FWHM) of the diffraction peak and θ is the Bragg angle. The crystallite sizes of the Co_3O_4 phase calculated based on the FWHM of the diffraction peaks were in the range of 31 to 46 nm for all as-synthesized samples representing their nano-structure nature. The effect of plasma treatment on the crystallite structure has been evaluated by comparing two respective samples, plasma and non-plasma treated ones at the same pyrolysis temperature, e.g., CoZ@400 and P_CoZ@400.

Upon plasma treatment, the XRD patterns of the samples remain the same with those of the non-plasma treated samples. However, intensity reduction and peak broadening have been noticed for plasma treated samples, possibly owing to loss of long-range order and/or missing-linker defects formation. This may also be due to improved dispersion of cobalt oxide in carbon matrix. For pyrolysis temperature of 600°C, observed reduction in peak intensity was much more remarkable on plasma treated sample. XRD peaks have been shifted to the left upon plasma treatment. To show this shift precisely, the peak at the 311 plane has been given in Figure 4.6. According to Bragg's law ($n\lambda=2d\sin\theta$), peak shifting to smaller angles indicates the expanded space distance (d). This might occur due to the oxygen vacancies (OVs), in other words, more Co^{3+} formation with the larger ion radius compared to Co^{2+} as well as wider van der Waals gap.

Table 4.3. Crystallite size of the catalysts group 1.

Sample	2Θ (Deg)	FWHM	Crystallite Size (nm)
CoZ@400	37.08	0.3	31.02
P_CoZ@400	36.92	0.24	38.76
CoZ@500	37.08	0.2	46.53
P_CoZ@500	37.04	0.24	38.77
CoZ@600	37.08	0.2	46.53

Figure 4.6 shows the XRD patterns of catalysts in group 2: (a) CoZ@700, (b) P_CoZ@700, (c) CoZ@800, (d) P_CoZ@800 (e) CoZ@900 and (f) P_CoZ@900 in $2\boldsymbol{\theta}$ range of 10-85 ˚. The diffraction peaks at 19˚, 31.3˚, 37.1˚, 44.8˚, 55.65˚, 59.4˚, 65.2˚, 77.34˚ have been perfectly indexed to Co3O4 (111), (220), (311), (400), (442), (511), (440), (533) planes (JCPDS: 42-1467). For all six samples, no diffraction peaks related to CoO and other impurity phases were observed, indicating the complete decomposition of ZIF-67 precursor into pure Co_3O_4 phase for the carbonization temperature of 700-900 °C. All six samples prepared with various pyrolysis temperatures and plasma treatment have been seen to be composed of pure crystalline Co_3O_4 phase.

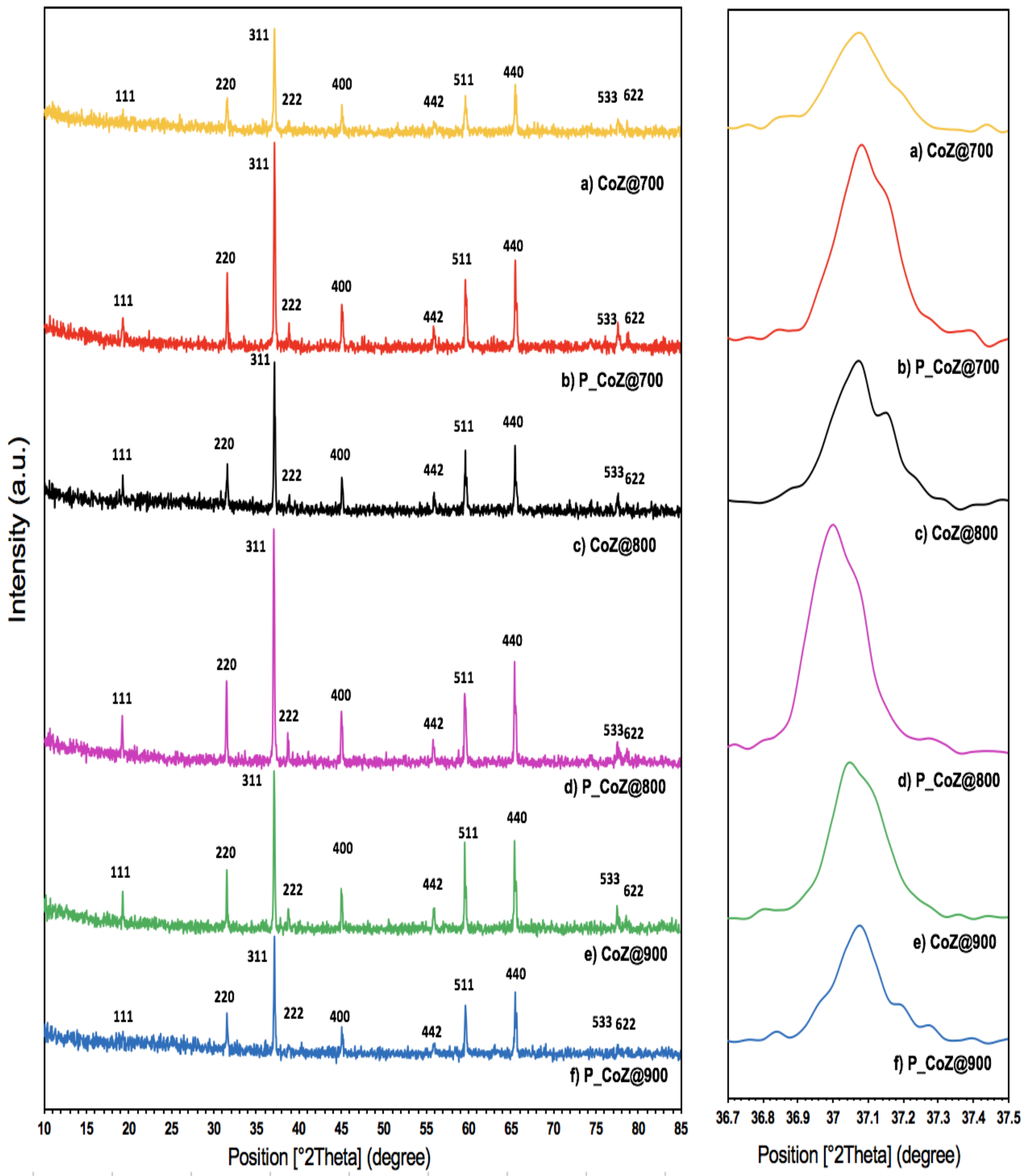

Figure 4.6: XRD patterns of catalysts: (a) CoZ@700, (b) P_CoZ@700, (c) CoZ@800, (d) P_CoZ@800 (e) CoZ@900 and (f) P_CoZ@900.

The calculated crystallite size of the catalysts in group 2 have been given in Table 4.4. The calculated crystallite sizes for the catalysts by Scherrer equation has shown their nano-structures. By comparing the XRD patterns of (a) CoZ@700, (c) CoZ@800, and (e) CoZ@900, it can be seen that by increasing the carbonization temperature the intensity of major peaks of Co_3O_4 have been increased. On the other hand, application of plasma treatment led to crystallinity increase at carbonization temperature of 700 and 800 °C but without no change for 900 °C.

Table 4.4. Crystallite size of the catalysts group 2.

Sample	2Θ (Deg)	FWHM	Crystallite Size (nm)
CoZ@700	37.08	0.2	46.53
P_CoZ@700	37.08	0.2	46.2
CoZ@800	37.08	0.2	46.53
P_CoZ@800	37	0.2	46.5
CoZ@900	37.08	0.16	58.16
P_CoZ@900	37.08	0.16	58.1

4.2.2 FTIR analysis

Figure 4.7 shows the FTIR transmittance spectrum of Co_3O_4 recorded at room temperature, in the frequency range of 400–4000 cm^{-1}: (a) CoZ@400, (b) P_CoZ@400, (c) CoZ@500, (d) P_CoZ@500 (e) CoZ@600 and (f) P_CoZ@600. The functional groups present in the material could be identified using FTIR characterization method. Two characteristic bands of the spinel-type Co_3O_4 structure at 676 (v_1) and 570 (v_2) cm^{-1} have been observed. The v_1 band was characteristic of Co^{3+}–O vibration in an octahedral site, and the v_2 band was for the Co^{2+}–O vibration in a tetrahedral site of the Co_3O_4 lattice.

FTIR results were in good agreement with the obtained XRD results in the previous section showing the pure phase of Co_3O_4. Pyrolysis temperature did not have any noticeable effect on the peak positions in the FTIR spectra. Only slight changes can be observed in the peaks at wavenumbers 1650 and 3450 cm^{-1} related to the adsorbed water and structural OH groups, respectively. Plasma treatment seemed to cause an increase in the intensity of the peak related to Co^{3+}–O and decreases the intensity of the peak Co^{2+}–O. Additionally, the observed weak peaks at 2920 and 2880 cm^{-1} can be assigned to the C−H bonds of aliphatic chain remained from organic linker of the pristine MOF. This confirmed the formation of carbon matrix upon pyrolysis.

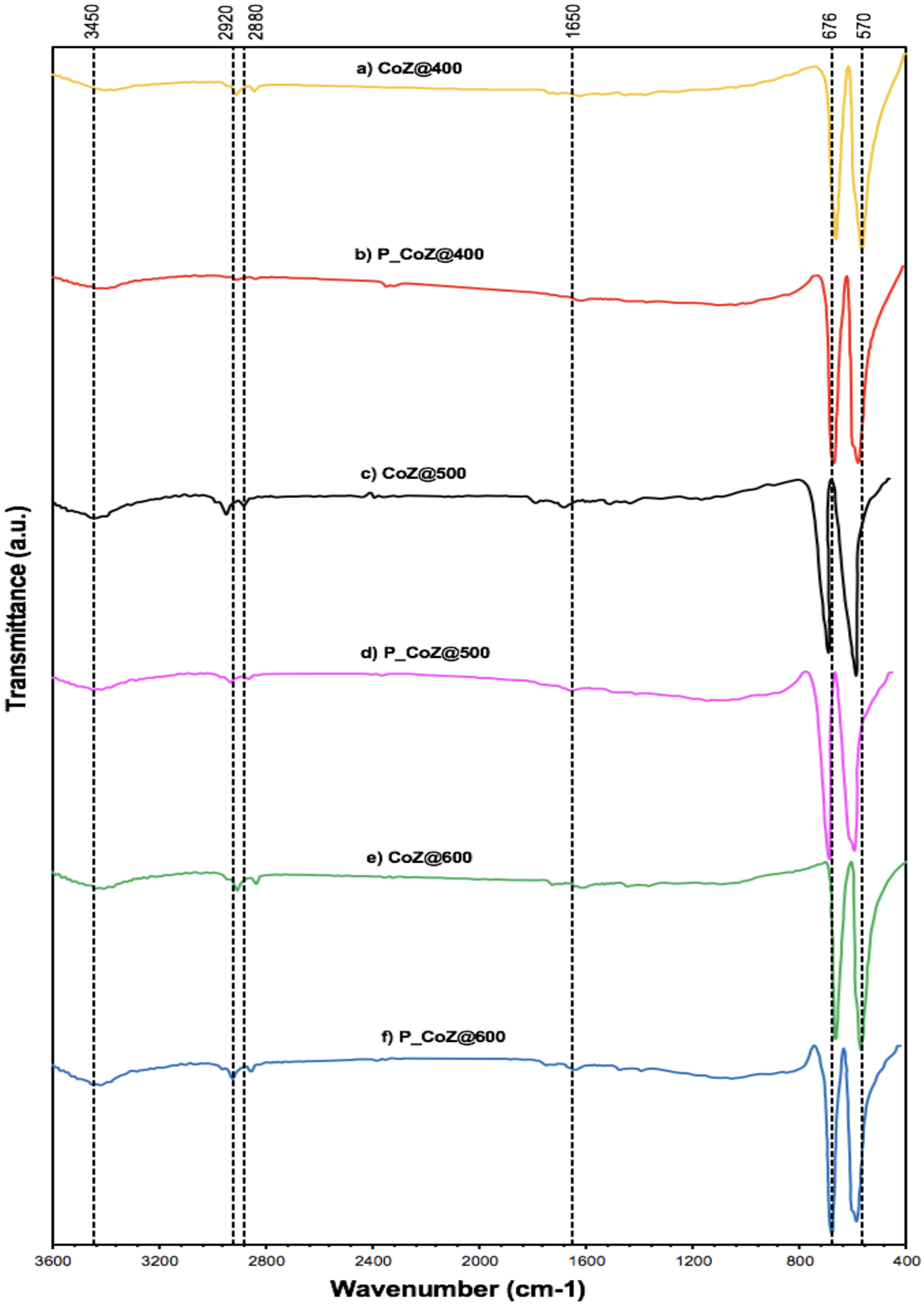

Figure 4.7: FTIR spectra of: (a) CoZ@400, (b) P_CoZ@400, (c) CoZ@500, (d) P_CoZ@500 (e) CoZ@600 and (f) P_CoZ@600.

Figure 4.8 has shown the FTIR transmittance spectrum of Co_3O_4 recorded at room temperature, in the frequency range of 400–4000 cm^{-1}: (a) CoZ@700, (b) P_CoZ@700, (c) CoZ@800, (d) P_CoZ@800 (e) CoZ@900 and (f) P_CoZ@900. For the second group of the catalysts pyrolyzed at high temperatures, similar FT-IR spectra have been recorded. Importantly, the two characteristic bands of the spinel-type Co_3O_4

structure at 676 (v_1) and 570 (v_2) cm^{-1} have been observed as well for the second group of the catalysts pyrolyzed at high temperatures. These two bands at 676 cm^{-1} and 570 cm^{-1} were attributed to Co^{3+}–O vibration in an octahedral site and Co^{2+}–O vibration in a tetrahedral site of the Co_3O_4 lattice, respectively (Makhlouf et al., 2013). While pyrolysis temperature did not have any remarkable effect on FT-IR peaks, plasma treatment might increase in peak intensities related to octahedral coordinated Co^{3+}–O and might decrease in peak intensities of the tetrahedrally coordinated Co^{2+}–O that all can be related with the structural changes by plasma treatment (Wang et al., 2010).

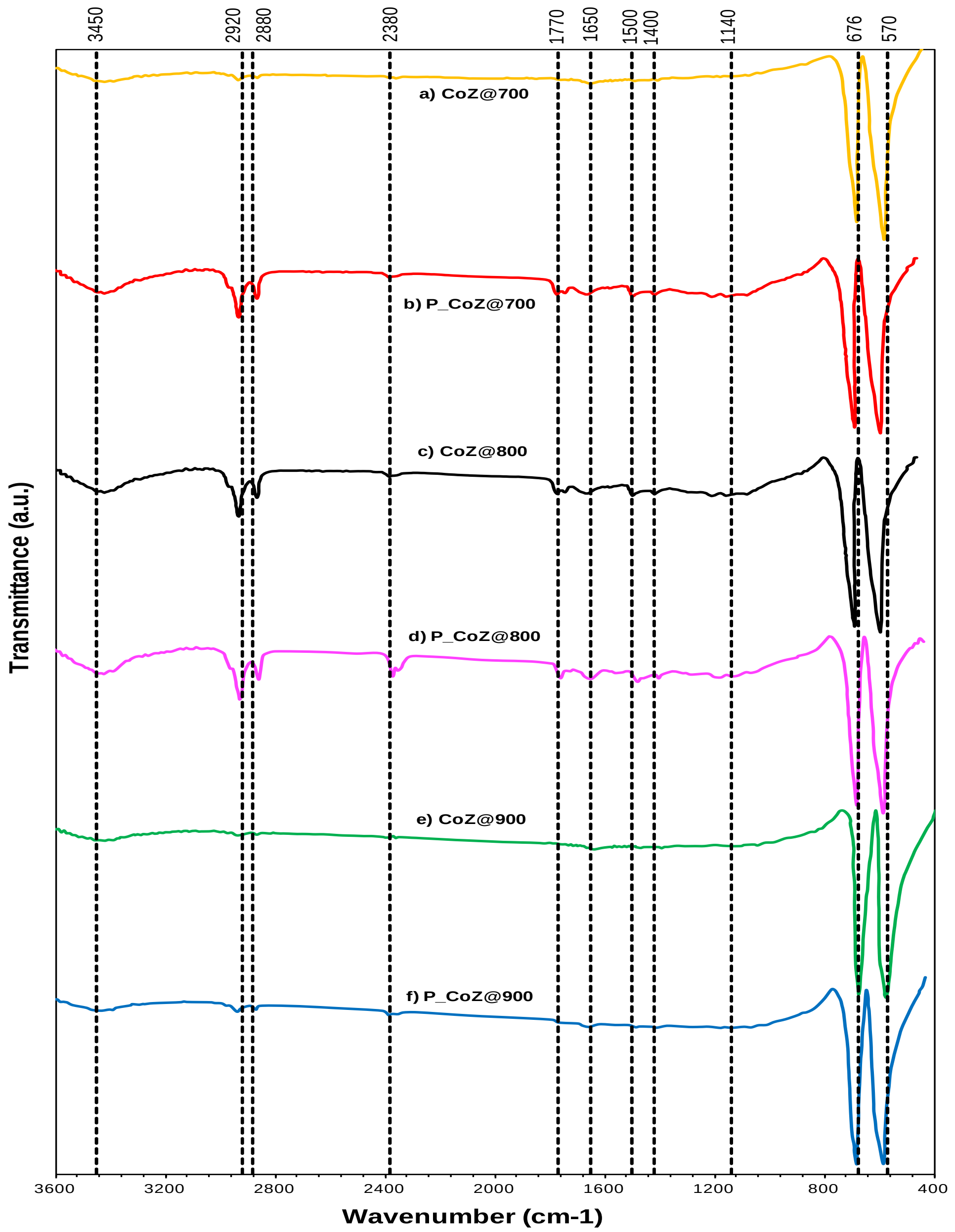

Figure 4.8: FTIR spectra of: (a) CoZ@700, (b) P_CoZ@700, (c) CoZ@800, (d) P_CoZ@800 (e) CoZ@900 and (f) P_CoZ@9004.1.2.3 FESEM Analysis.

4.2.3 FESEM analysis

The morphology of the catalysts have been investigated by FESEM shown in Figures 4.9 and 4.10.

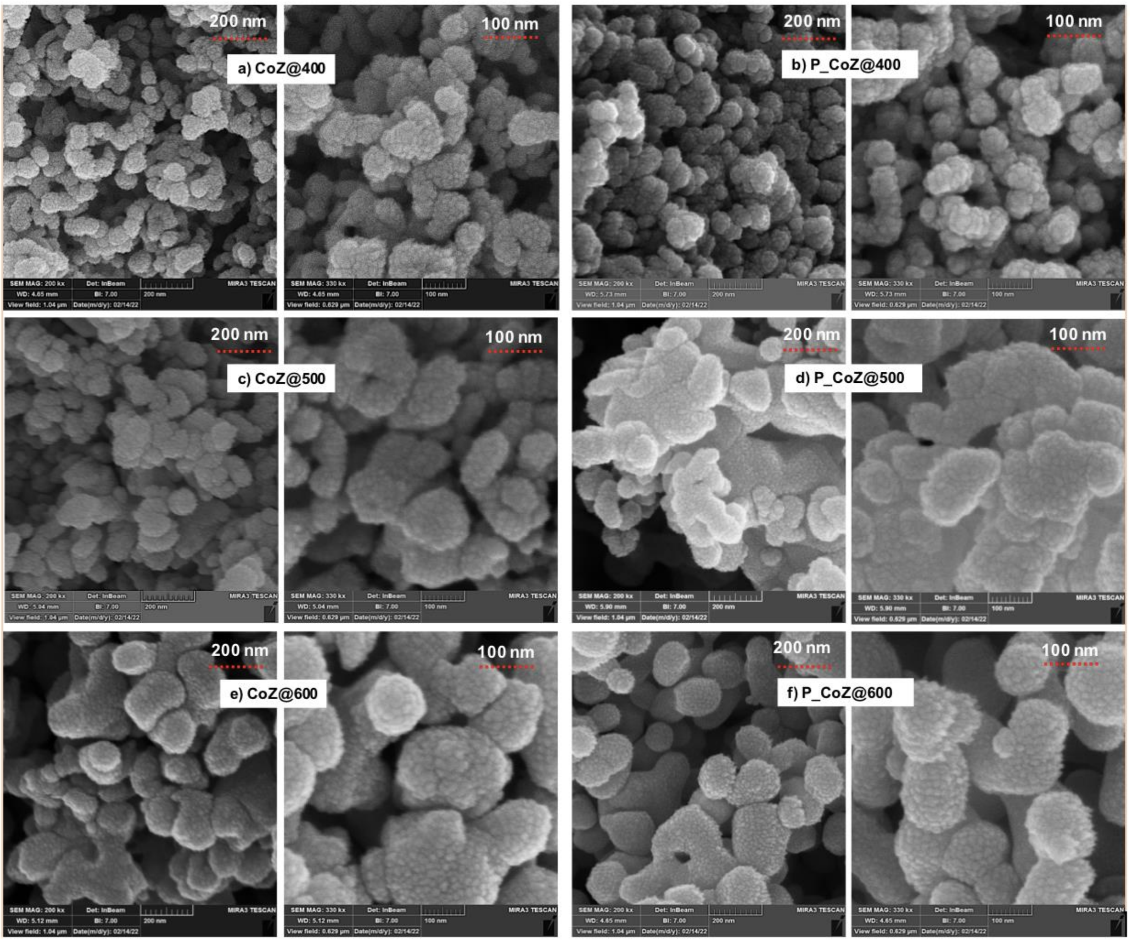

Figure 4.9: FESEM images of catalysts: (a) CoZ@400, (b) P_CoZ@400, (c) CoZ@500, (d) P_CoZ@500 (e) CoZ@600 (f) P_CoZ@600.

Two different magnifications (100 and 200 nm) have been selected to observe the morphology of the Co_3O_4 particles. From the FESEM images in Figure 4.9, it was seen that upon pyrolysis treatment, hexagonal shaped particles of ZIF-67 in the range of 500 nm have been changed into berry-like spherical clusters in size below 100 nm. These clusters have tended to agglomerate by increasing the pyrolysis temperature. For example, spherical clusters of CoZ@400 were in the range of 59-75 nm while the size of CoZ@600 clusters have varied in a wide range of 39-149 nm. When plasma treated sample morphologies were evaluated, it can be seen that the surface roughness of plasma-treated ones has become more visible than that of pristine cobalt oxide in non-plasma treated ones. The observed roughness was the indicative of sputtering the metal oxide atoms out of the surface and etching by the bombardment of energetic particles during plasma treatment. However, the spherical structures have been well preserved for both of them. Figure 4.10 shows the FESEM images of the catalysts in group 2 which were pyrolyzed at high temperatures. It was obvious that particles tend to continue to aggregate at high temperatures.

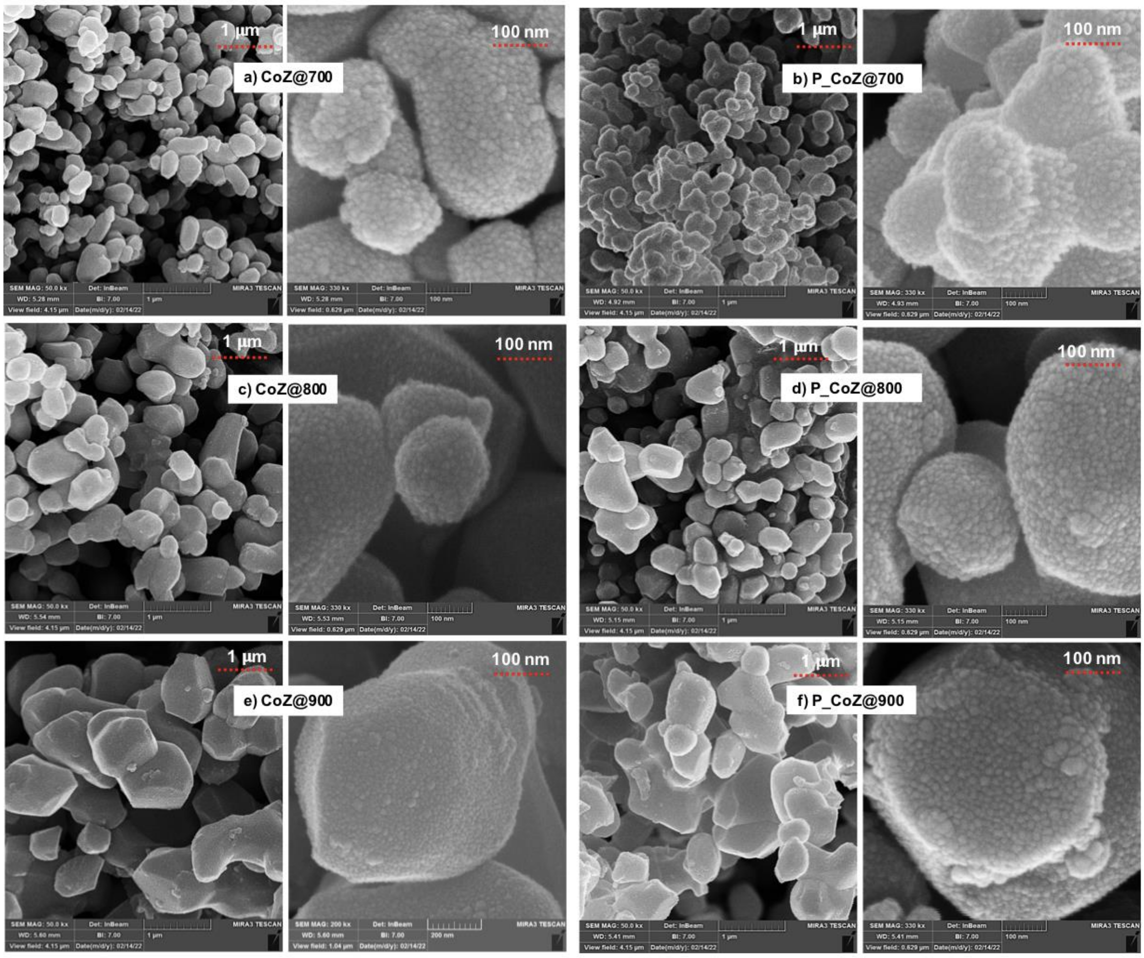

Figure 4.10: FESEM images of catalysts: (a) CoZ@700, (b) P_CoZ@700, (c) CoZ@800, (d) P_CoZ@800 (e) CoZ@900 and (f) P_CoZ@900.

4.2.4 N_2 Sorption measurements

Nitrogen adsorption/desorption isotherms were taken to calculate BET surface area, pore volume and average pore size of the catalysts. A sharp decrease in BET surface area and pore volume was observed in comparison with those of fresh ZIF-67. As seen from Figures 4.11, 4.12, 4.13, 4.14, 4.15, 4.16, 4.17, 4.18, 4.19, 4.20, 4.21 and 4.22, and given textural properties in Table 4.5 and 4.6, BET surface area and pore volume of fresh ZIF-67 were 1824 m^2/g and 0.6 cc/g while their pyrolyzed forms had BET surface areas and pore volumes around 10 to 40 m^2/g and 0.01 to 0.05 cc/g, respectively.

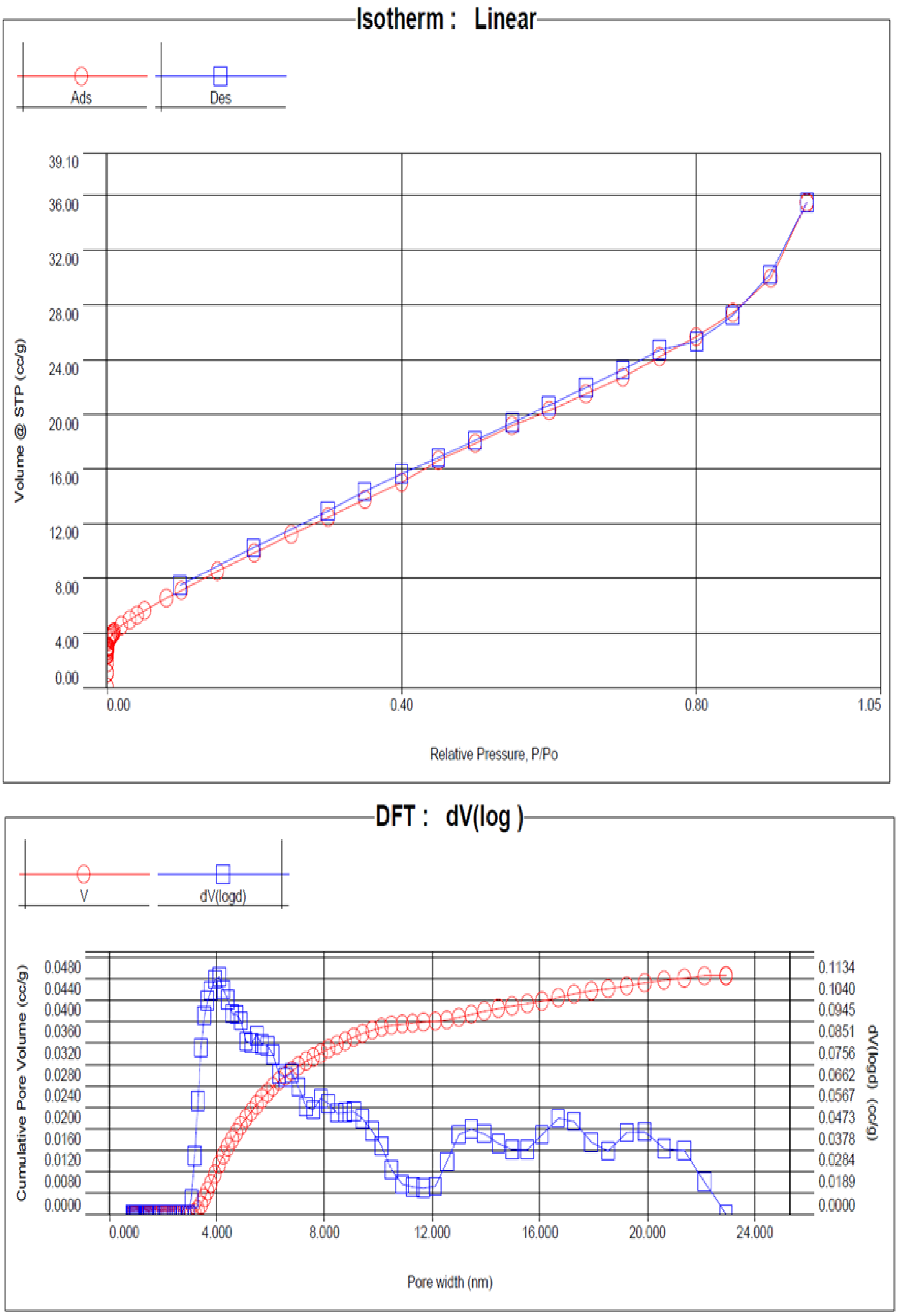

Figure 4.11: Adsorption/desorption isotherm and DFT pore volume vs pore width for the catalyst: CoZ@400.

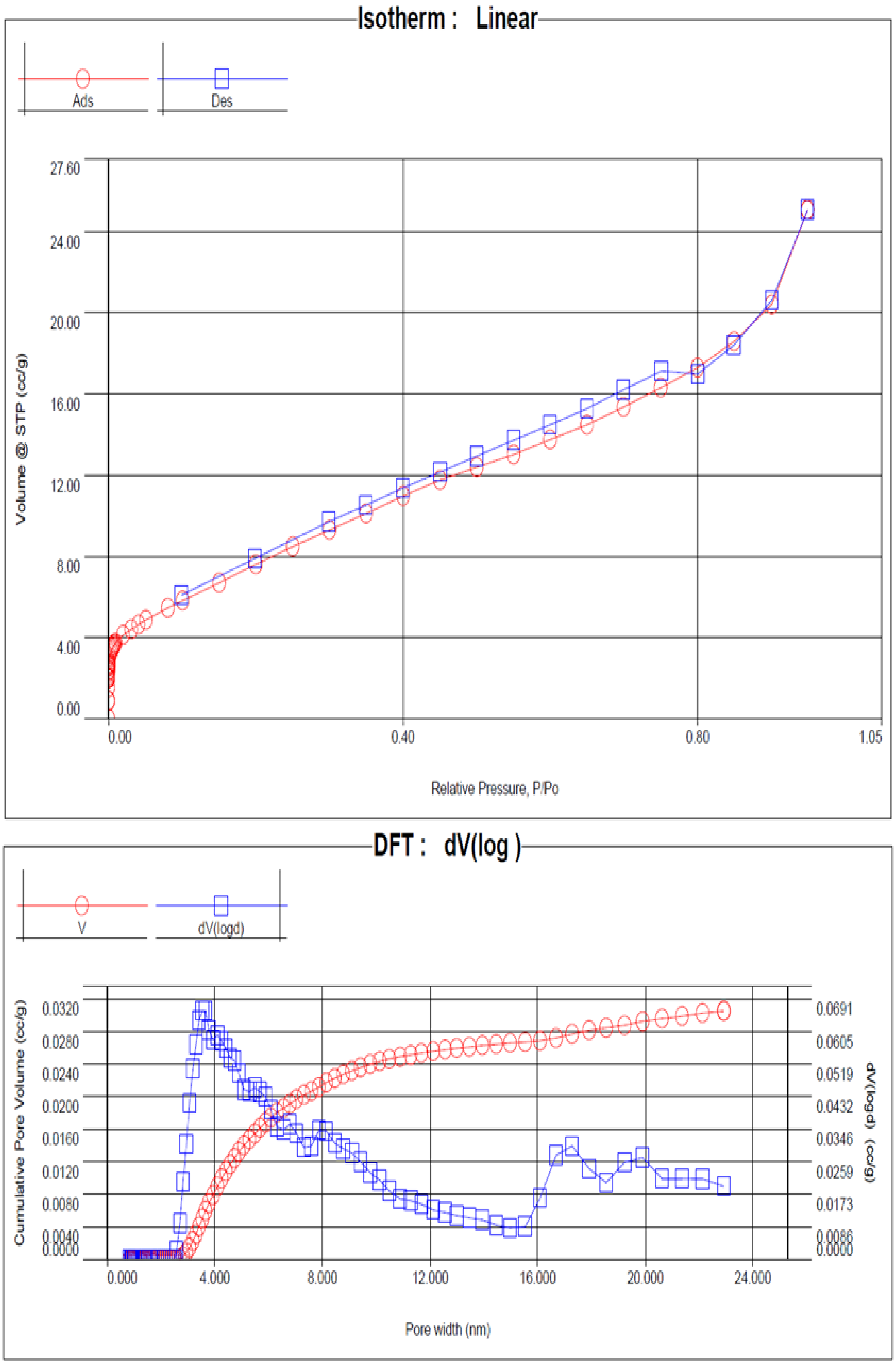

Figure 4.12: Adsorption/desorption isotherm and DFT pore volume vs pore width for the catalyst: P_CoZ@400.

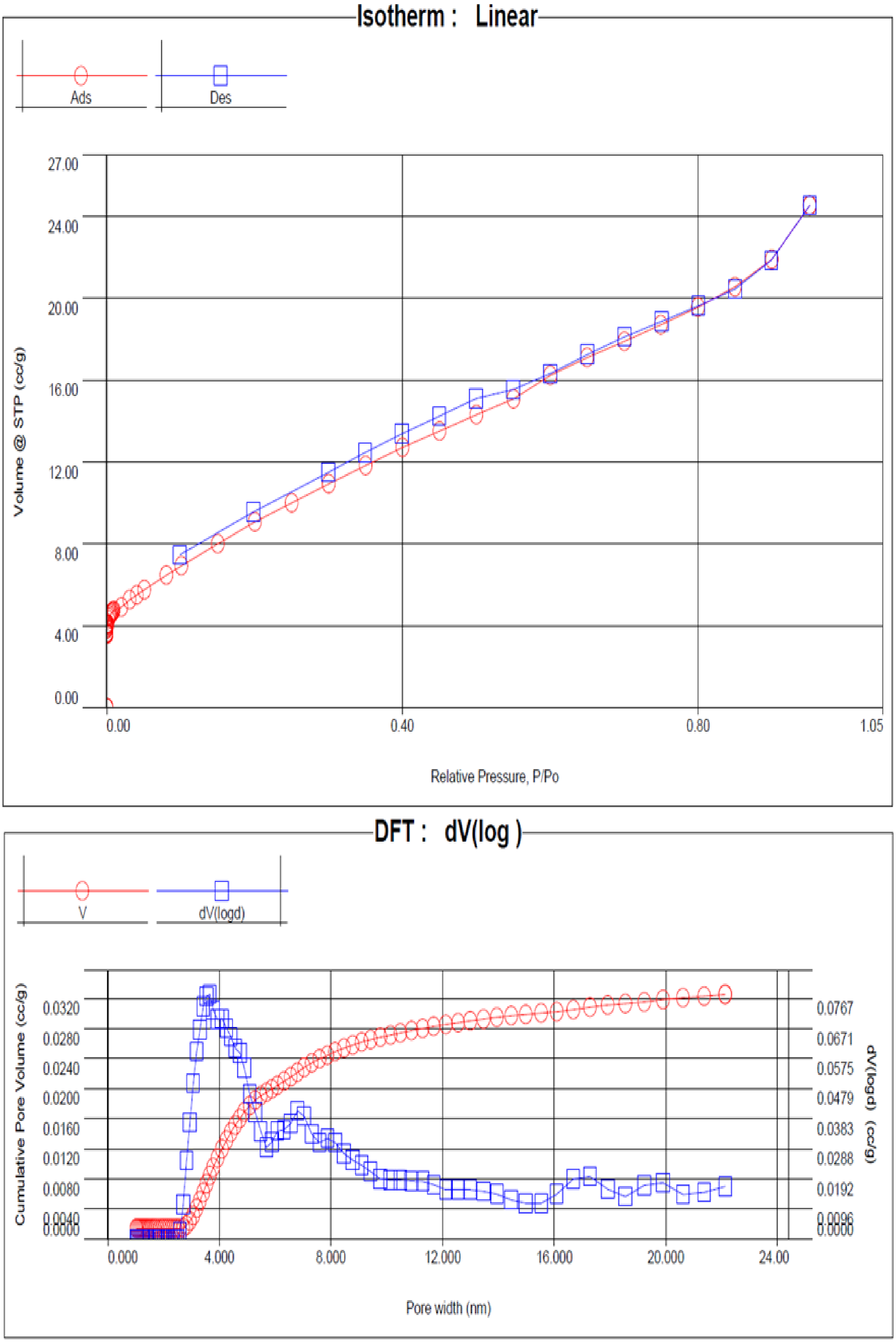

Figure 4.13: Adsorption/desorption isotherm and DFT pore volume vs pore width for the catalyst: CoZ@500.

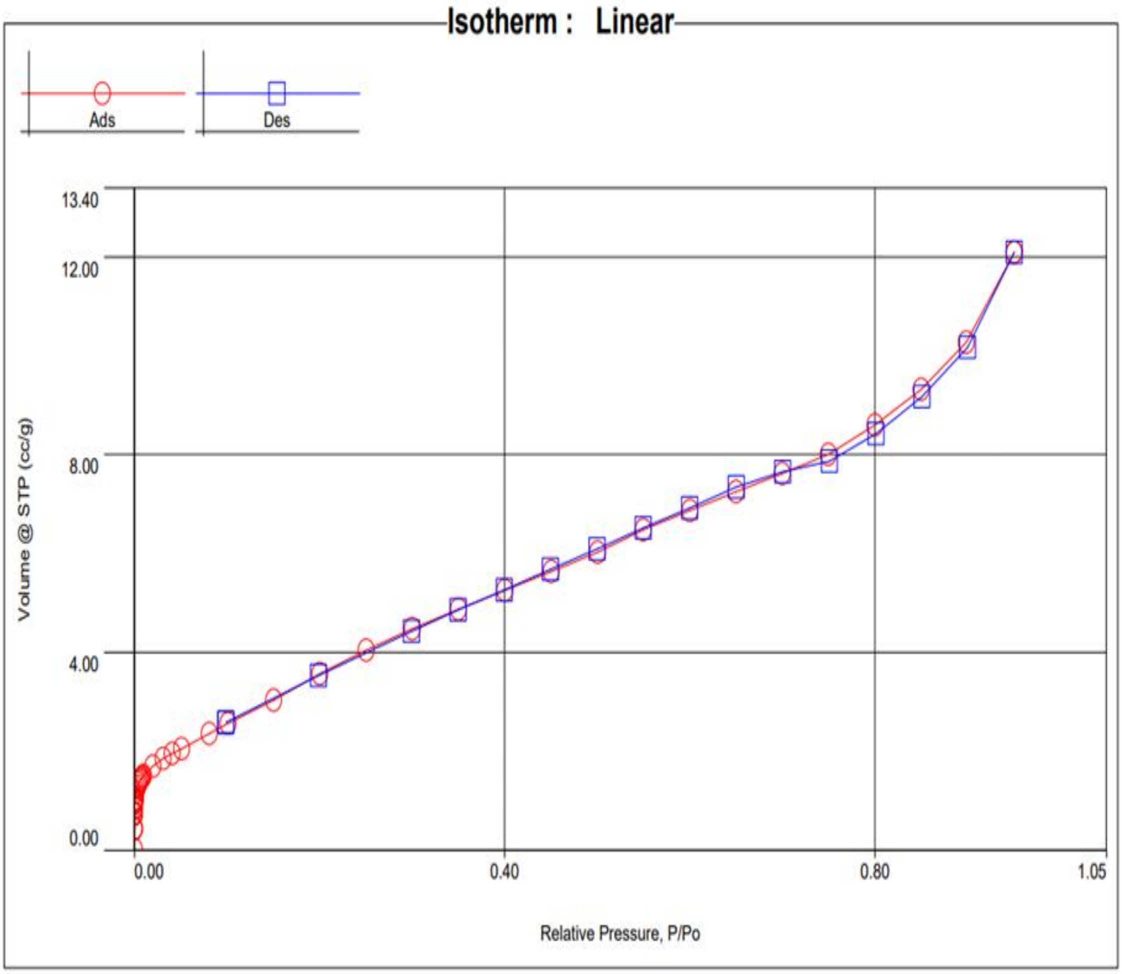

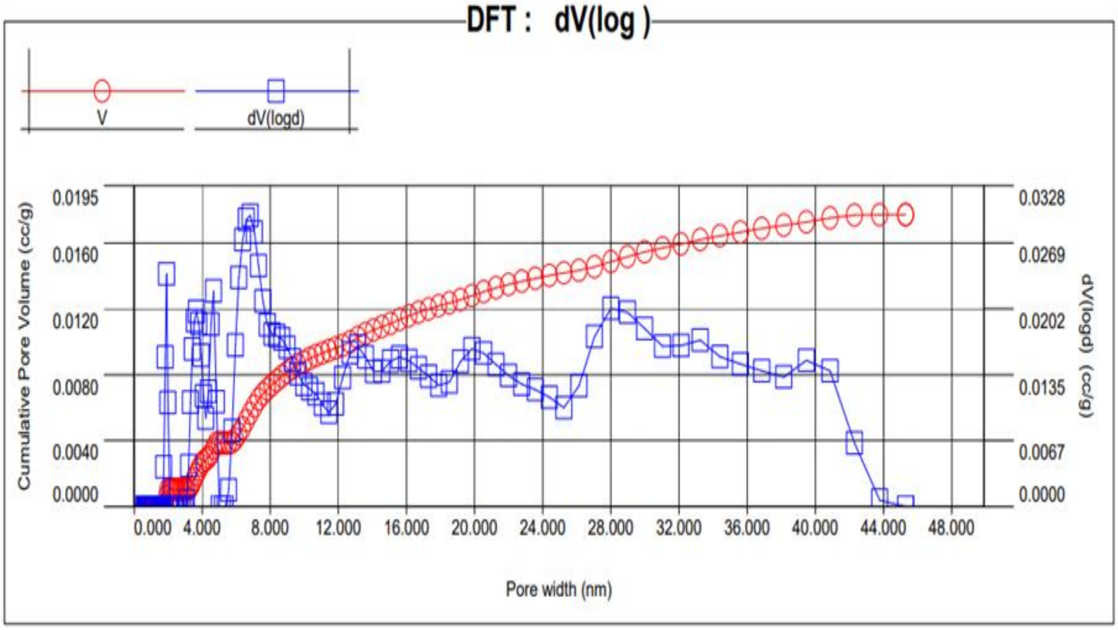

Figure 4.14: Adsorption/desorption isotherm and DFT pore volume vs pore width for the catalyst: P_CoZ@500.

It appeared that all catalyst samples lost their texture to a large extent due to the pyrolysis and calcination. Another points that should be remarked here that an increase in pore widths was noticeable. Mesopores seemed to be formed depending on the pyrolysis conditions over the Co/C catalysts. Such a sharp change in the textural properties indicated that the metal organic framework structure was lost by decomposition and/or calcination at their applied temperatures.

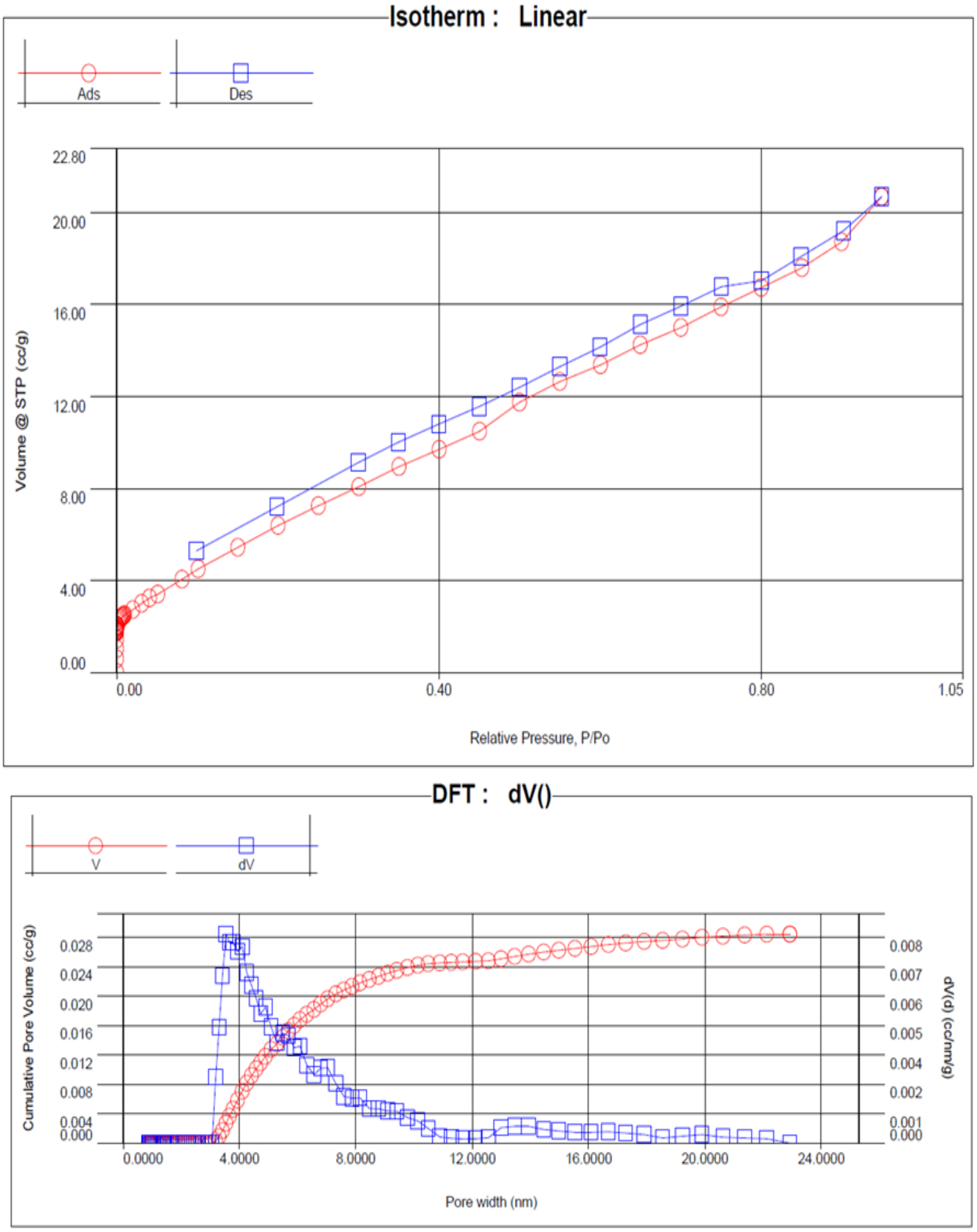

Figure 4.15: Adsorption/desorption isotherm and DFT pore volume vs pore width for the catalyst: CoZ@600.

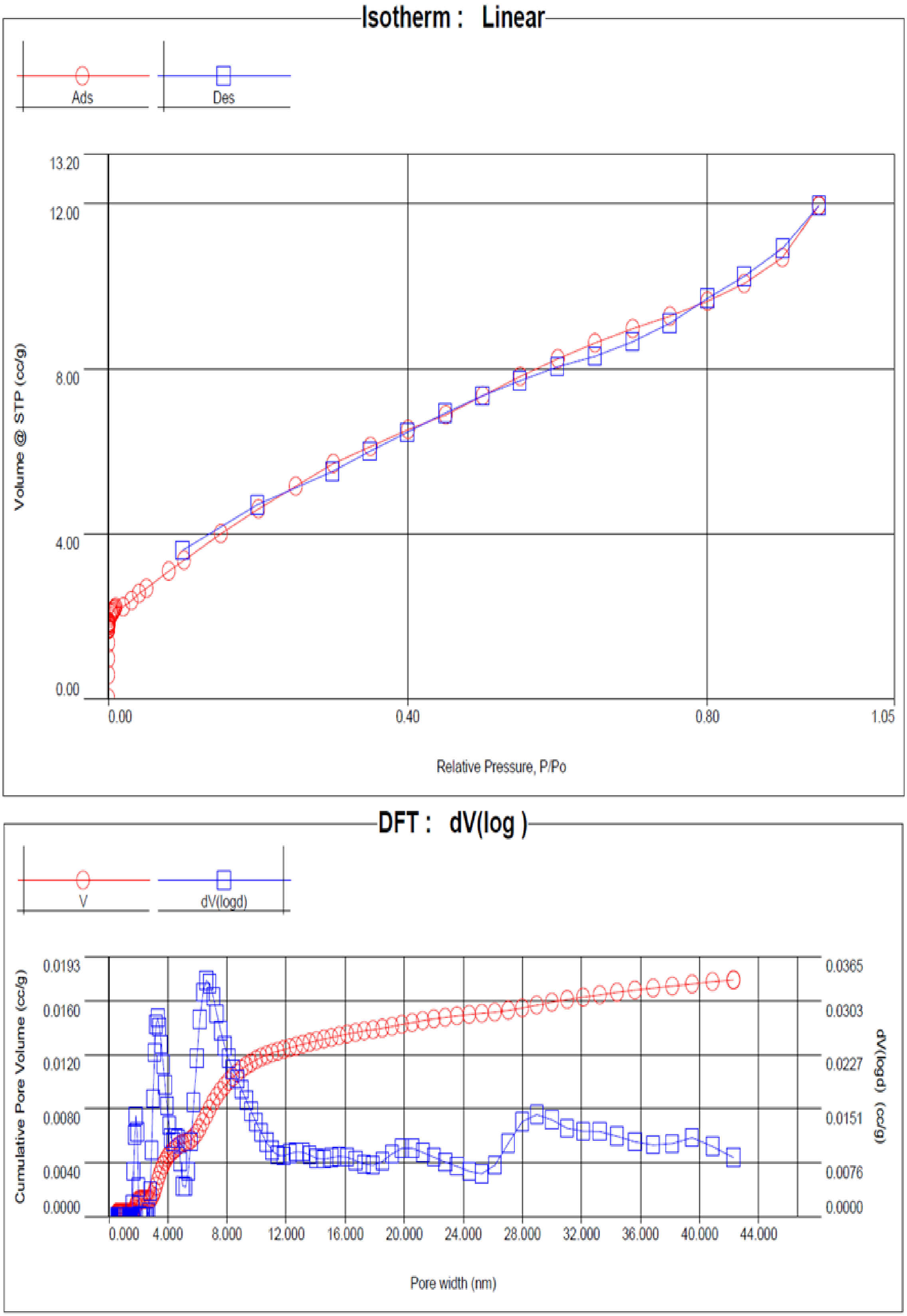

Figure 4.16: Adsorption/desorption isotherm and DFT pore volume vs pore width for the catalyst: CoZ@600.

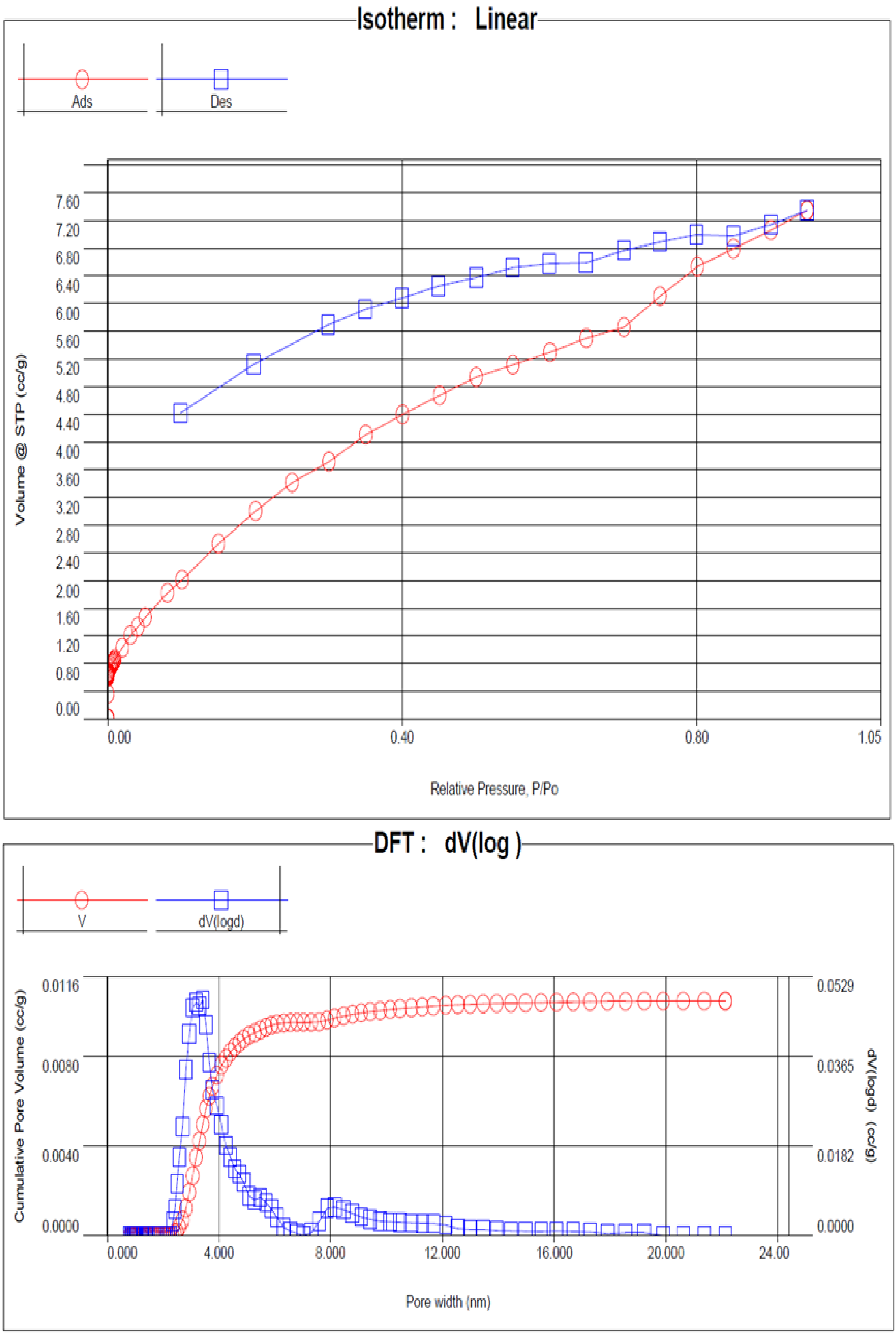

Figure 4.17: Adsorption/desorption isotherm and DFT pore volume vs pore width for the catalyst: CoZ@700.

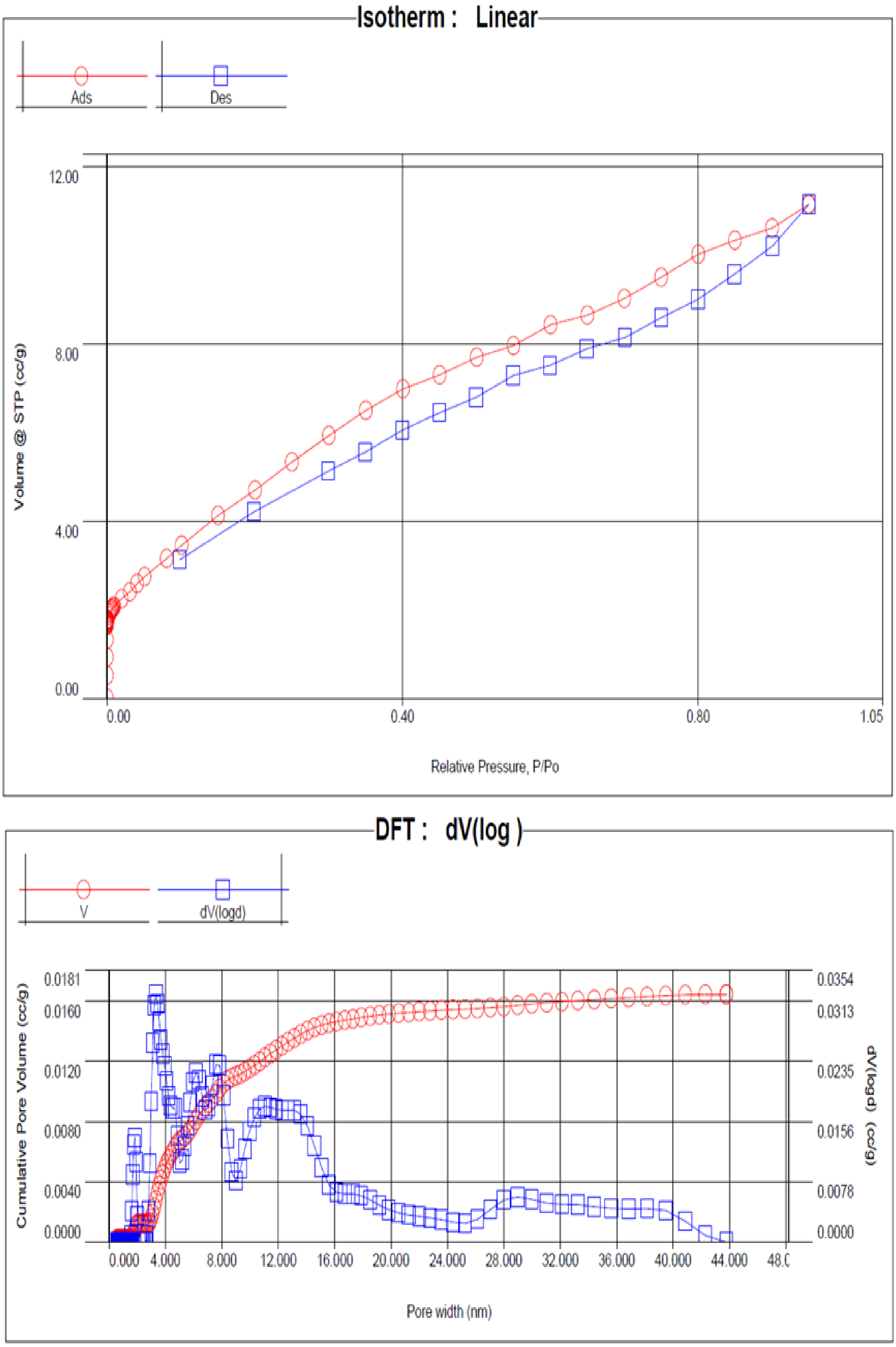

Figure 4.18: Adsorption/desorption isotherm and DFT pore volume vs pore width for the catalyst: CoZ@700.

And as we can see in the Figures 4.17-4.22, decomposition counld be increased by increasing the temperature that affects the catalysts. But trends are also similiar with low temperature pyrolyzed catalysts, textural properties of ZIF-67 was lost due to the high temperatures.

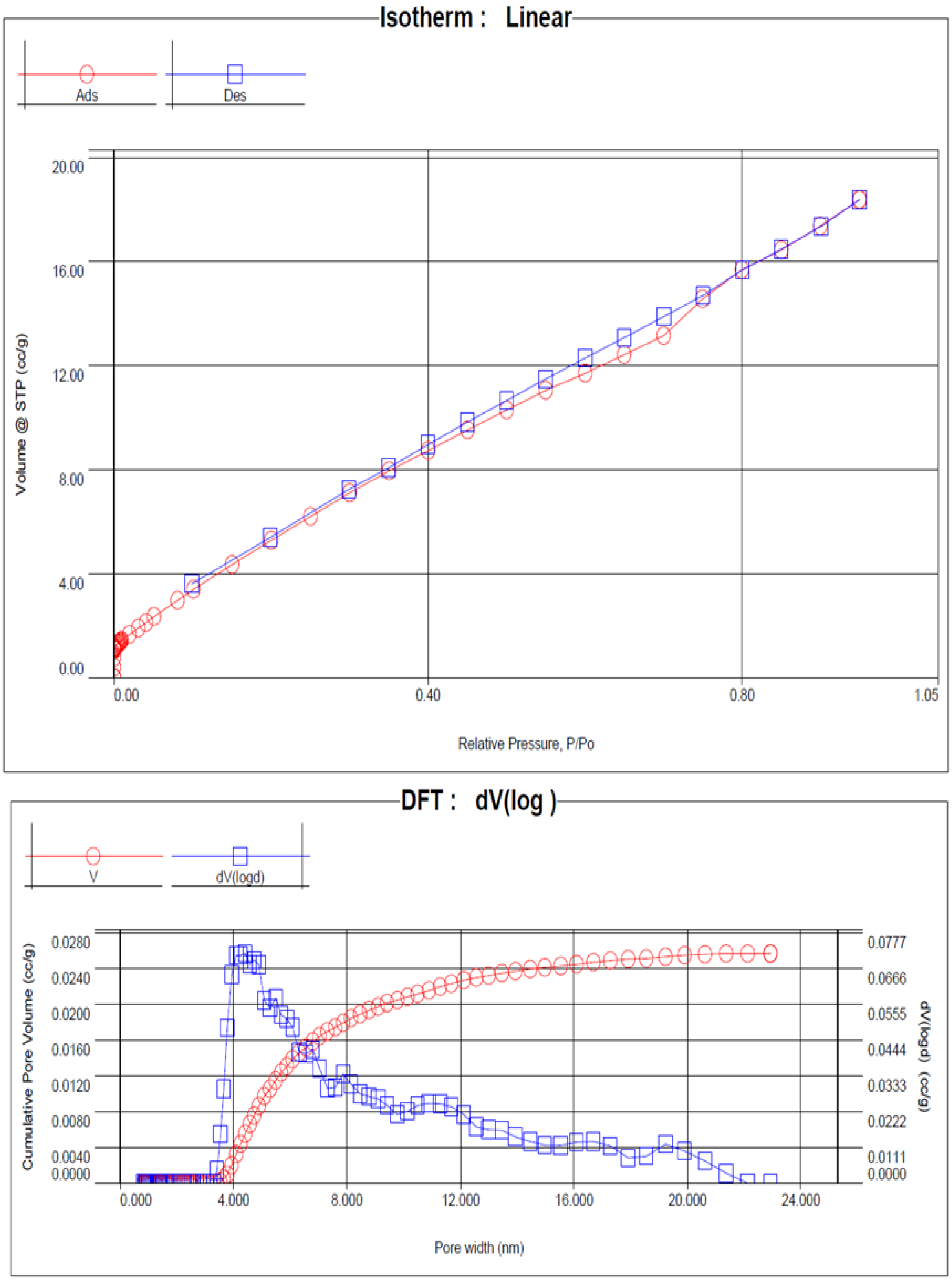

Figure 4.19: Adsorption/desorption isotherm and DFT pore volume vs pore width for the catalyst: CoZ@800.

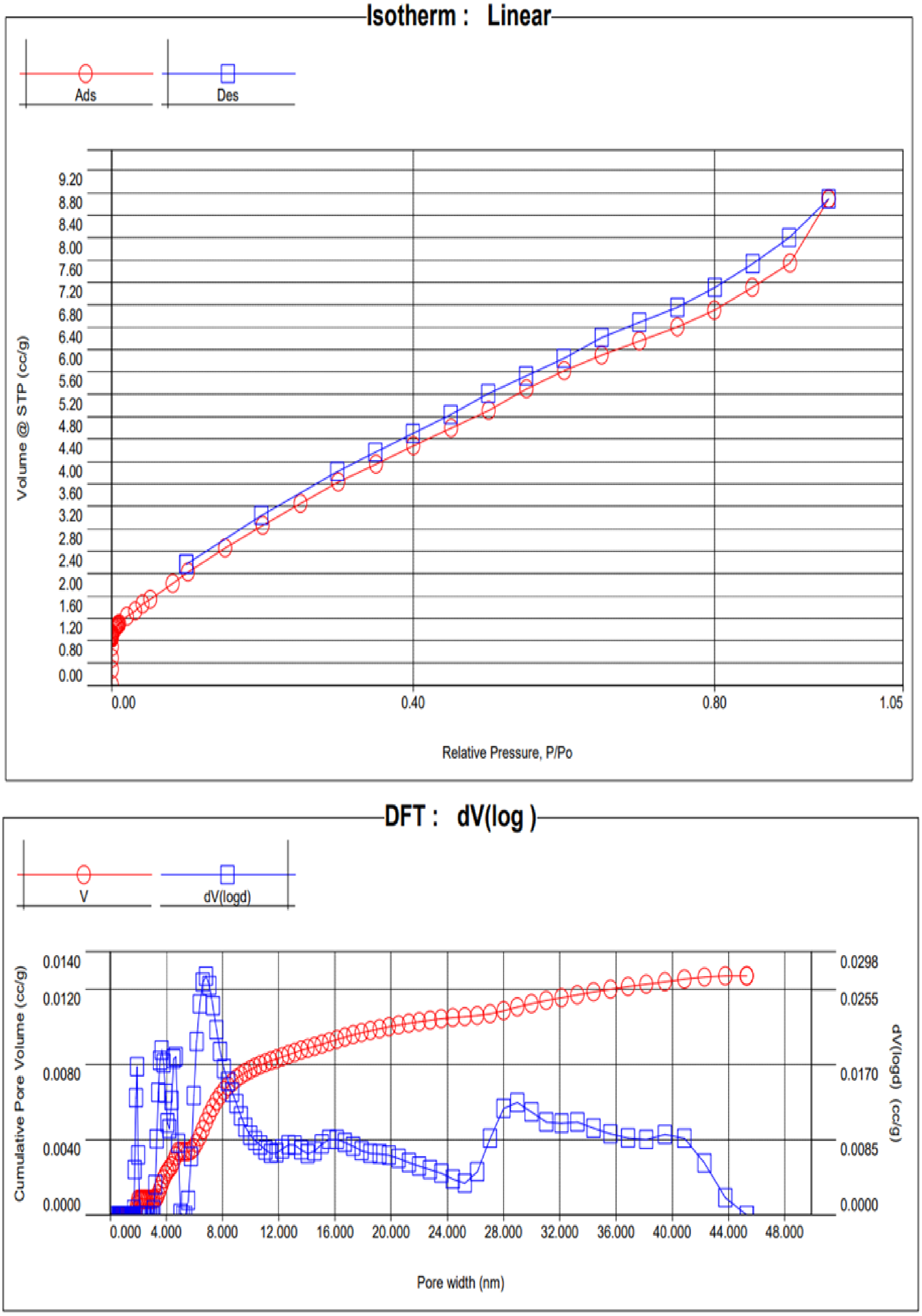

Figure 4.20: Adsorption/desorption isotherm and DFT pore volume vs pore width for the catalyst: CoZ@800.

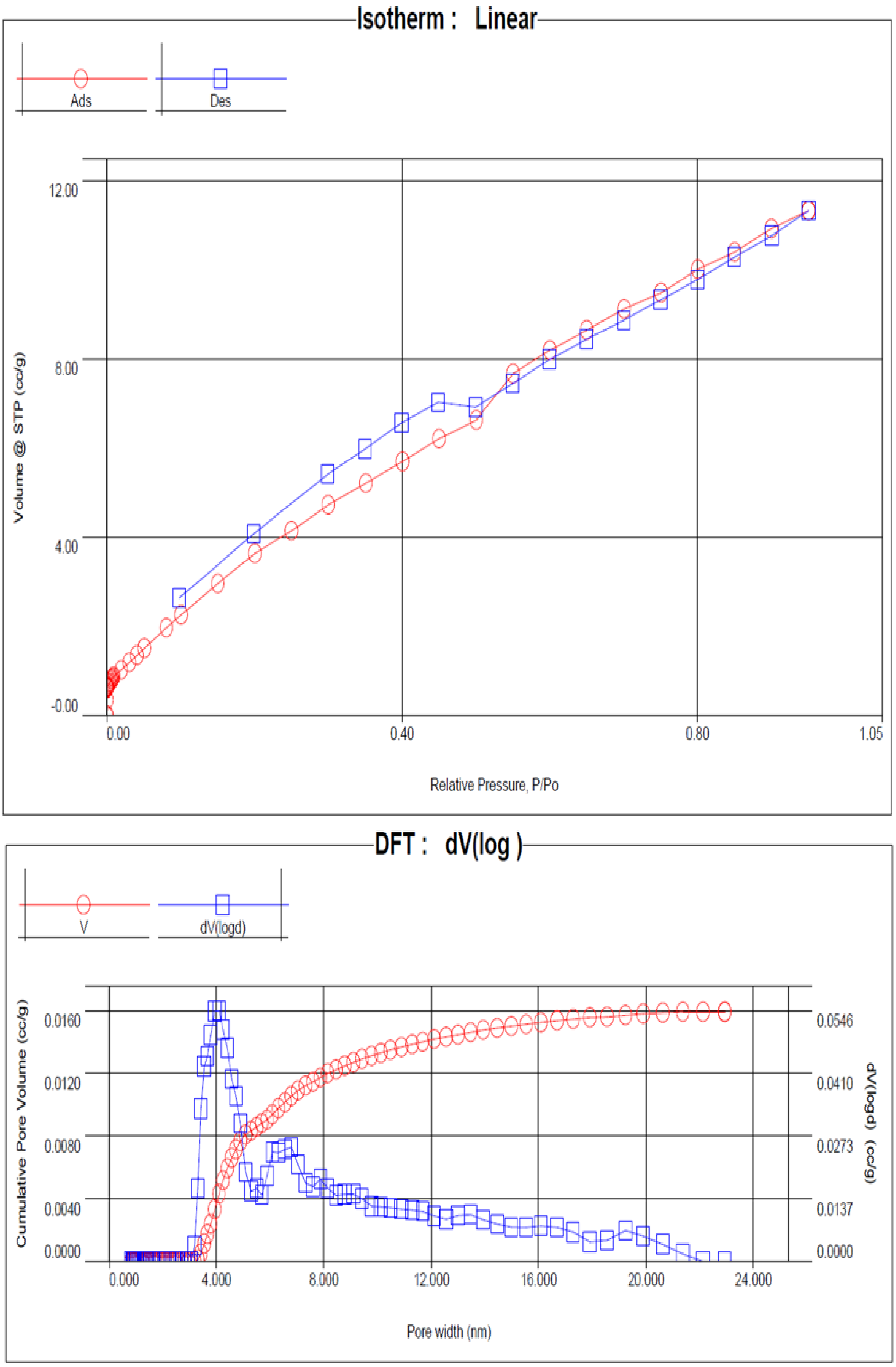

Figure 4.21: Adsorption/desorption isotherm and DFT pore volume vs pore width for the catalyst: CoZ@900.

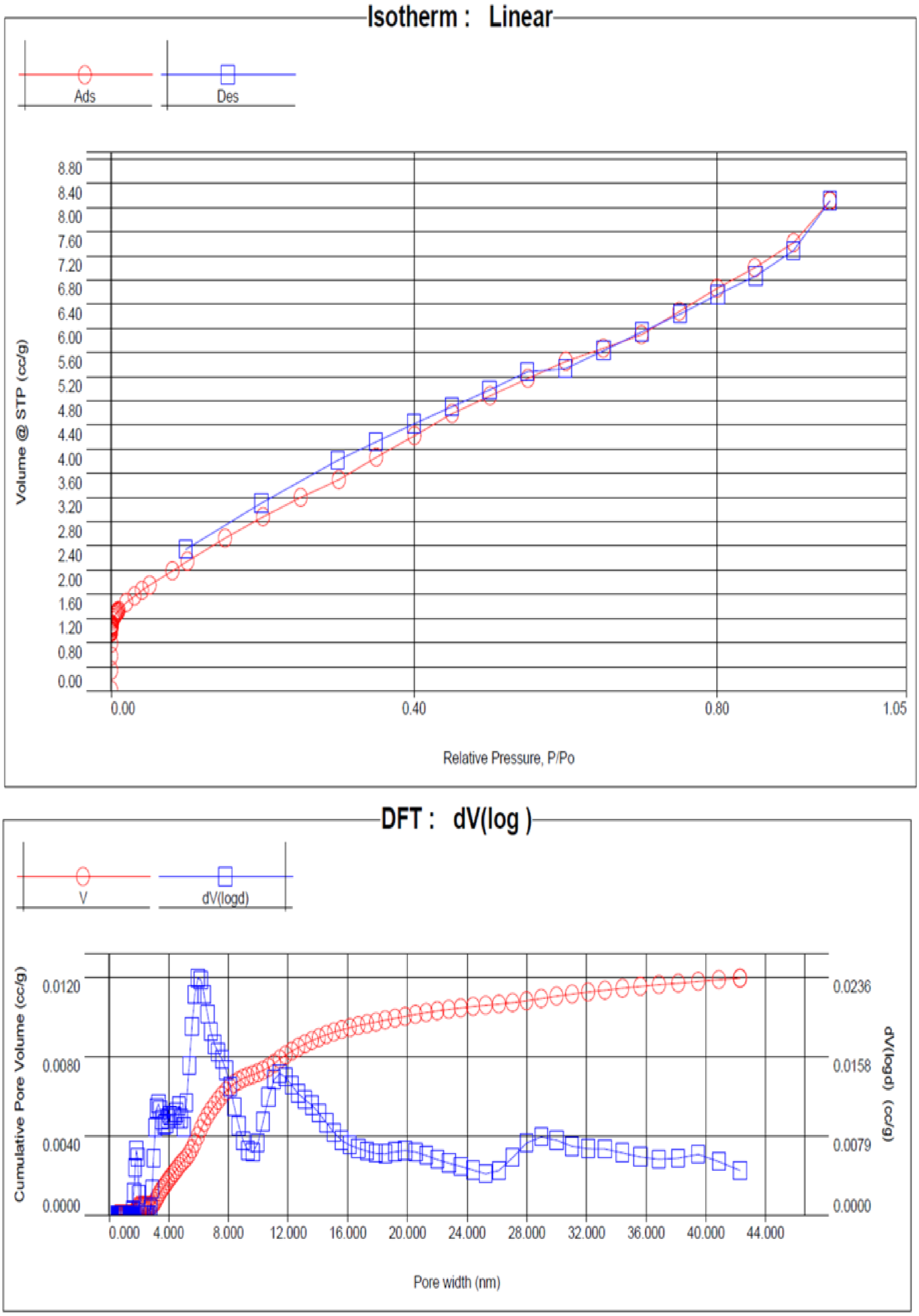

Figure 4.22: Adsorption/desorption isotherm and DFT pore volume vs pore width for the catalyst: CoZ@900.

Table 4.1. Multipoint BET, DFT pore volume and pore with of the catalysts group 1.

Sample	Multipoint BET m^2/g	Total Pore Volume cc/g	Pore width (mode) nm
ZIF-67	1824	0.62	1.43
CoZ@400	40.4	0.045	4.09
P_CoZ@400	29.5	0.031	3.54
CoZ@500	34.9	0.033	3.54
P_CoZ@500	15.1	0.02	2.0
CoZ@600	26.8	0.028	3.54
P_CoZ@600	18.5	0.018	3.32

Table 4.6. Multipoint BET, DFT pore volume and pore with of the catalysts group 2.

Sample	Multipoint BET m^2/g	Total Pore Volume cc/g	Pore width (mode) nm
CoZ@700	13.2	0.011	3.18
P_CoZ@700	19.1	0.016	3.32
CoZ@800	25	0.026	4.09
P_CoZ@800	12.5	0.014	1.9
CoZ@900	17.4	0.016	4.09
P_CoZ@900	11.6	0.012	5.95

4.2.5 Thermogravimetric analysis (TGA)

As seen in Figure 4.4, the first small peak at ~200 °C was due to the removal of remaining organic linkers and the second one between ~280°C and ~440°C might be attributed to the decomposition of the organic framework of ZIF-67. Thermogravimetric profiles of CoZ@400, CoZ@500, CoZ@600, CoZ@700, CoZ@800 and CoZ@900 catalysts were given in Figure 4.23, 4.24, 4.25, 4,26, 4.27

and 4.28, respectively. Above 800 °C a sharp but small weight loss of 5.3-6.8% were observed for these samples. As a plausible explanation, the nitrogen atoms incorporated into the carbon residue might be released as ammonia with increasing the pyrolysis temperature as a possible reason of the weight loss recorded beyond 800°C.

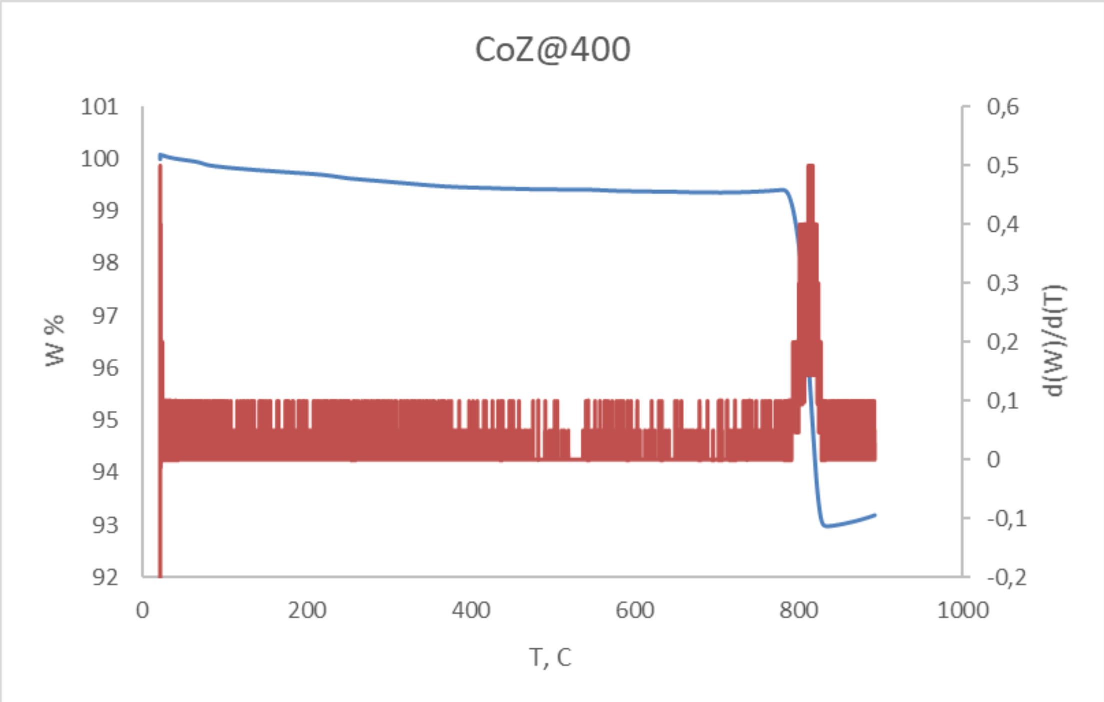

Figure 4.23: Thermogravimetric analysis (TGA) of CoZ@400 catalyst.

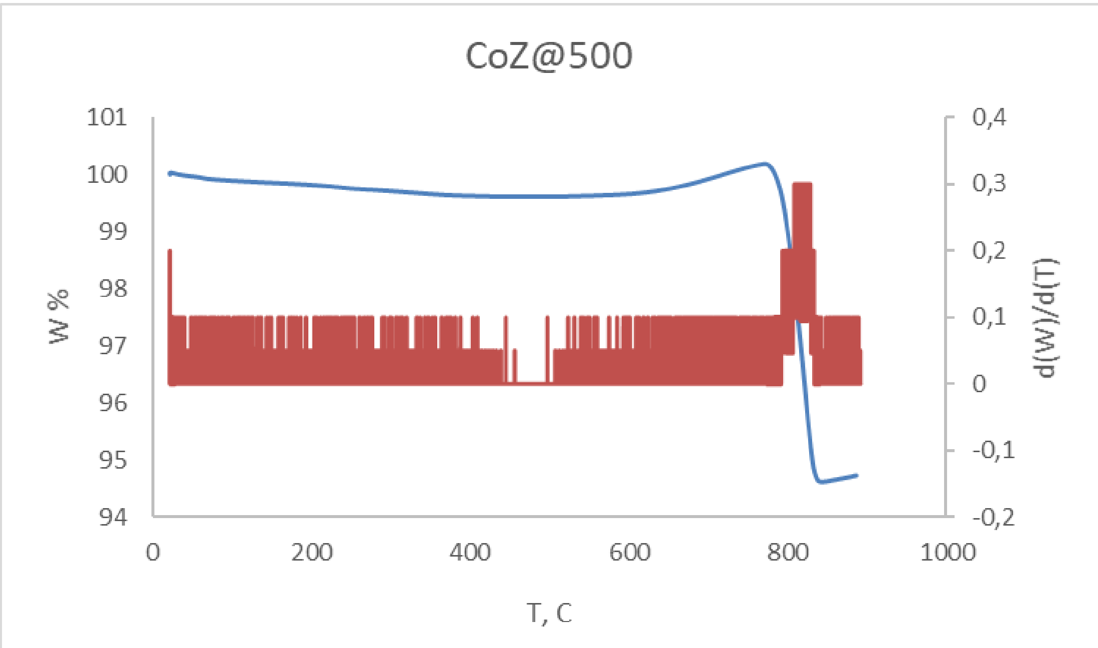

Figure 4.24: Thermogravimetric analysis (TGA) of CoZ@500 catalyst.

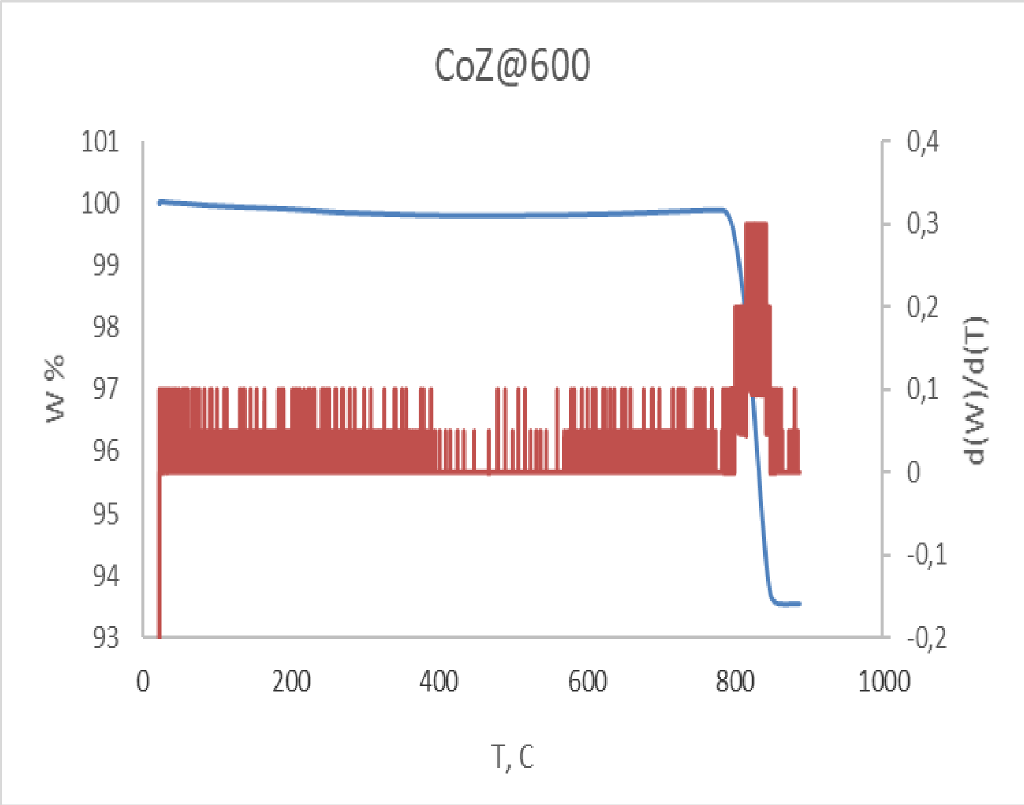

Figure 4.25: Thermogravimetric analysis (TGA) of CoZ@600 catalyst.

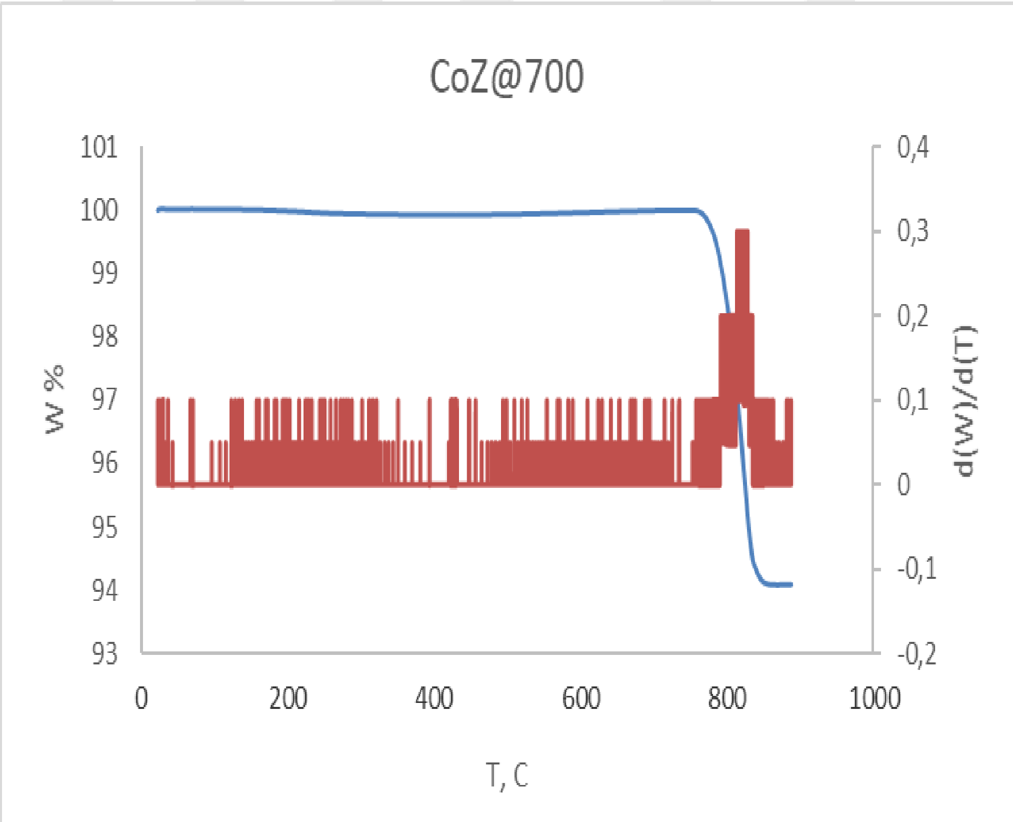

Figure 4.26: Thermogravimetric analysis (TGA) of CoZ@700 catalyst.

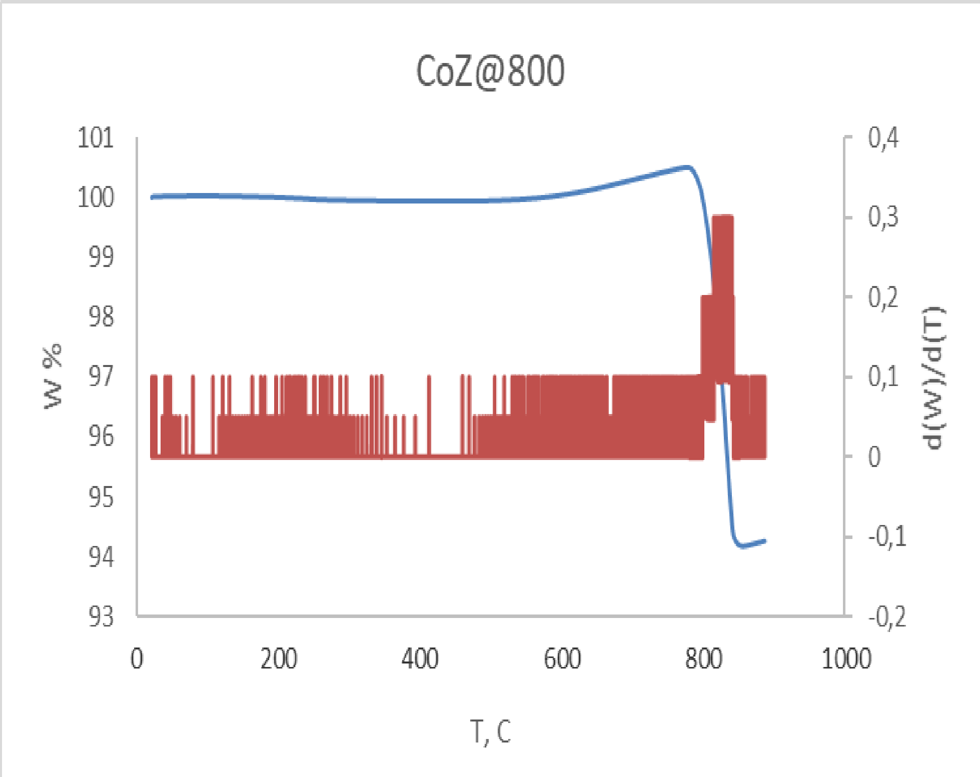

Figure 4.27: Thermogravimetric analysis (TGA) of CoZ@800 catalyst.

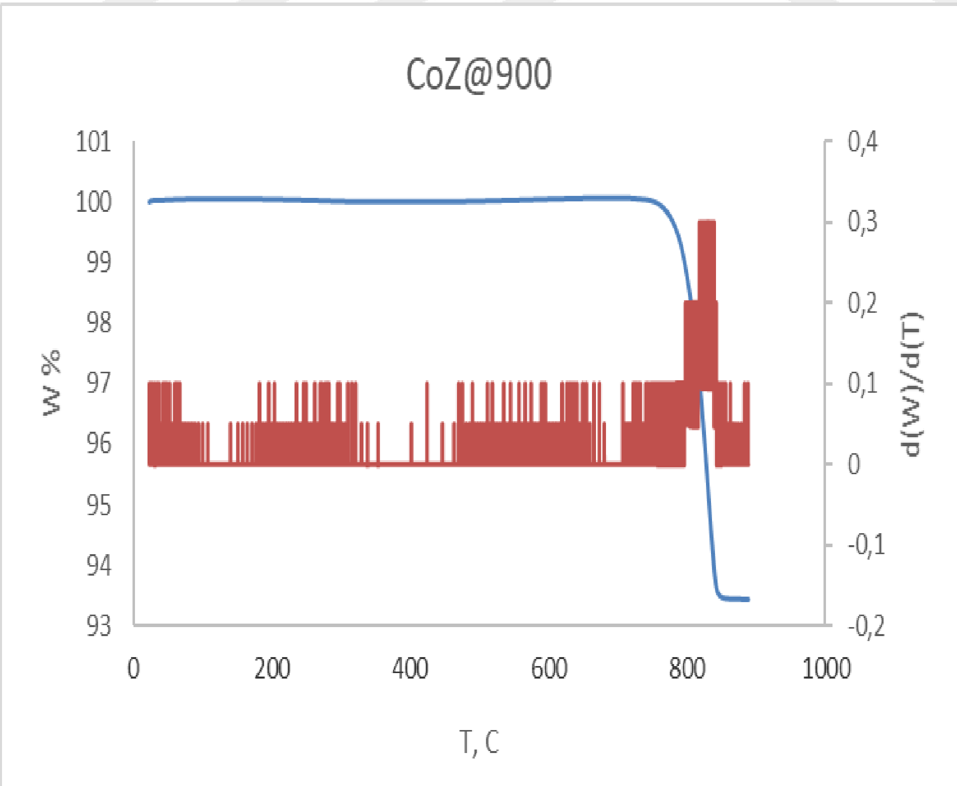

Figure 4.28: Thermogravimetric analysis (TGA) of CoZ@900 catalyst.

4.2.6 Temperature program reduction (TPR)

The TGA profiles of Co_3O_4 reduction were given in Figure 4.29 and Figure 4.30. In general, the H_2-TPR profiles of Co_3O_4 show two distinct peaks, $Co^{3+} \rightarrow Co^{2+}$ at low temperature and $Co^{2+} \rightarrow Co°$ at higher temperature according to Cheng and his colleagues study (Cheng et al., 2017). As seen in Figure 4.29 showing TPR profiles for low temperature pyrolysis (Group 1), two TPR peaks at 298 C and 397 °C were observed for the catalyst, CoZ@400 whereas the others have shown only one distinct TPR peak at around 350-400°C.

In some of them, the low temperature peak of 298 °C can be vaguely distinguished as in shoulder, e.g., CoZ@500 and P_CoZ@400. Moreover, a small peak above 550 C has been noticed due to the residual carbon possibly leaving in the form of methane in the presence of catalytic effect of cobalt. From TGA profiles, it cannot be concluded a systematic change of TPR peak temperatures with or without plasma treatment. However, TPR peaks have been noted shifting to higher temperatures when plasma was applied on.

Higher temperatures of TPR peak maxima might come from enhanced "strong metal surface interaction" (SMSI) effect for plasma-treated samples. Since the reduction temperature has been affected by the crystallite size, reduction percentage, support-metal oxide interaction and intermediate compound formation, the differences in the main TPR peak temperatures can also be attributed to the differences in crystal sizes of cobalt oxides depending on the pre-treatment conditions.Similar trends were clear for the catalysts in Group 2, namely the high temperature pyrolysis ones in Figure 4.30. Plasma treatment had a marked effect on shifting the TPR peak temperatures to the right. The TPR temperatures of CoZ@700, CoZ@800 and CoZ@900 catalysts were recorded as 409°C, 410°C and 382°C, respectively. Upon plasma treatment, these TPR peaks were shifted to 423°C, 414°C and 426°C, respectively.

In general, the TPR peak temperatures were seen to increase with increasing pyrolysis temperature with or without plasma induction as well. So, we may claim that reduction occurs on the surface Co_3O_4 nanoparticles and in consistent with literature that the reduction peak shifting to high temperatures is the indicative of increasing the particle size. (Chen et al., 2020)

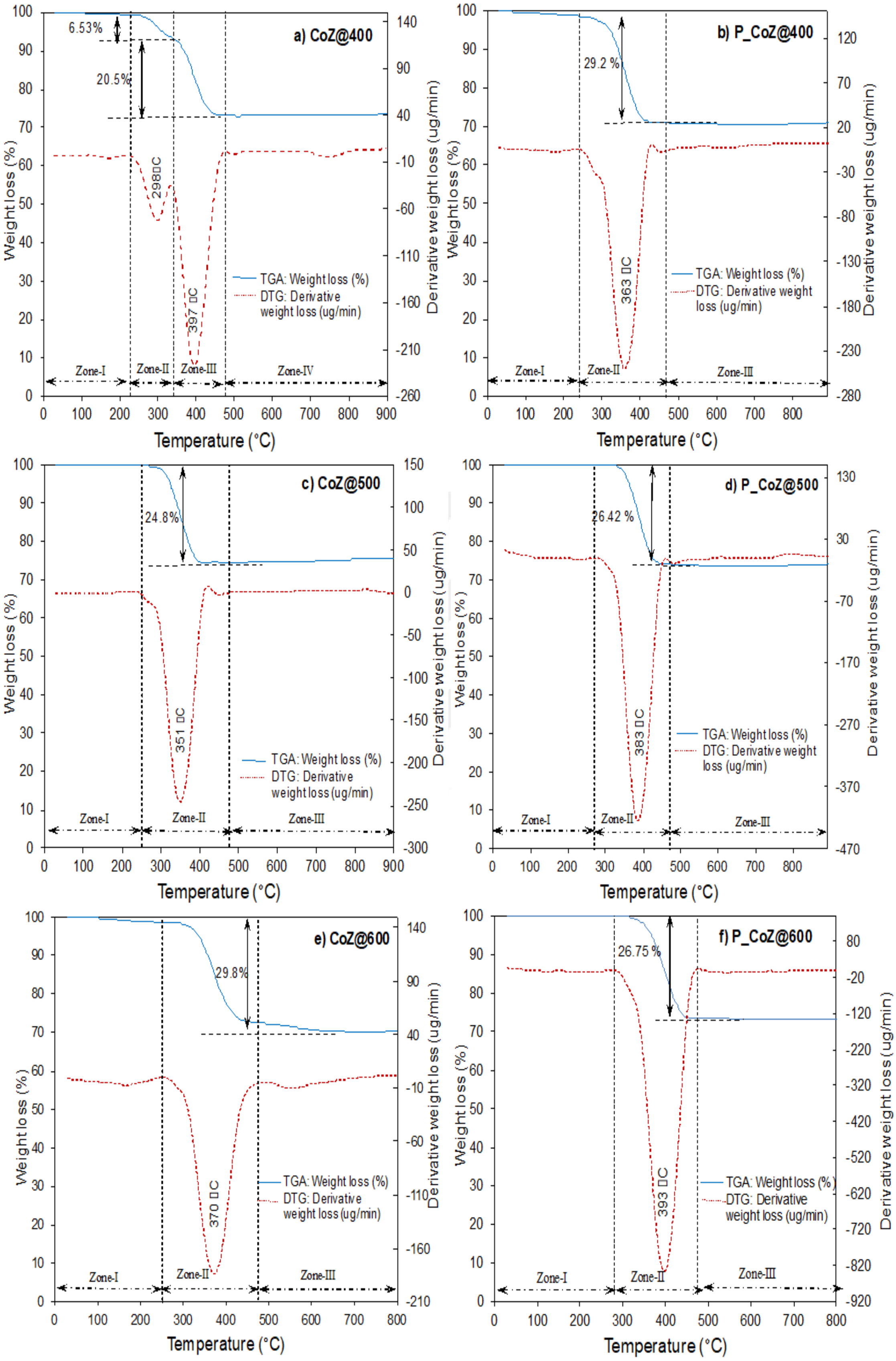

Figure 4.29: H_2 TG/DTG analysis of: (a) CoZ@400, (b) P_CoZ@400, (c) CoZ@500, (d) P_CoZ@500 (e) CoZ@600 and (f) P_CoZ@600.

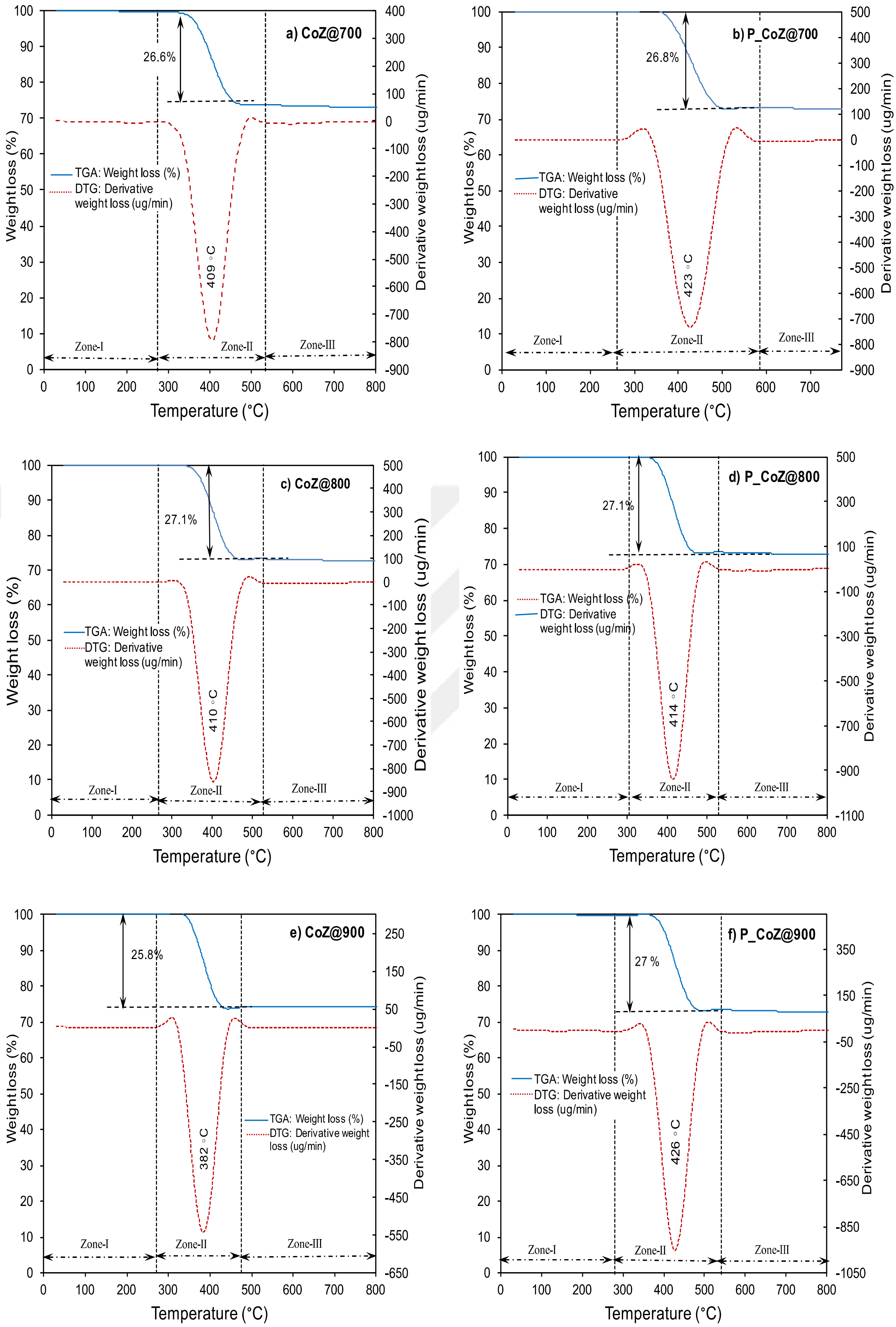

Figure 4.30: H_2 TG/DTG analysis of: (a) CoZ@700, (b) P_CoZ@700, (c) CoZ@800, (d) P_CoZ@800 (e) CoZ@900 and (f) P_CoZ@900.

4.2.7 Elemental Analysis

To investigate the effect of calcination on the carbon content of the catalysts, two catalysts one prepared with pyrolysis and calcination, that is CoZ@700, and the other one prepared with pyrolysis but without calcination were compared in terms of their elemental analysis. Elemental analysis results of these two catalysts were given in Table 4.7. As seen below, calcination has removed all hydrocarbons from the content of the catalyst.

Table 4.7. Elemental analysis results of the fresh catalysts CoZ@700 and CoZ@700-without calcination on weight percentage basis.

Sample	Carbon	Hydrogen	Nitrogen	Sulphur
CoZ@700	0.02	0.02	0.01	0.01
CoZ@700-without calcination	44.07	0.542	3.37	0.01

All these apparently has shown that the textural properties coming from MOF structure were significantly lost upon calcination. However, it is commonly accepted that the metallic cobalt (Co^0) was the active centre for Fischer-Tropsch Synthesis (FTS). Controlling the size of Co^0 over a support surface is quite challenging since reducibility is decreased with an increase in dispersion as a result of strong metal oxide-support interaction. In this term, thermal decomposition of metal complexes still keeps its importance to control the size and morphology of the active metal sites. In this framework, decomposition of ZIF67 to prepare nano-sized cobalt oxides interacted with nitrogen doped carbon might be secured by a secondary metal oxide shell. So, further encapsulation of the cobalt metal core with a metal oxide shell gain interest in order to control both the size of cobalt and diffusion of reaction products.

4.2.8 Characterization results of Co/ZIF-67 core and K_2O, ZnO or MnO metal oxide shell catalysts

As seen in Figure 4.31, 4.32, 4.33 and 4.34 and Table 4.8, although core-shell catalysts have similar BET surface areas and total pore volumes, their pore widths were noticed to be larger than the pyrolysis ones. This shows that mesopores have been generated during shell formation to enhance the mass transport efficiency for the reaction. Size selectivity comes from the catalyst pore size from where molecules with the right size below the pore aperture can pass and reach the active centers. The size of the pores also limits the chain growth reaction to a certain size of molecules diffusing out the pores. Probably, the catalytic stability may come from the diffusion controlled selectivity of core-shell catalysts.

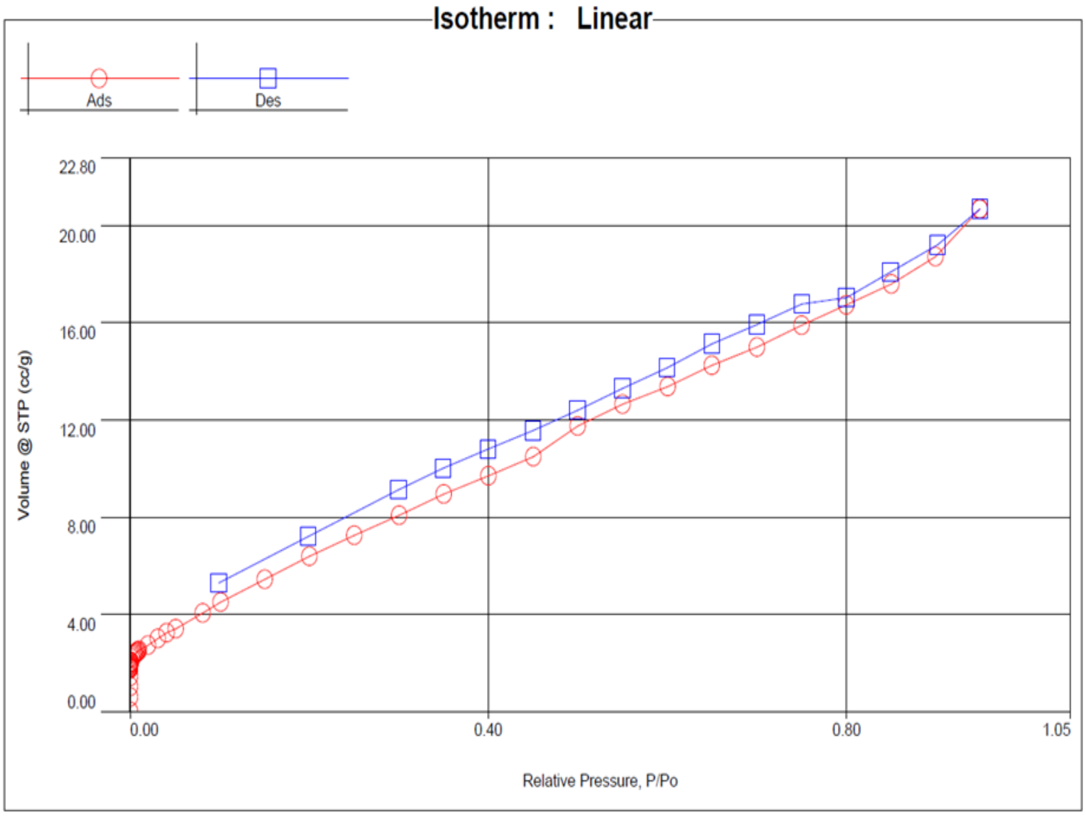

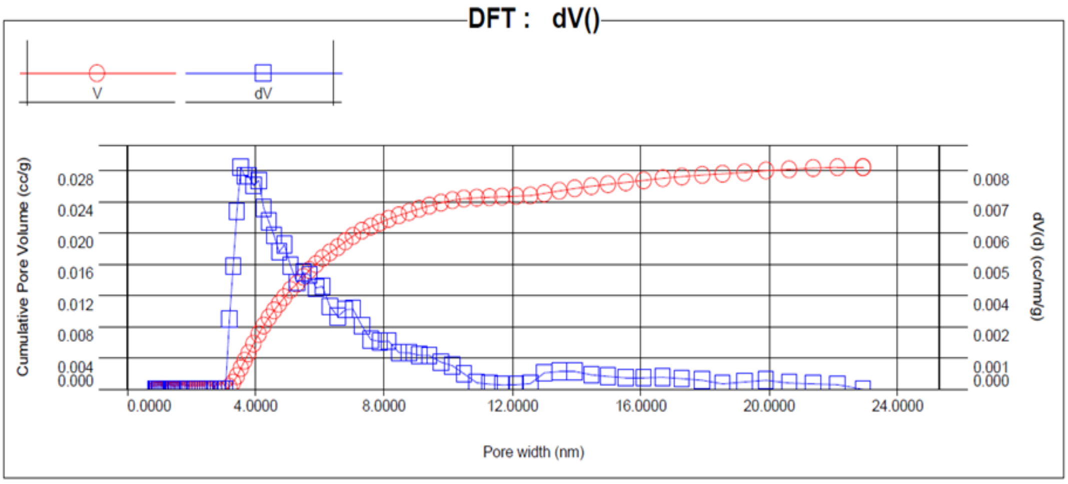

Figure 4.31:: Adsorption/desorption isotherm and DFT pore volume vs pore width for the catalyst: CoZ@600.

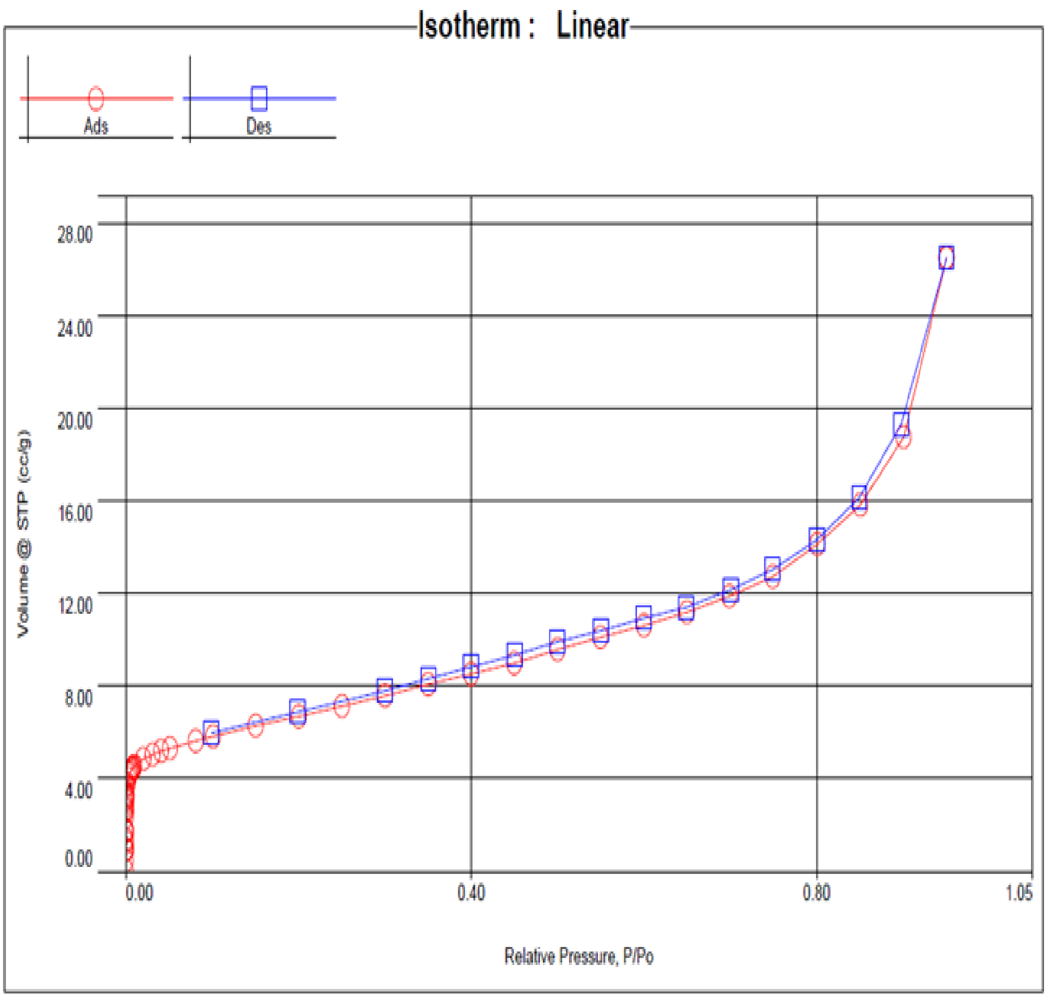

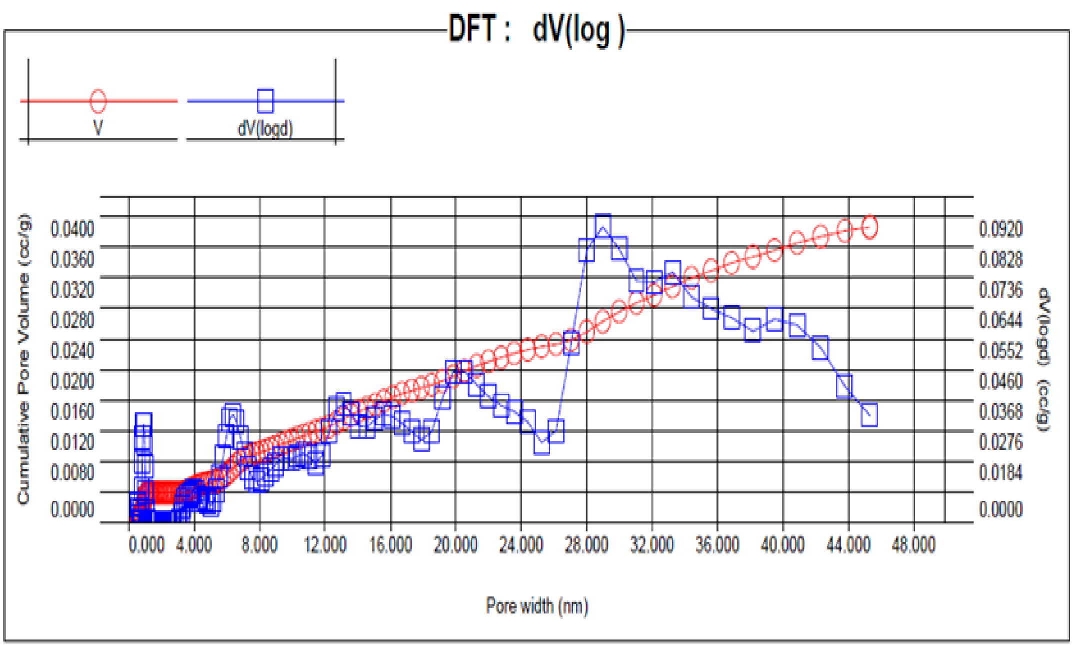

Figure 4.32: Adsorption/desorption isotherm and DFT pore volume vs pore width for the catalyst: CoZ@K2O.

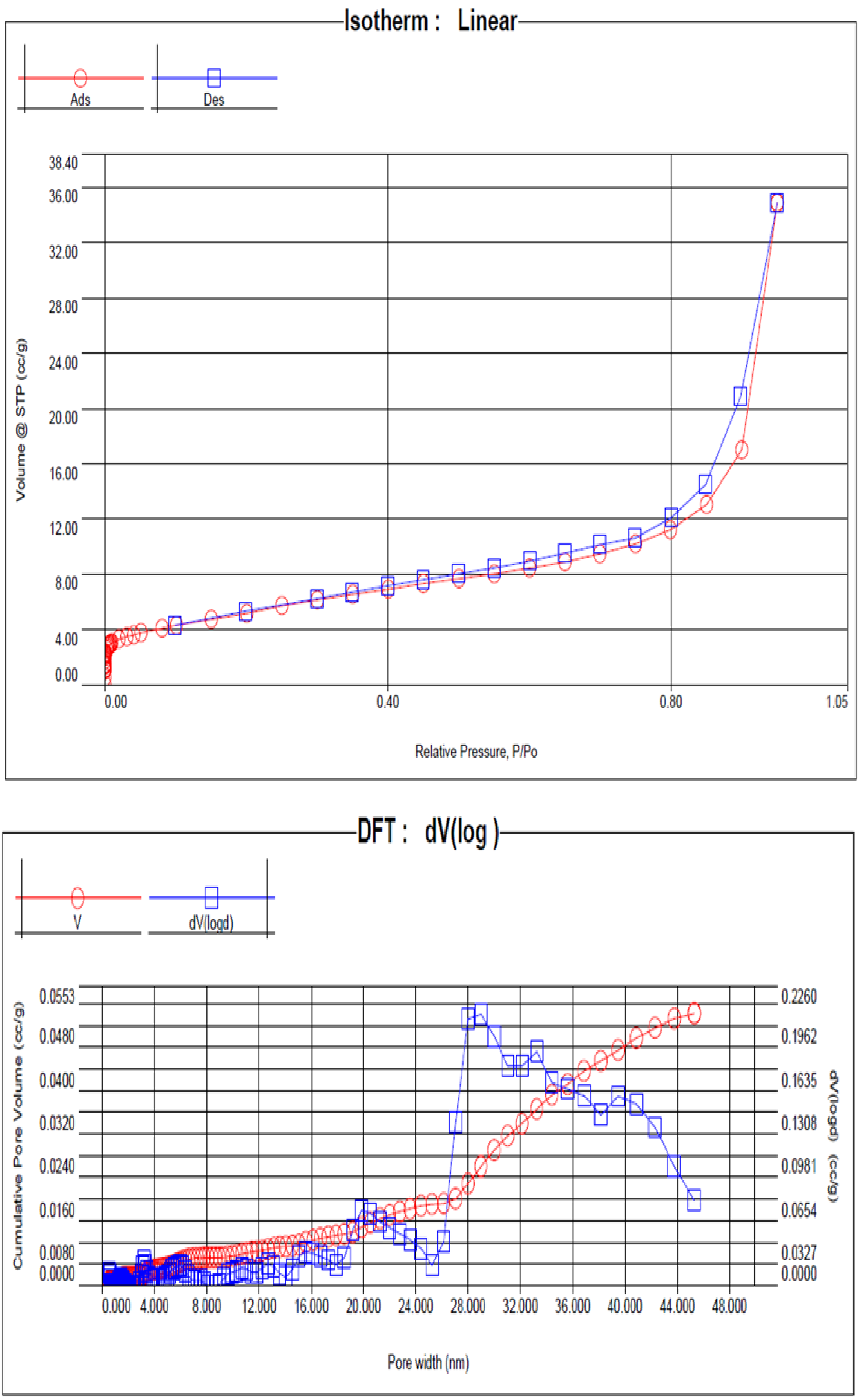

Figure 4.33: Adsorption/desorption isotherm and DFT pore volume vs pore width for the catalyst: CoZ@ZnO.

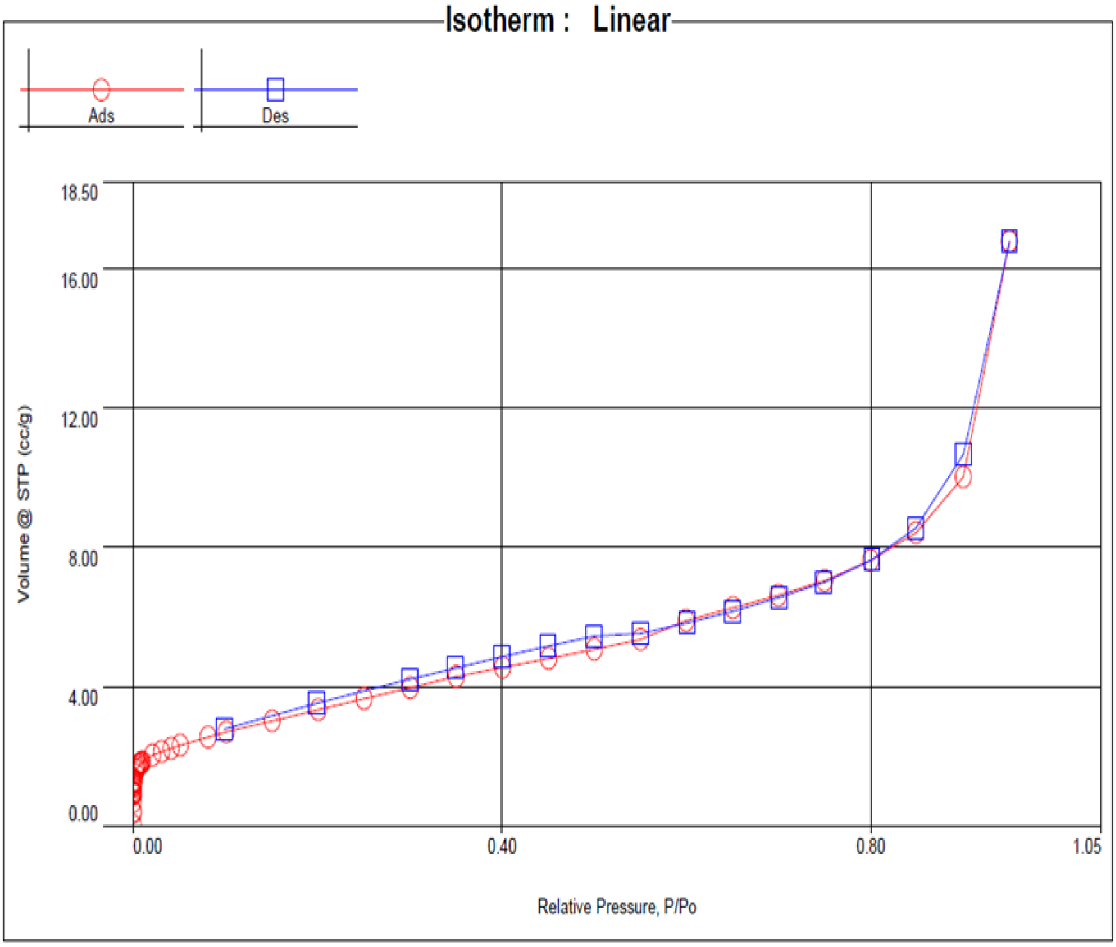

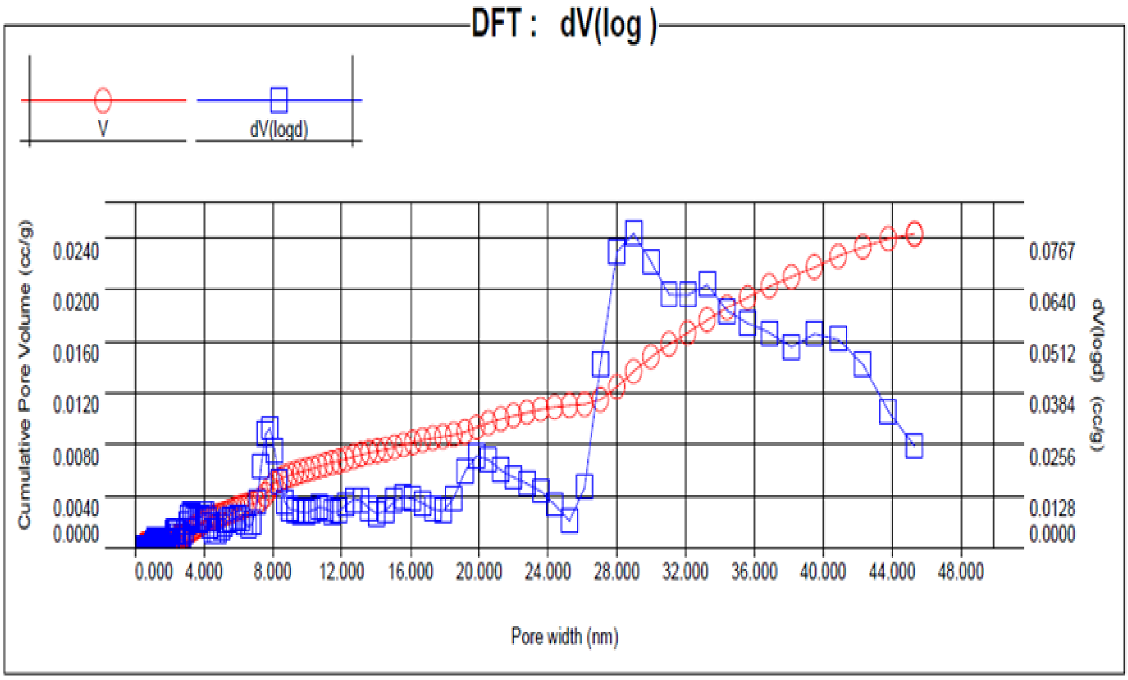

Figure 4.34: Adsorption/desorption isotherm and DFT pore volume vs pore width for the catalyst: CoZ@MnO.

Table 4.2. Multipoint BET, DFT pore volume and pore with of core-shell catalysts.

Sample	Multipoint BET m^2/g	Total Pore Volume cc/g	Pore width (mode) nm
ZIF-67	1824	0.62	1.37
CoZ@600	26.8	0.027	3.83
P_CoZ@600	18.5	0.018	4.01
CoZ@K_2O	23.4	0.041	7.0
CoZ@MnO	19.4	0.054	11.1
CoZ@ZnO	12.6	0.026	8.2

TGA profiles of core-shell catalysts were given in Figure 4.35, 4.36 and 4.37. The weight losses were observed starting from 750 °C and lasts to 850°C. In total, 6-7% weight loss was recorded for CoZ@K_2O and CoZ@ZnO catalysts while it was quite less for CoZ@MnO. The weight loss observed under N_2 atmosphere was attributed to the volatile carbon residues left upon calcination and hosting cobalt oxide.

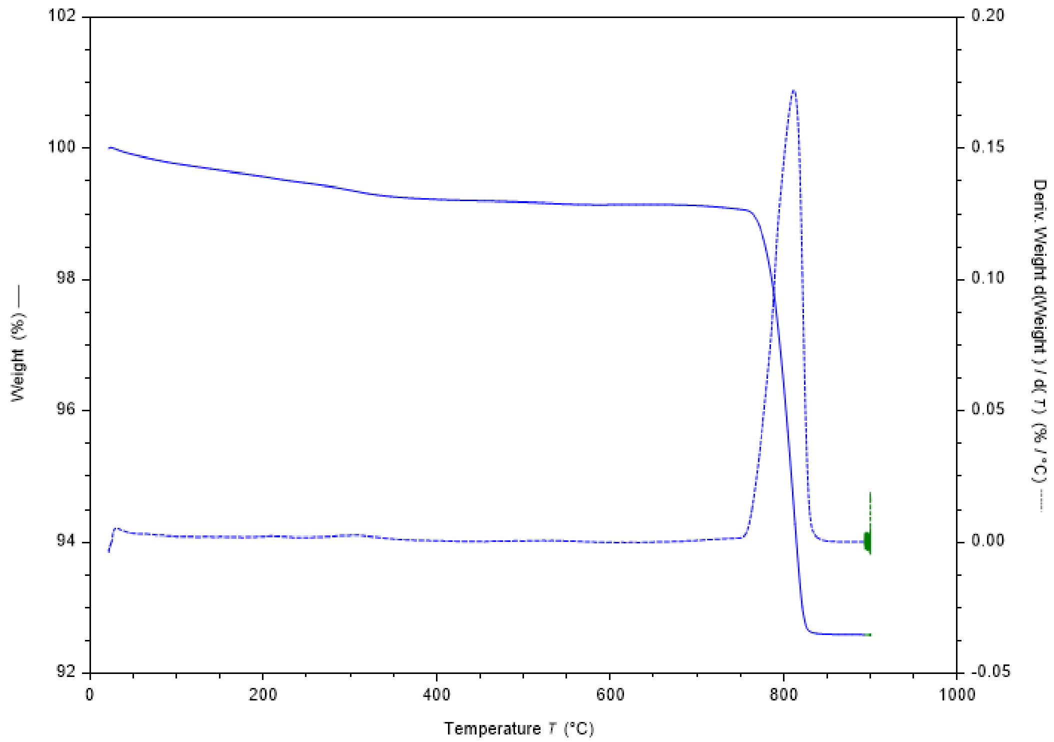

Figure 4.35: TGA profile of the catalyst: CoZ@K2O.

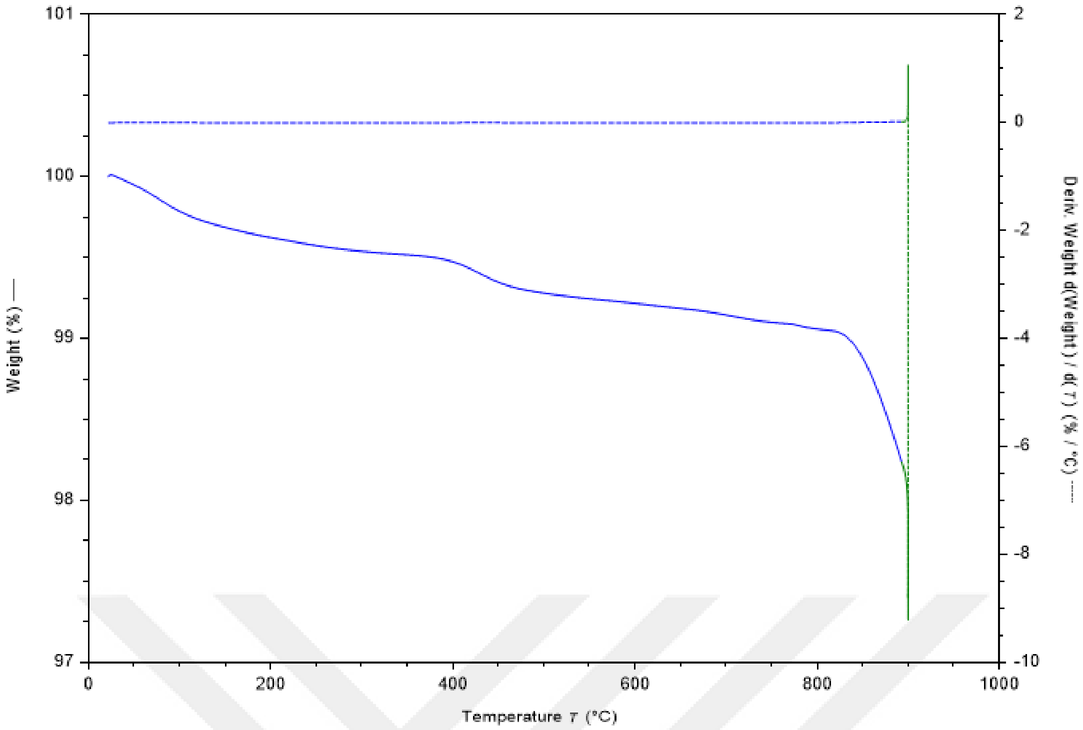

Figure 4.36: TGA profile of the catalyst: CoZ@MnO.

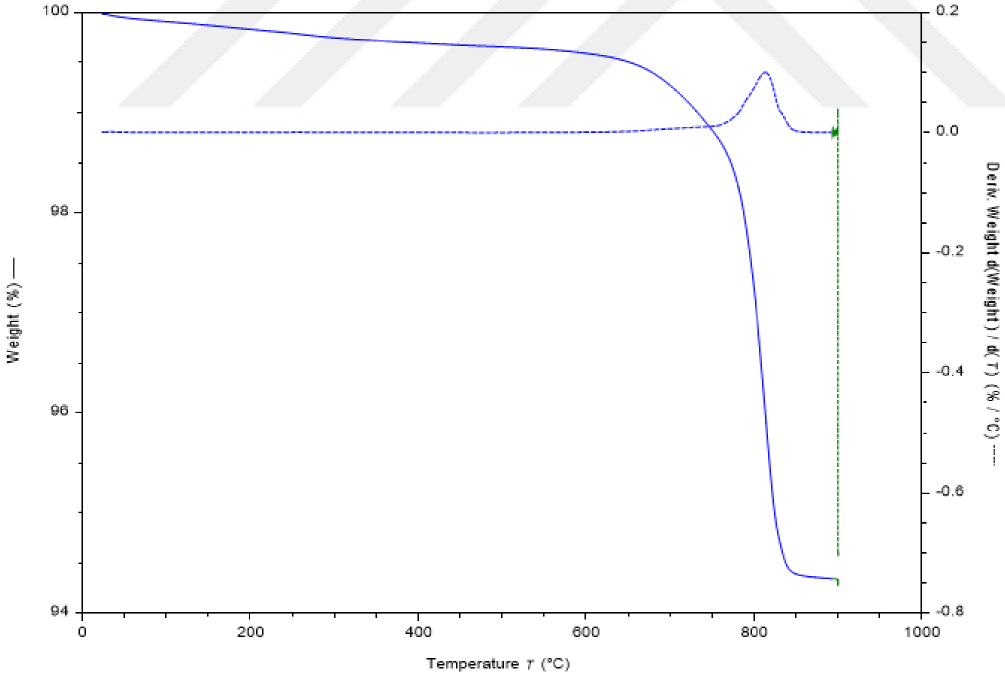

Figure 4.37: TGA profile of the catalyst: CoZ@ZnO.

TPR profiles of the core-shell catalysts were given in Figures 4.38. As apparently seen from the Figure, CoZ@ZnO was reduced at a lower temperature compared to the catalysts with K_2O and MnO shells. CoZ@MnO catalysts appeared to be hardly reducible probably due to the stronger interaction of manganese oxide with cobalt. This interaction might give mixed oxides resistant to reduction. Thereby, high conversions achieved over CoZ@ZnO might originate from its easy reducibility compared to the others.

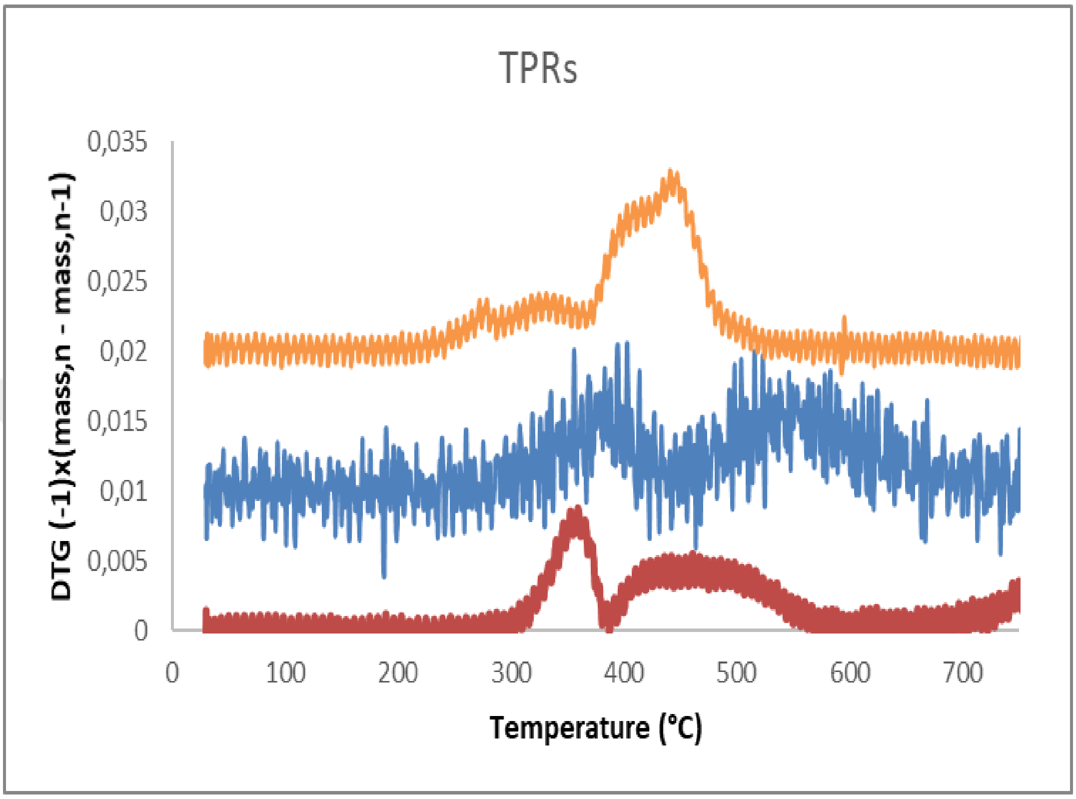

Figure 4.38: TPR profile of the catalysts on the same axis.

4.3 Catalytic Performance

12 catalysts were synthesized using ZIF-67, and promising catalyst were selected for creating core-shell structure on the purpose for improvement of the catalyst activity, durability and selectivity. Three sets of catalysts with Co/ZIF-67 core and K_2O, ZnO or MnO metal oxide shell have been prepared as well in order to improve the catalytic performance further. In the following section their performance test results have been presented.

4.3.1 CO and H_2 conversions of ZIF-67 based catalysts without a shell structure

CO conversion with time on stream for low temperature pyrolyzed catalysts (group I) were shown below in Figure 4.39. The highest and the lowest initial CO conversions of around 60.5% and 25.5% were achieved over P_CoZ@400 and CoZ@500, respectively.

However, since deactivation in different extends occurs for all catalysts, the best way to evaluate the catalytic performance was considered to be the average values for specific time intervals such as 0-10 h, 10-20 h etc. Regarding this, CoZ@600 has shown the highest CO conversion trend in between 37% - 40% with a reasonable stability in the first 20 h on stream. Although a sudden drop of CO conversion from 37% to 27% was observed on CoZ@600, the highest overall CO conversion on average of 31.3% was achieved on CoZ@600. It is also worth to mention that plasma treated samples (P_CoZ@400, P_CoZ@500 and P_CoZ@600) initially has shown high CO conversions, namely around 60.5%, 53.5% and 47.4%, but they were deactivated fast with a decrease in their conversions to 15.5%, 20.9% and 20.9%, respectively.

In general, non-plasma treated catalysts were more stable than the plasma treated ones. H_2 conversion with time on stream for the applied catalysts during Fisher-Tropsch Synthesis were shown in Figure 4.40. When H_2 conversions were compared with CO conversions, it was seen that more or less H_2 conversions were lower than CO conversions.

For the pyrolyzed catalyst, the difference between H_2 and CO conversions were less in the period of 0-20 h on stream due to the poor water gas shift activity of cobalt-based catalyst. For example, the average values of H_2 and CO conversions over CoZ@600 were 40.5% and 38.8%, respectively. However, this difference was more noticeable for plasma treated samples. Initial and final CO conversions of P_CoZ@500 were 53.5% and 20.9% while those of H_2 conversions were 46.0% and 15.7%, respectively. This unexpected situation can only be speculated by the existence of another reaction that would lead to the consumption of carbon monoxide and/or hydrogen production via water gas shift or dehydrogenation of intermediate surface species. However, there is no evidence to support this.

All in all, it is clear that non-plasma treated catalysts were less prone to deactivation and among them, the CoZ@600 catalyst had the highest CO and H_2 conversions in the first 20 h on stream. Last, even if there was a small but sharp decrease in CO and H_2 conversion after 20 hours on stream over CoZ@600, this situation can be improved by using promoters.

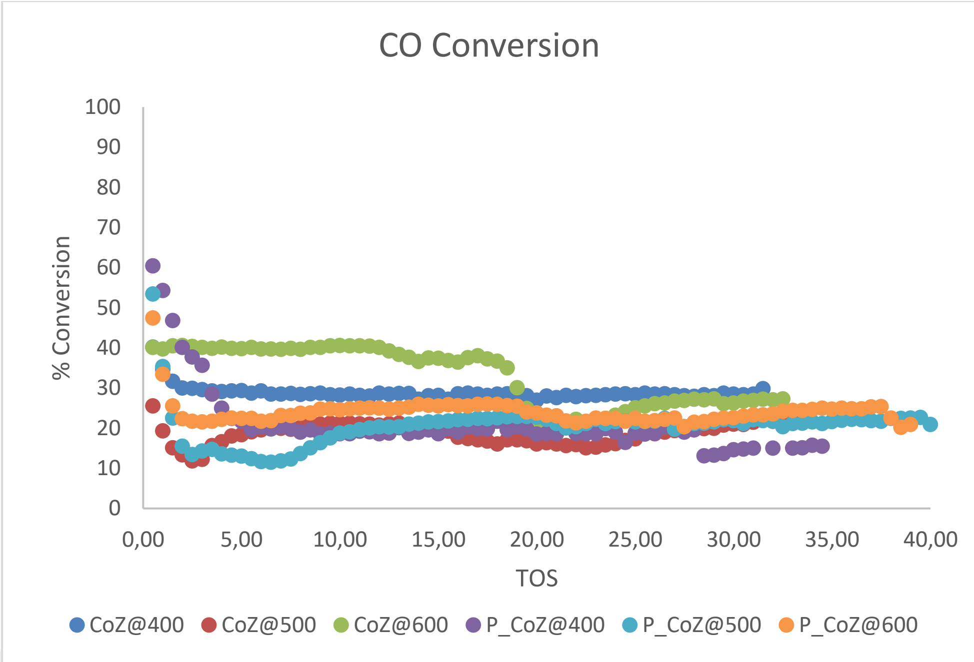

Figure 4.39: CO conversions with time on stream for the catalysts group 1, low temperature pyrolysis.

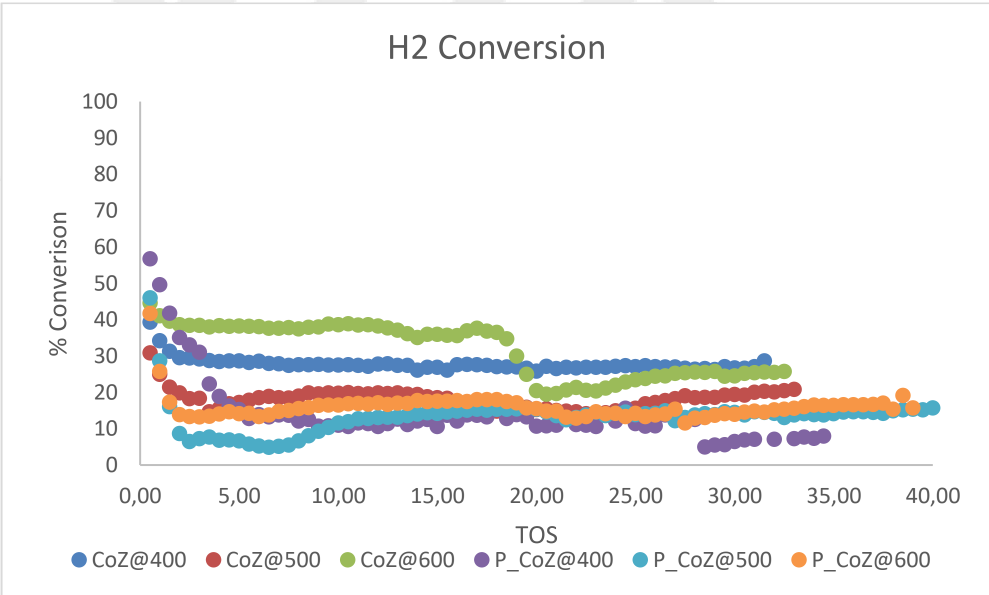

Figure 4.40: H_2 conversions with time on stream for the catalysts group 1, low temperature pyrolysis.

Figure 4.41 and 4.42 have shown CO and H_2 conversions with time on stream for high temperature pyrolyzed catalysts (group II).). For all catalysts, initially high CO conversions were observed. As in the case of group I low temperature pyrolyzed catalysts, the highest CO conversions were achieved over plasma treated catalysts. Plasma-induced samples have shown more severe loss of conversion compared to non-plasma induced ones. Among all catalysts, the highest initial CO conversion of 67.8%

was achieved over P_CoZ@800. However, CO conversion over Co@Z@700 seemed decreasing more steadily compared to the others in this set of catalysts. As it was remarked for the catalysts in group I, comparably lower H_2 conversions were seen for the catalysts in group II. For example, while initial CO conversions over CoZ@700, CoZ@800 and CoZ@900 were 33.5%, 28.8% and 47.6%, the corresponding H_2 conversions were 29.4%, 27.1% and 38.6%, respectively.

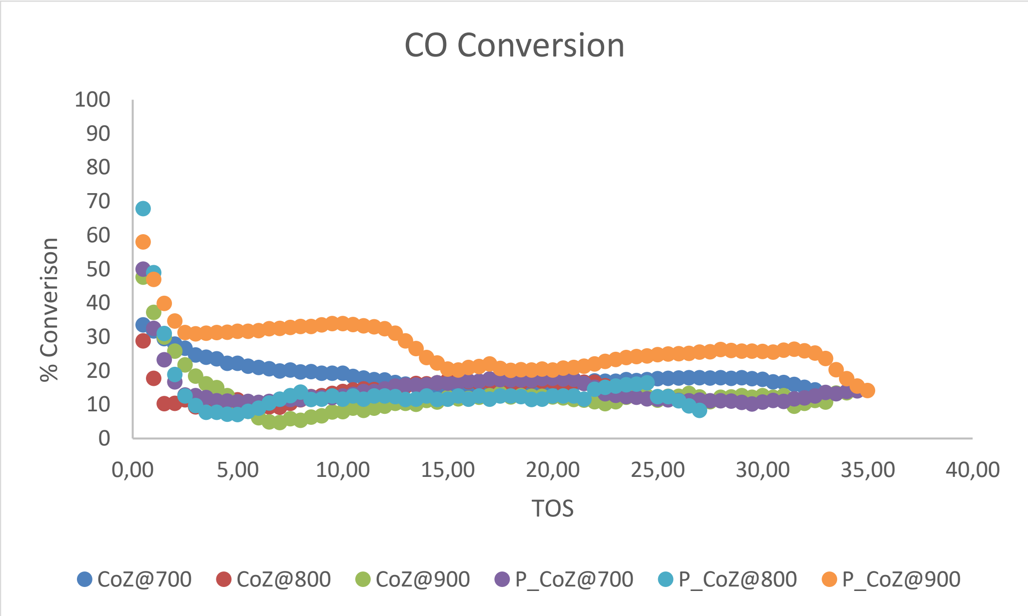

Figure 4.41: CO conversions with time on stream for the catalysts group 2, high temperature pyrolysis.

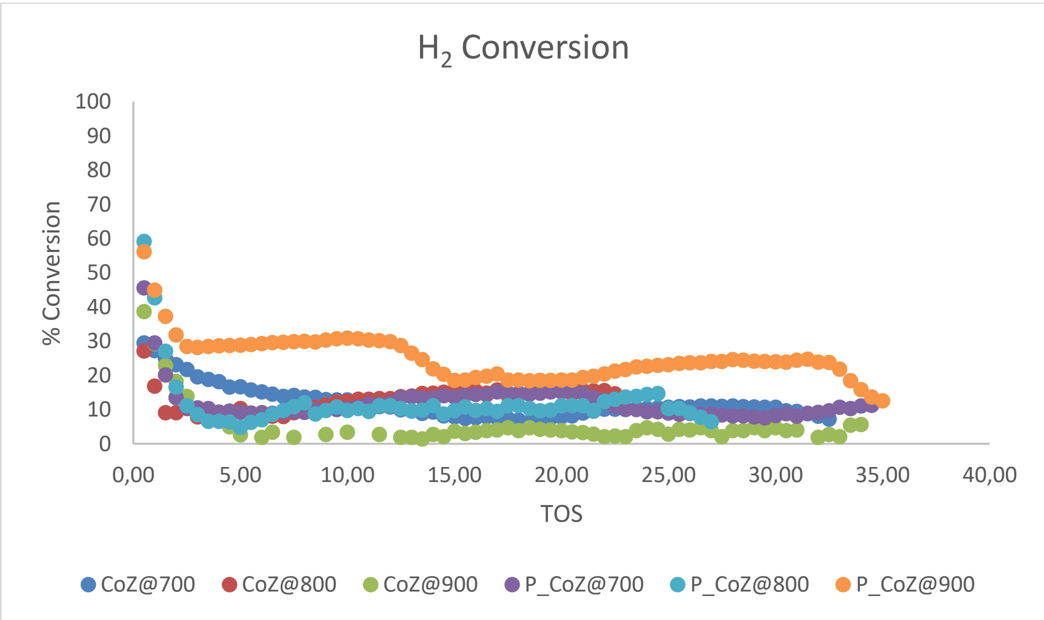

Figure 4.42: H_2 conversions with time on stream for the catalysts group 2, high temperature pyrolysis.

4.3.2 Product selectivity of ZIF-67 based catalysts without a shell structure

The average values of olefin selectivity in every 10 h intervals of test duration were given in bars in Figures 4.43, 4.44 and 4.45 for the low and high temeprature pyrolyzed catalysts separately. As seen in the Figure 4.43 and 4.44, plasma tretaed catalysts were more selective to C2-C4 olefins compared to non-plasma treated ones.

Among the non-plasma treated catalysts, CoZ@400 and CoZ@600 were the ones showing the lowest C2-C4 olefin selectivity. The average olefin selectivities obtained with CoZ@400, CoZ@500 and CoZ@600 catalysts were 13.2%, 19.9% and 13.8%, while the those obtained for P_CoZ@400, P_CoZ@500 and P_CoZ@600 catalysts were 22.5%, 22.3% and 21.33%, respectively.

Since it was widely accepted that inhibited re-adsorption of olefinic intermediates and relatively low hydrogen transfer rates were in responsible for high olefin selectivity, it had been argued that plasma treated catalysts might have an altered catalytic surface feature promoting olefinic products.

On the other side, even the reaction started with high CO conversions on the plasma treated catalysts, their fast deactivation had been considered as one of the reasons for the observed high olefin selectivity due to the altered nature and decreased number of active sites over them.

Similar selectivity profile for C2-C4 olefins were observed for the high temperature pyrolyzed catalysts (group II). Average C2-C4 olefins selectivity values for non-plasma treated catalysts were 22.9%, 20% and 25.12%, all were well above the the ones as measured for low temperature pyrolyzed catalysts. In similar to the low temperature pyrolyzed catalysts (group I), plasma treatment gave higher C2-C4 olefins selectivity on average except for P_CoZ@900. Namely C2-C4 olefin selectivity on P_CoZ@700), P_CoZ@800 and P_CoZ@900 were calculated as 28.1%, 30.1% and 18.3%.

Olefin products may favourably form possibly due to the less extended growth of hydrocarbon chain under the effect of low CO conversion. So, one reason of the unexpectedly lower olefin selectivity on P_CoZ@900 may be due the highest CO and H_2 conversions among all high temperature pyrolyzed catalysts..

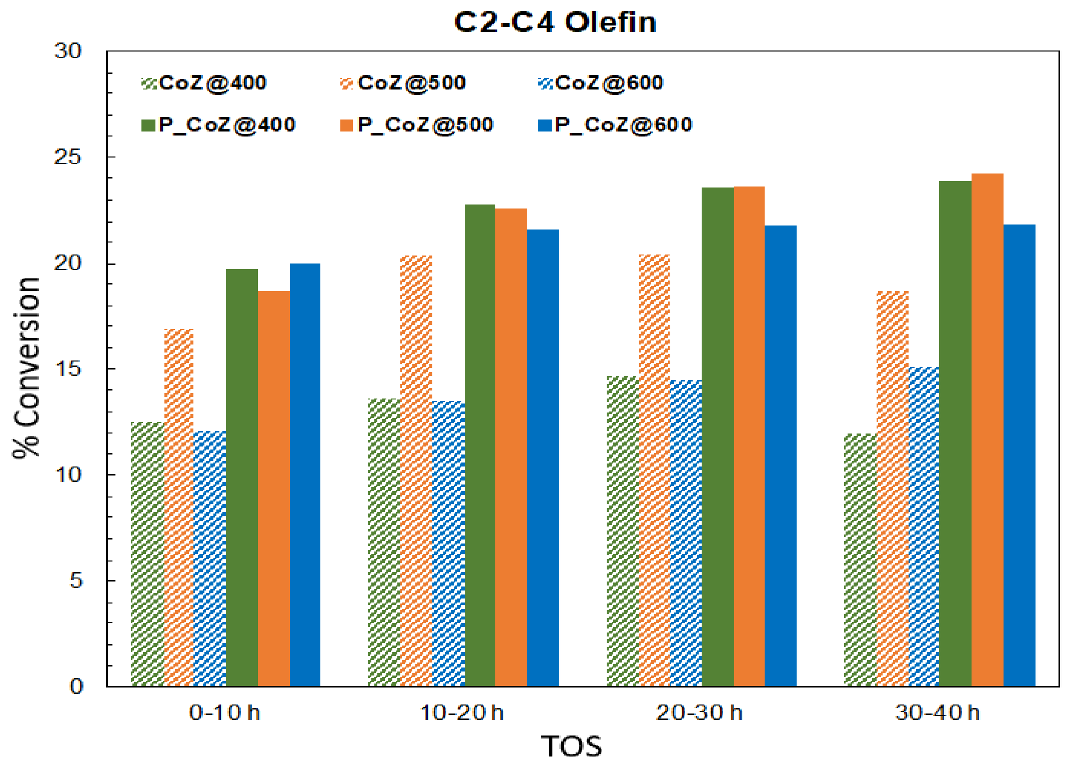

Figure 4.43: Average C_2-C_4 olefin selectivity in every 10 h time on stream for the applied catalysts during Fisher-Tropsch Synthesis.

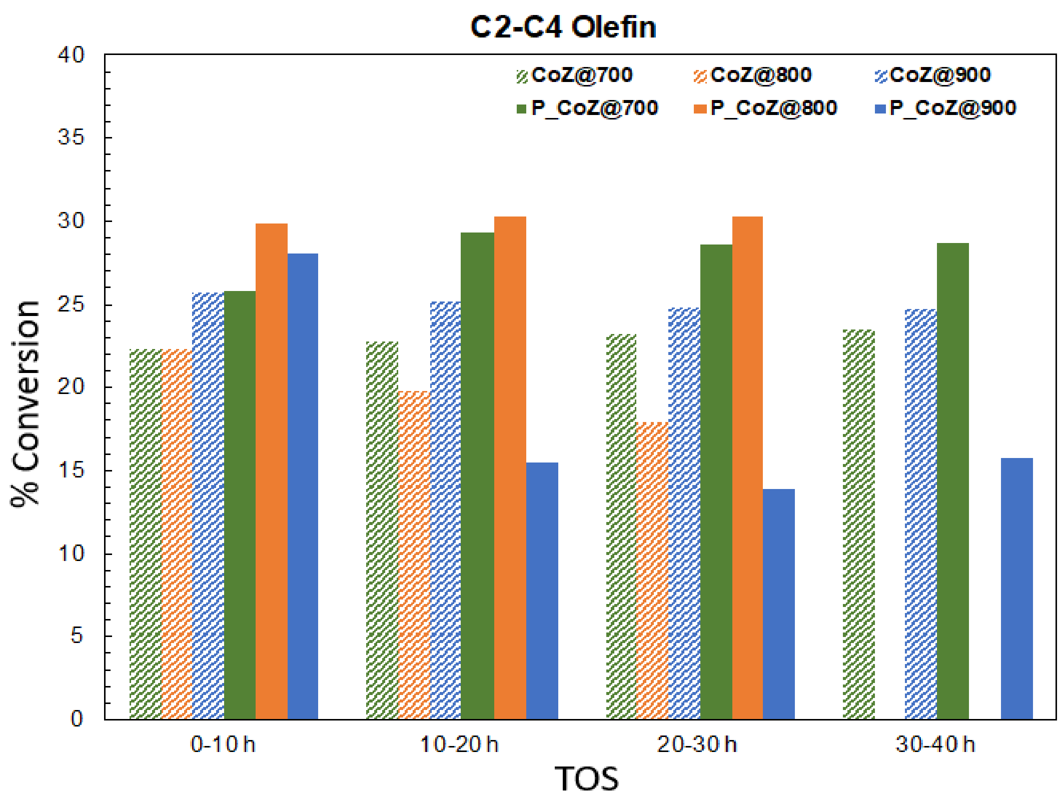

Figure 4.44: Average C_2-C_4 olefin selectivity in every 10 h time on stream for the applied catalysts during Fisher-Tropsch Synthesis.

C_2-C_4 paraffin selectivity for low temperature pyrolyzed catalysts (group I) and high temperature pyrolyzed catalysts (group II) were given in Figure 4.45 and 4.46, respectively. When the C_2-C_4 paraffin selectivity profiles were examined, higher paraffin selectivity at the expense of olefin selectivity was the most noticeable point. For example, a high paraffin selectivity of 25.2% and 24.2% were obtained on the catalysts, CoZ@400 and CoZ@600 versus their low olefin selectivity values of 13.2% and 13.8%. When the pyrolysis temperature was increased to 700-900°C, the situation was reversed by the effect of low CO conversion and olefin products favourably forms due to less extended growth of hydrocarbon chain. Under this circumstance, CoZ@800 and CoZ@900 have shown the lowest paraffin selectivity of 13.8% and 14.6% on average. When the effect of plasma was examined, it was clear that whatever the pyrolysis temperature was, plasma treated samples have shown higher olefin selectivity at the expense of paraffin selectivity. This implies again the fact that plasma treatment affects the selectivity towards olefins. In the other side, it should also be kept in mind that although the reaction started with high CO conversions on the plasma treated catalysts, their fast deactivation might lead to high olefin selectivity due to the altered nature and reduced number of active sites.

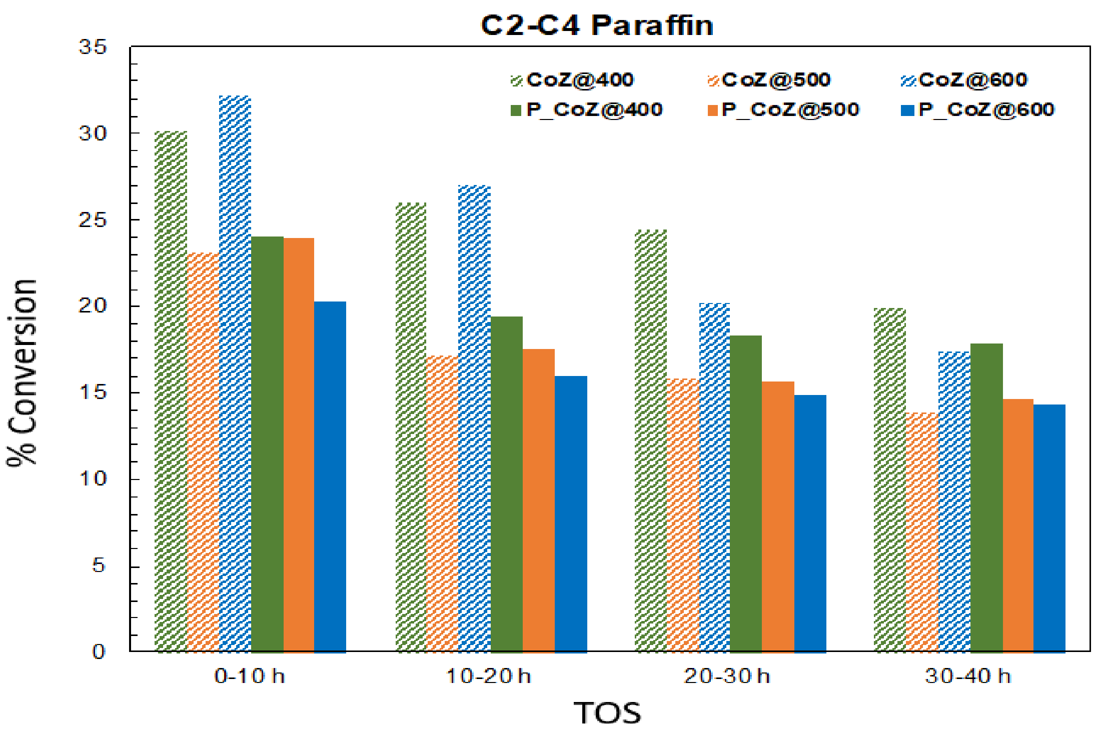

Figure 4.45: Average C_2-C_4 paraffin selectivity in every 10 h time on stream for the applied catalysts during Fisher-Tropsch Synthesis.

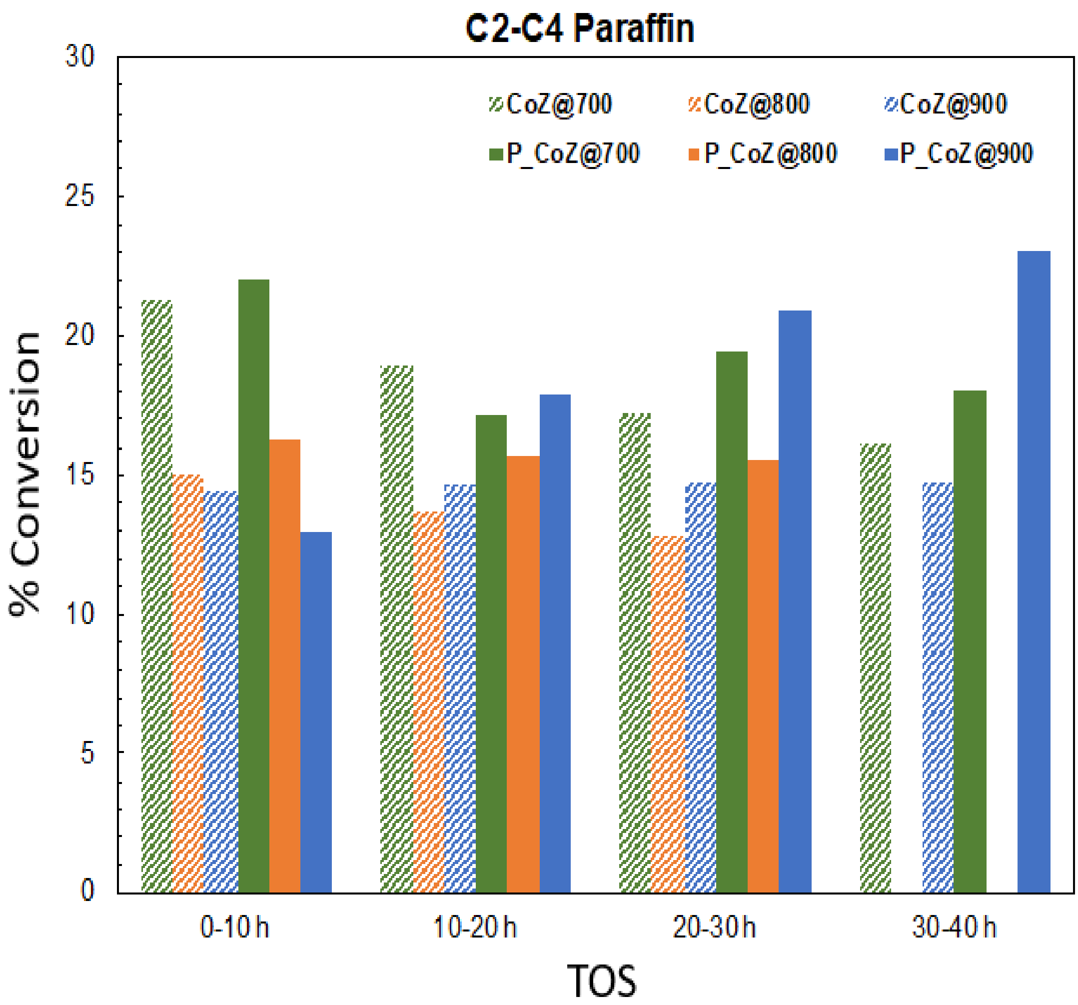

Figure 4.46: Average C_2-C_4 paraffin selectivity in every 10 h time on stream for the applied catalysts during Fisher-Tropsch Synthesis.

Figures 4.47, 4.48, 4.49 and 4.50 have shown C_{5+} and CH_4 selectivity for the low and high temperature pyrolyzed catalysts, respectively. As seen from Figures that average C_{5+} selectivity increases with time on stream for all catalysts.

When the low temperature pyrolyzed catalysts were examined, it was seen that the highest increase in C_{5+} selectivity was recorded for CoZ@400, CoZ@500 and CoZ@600. For example, C_{5+} selectivity was increased from 15.2% to 35.8 for CoZ@600 catalysts. Although initially high C_{5+} selectivity values were obtained over plasma treated catalysts for the 0-10 h period of stream, the increase in C_{5+} selectivity was less pronounced.

In general, plasma treated samples gave lower C_{5+} selectivity compared to the ones without plasma treatment, specifically at the second half of the test duration. For example, the highest C_{5+} selectivity was achieved on both CoZ@500 and CoZ@600 as 39.3% and 35.8%, respectively for the last period of 30-40 h. On the other hand, a systematic change in C_{5+} selectivity values were not observed for high temperature pyrolyzed catalysts. However, more stable C_{5+} selectivity values were noticed for the high temperature pyrolyzed catalysts. For example, C_{5+} selectivity on CoZ@900 was in between 28.6% and 32.3%.

Regarding methane selectivity, any relation on neither pyrolysis temperature not plasma treatment with CH_4 selectivity could not be deduced from the results. However, high methane selectivity was observed for all cases with or without plasma treatment. For example, CH_4 selectivity values on CoZ@600 and P_CoZ@600 catalysts were 38.3% and 32.5% for 0-10 h and 27.3% and 31.3% for 30-40 h, respectively.

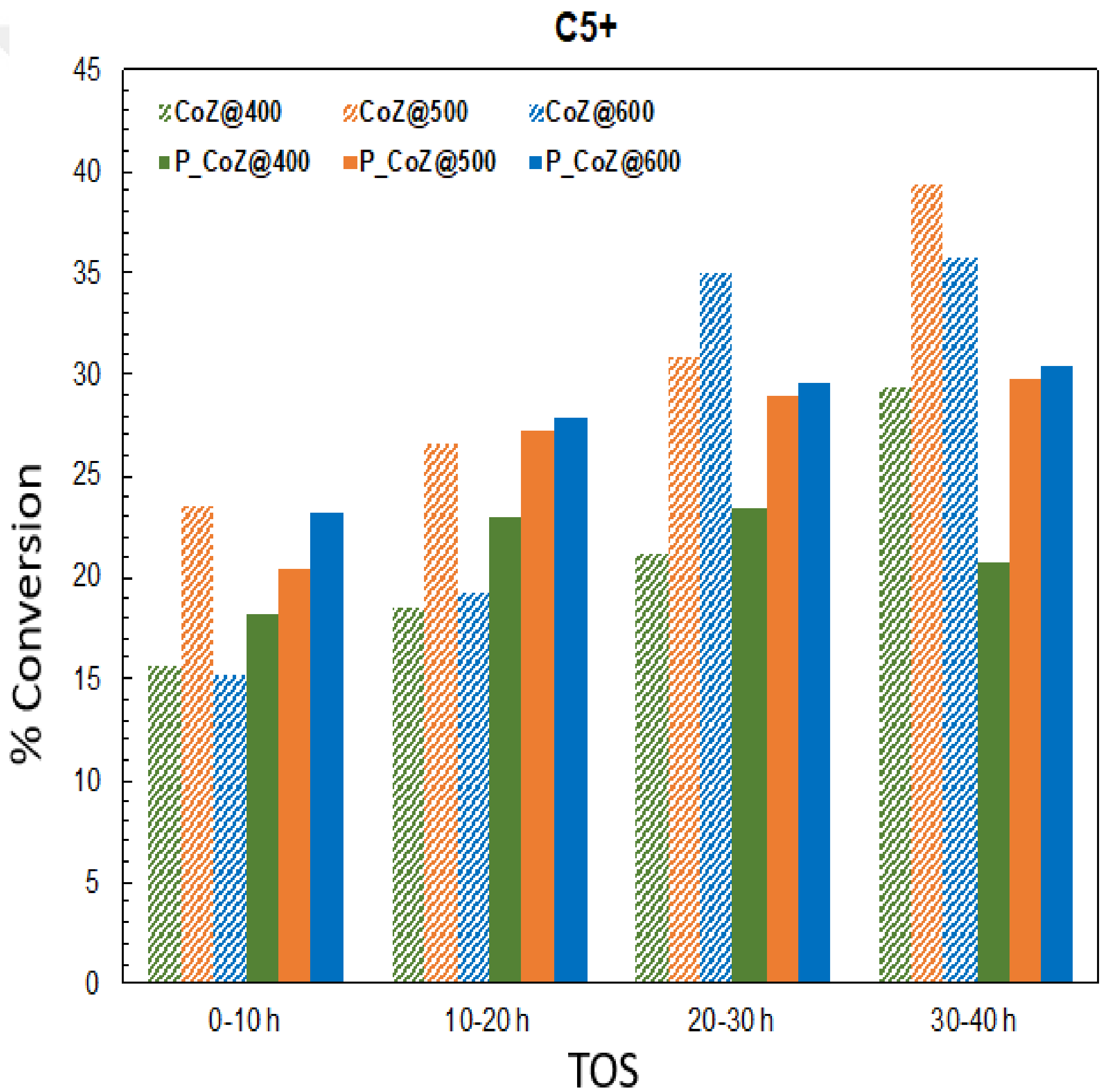

Figure 4.47: Average C5$^+$ selectivity in every 10 h time on stream for the applied catalysts during Fisher-Tropsch Synthesis.

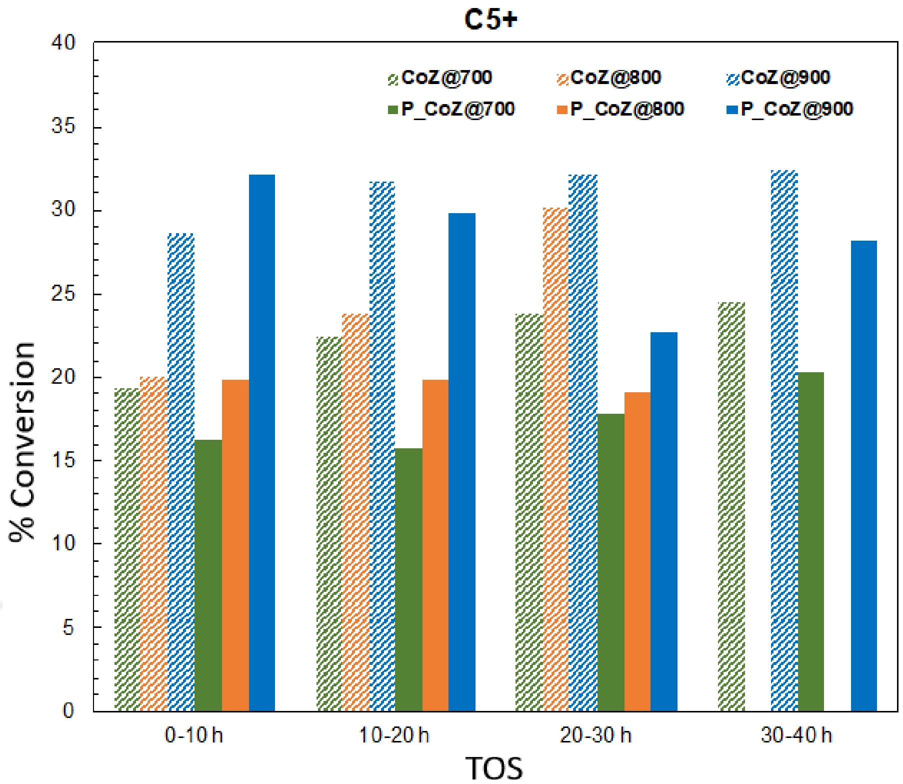

Figure 4.48: Average C5^{+} selectivity in every 10 h time on stream for the applied catalysts during Fisher-Tropsch Synthesis.

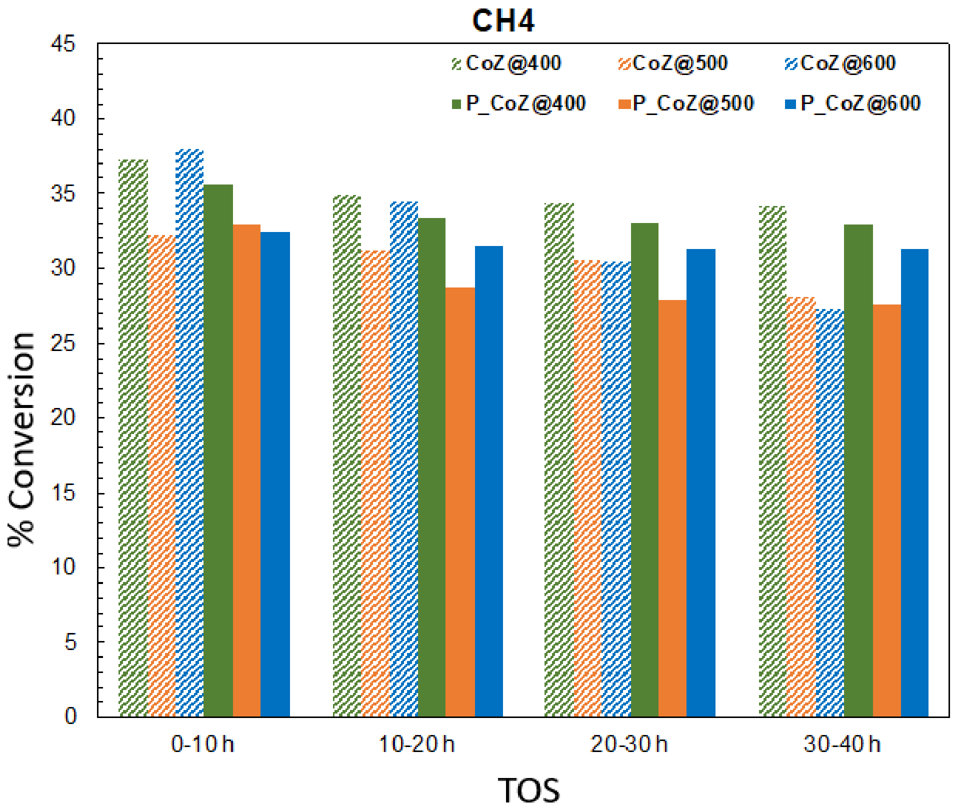

Figure 4.49: Average CH_4 selectivity in every 10 h time on stream for the applied catalysts during Fisher-Tropsch Synthesis.

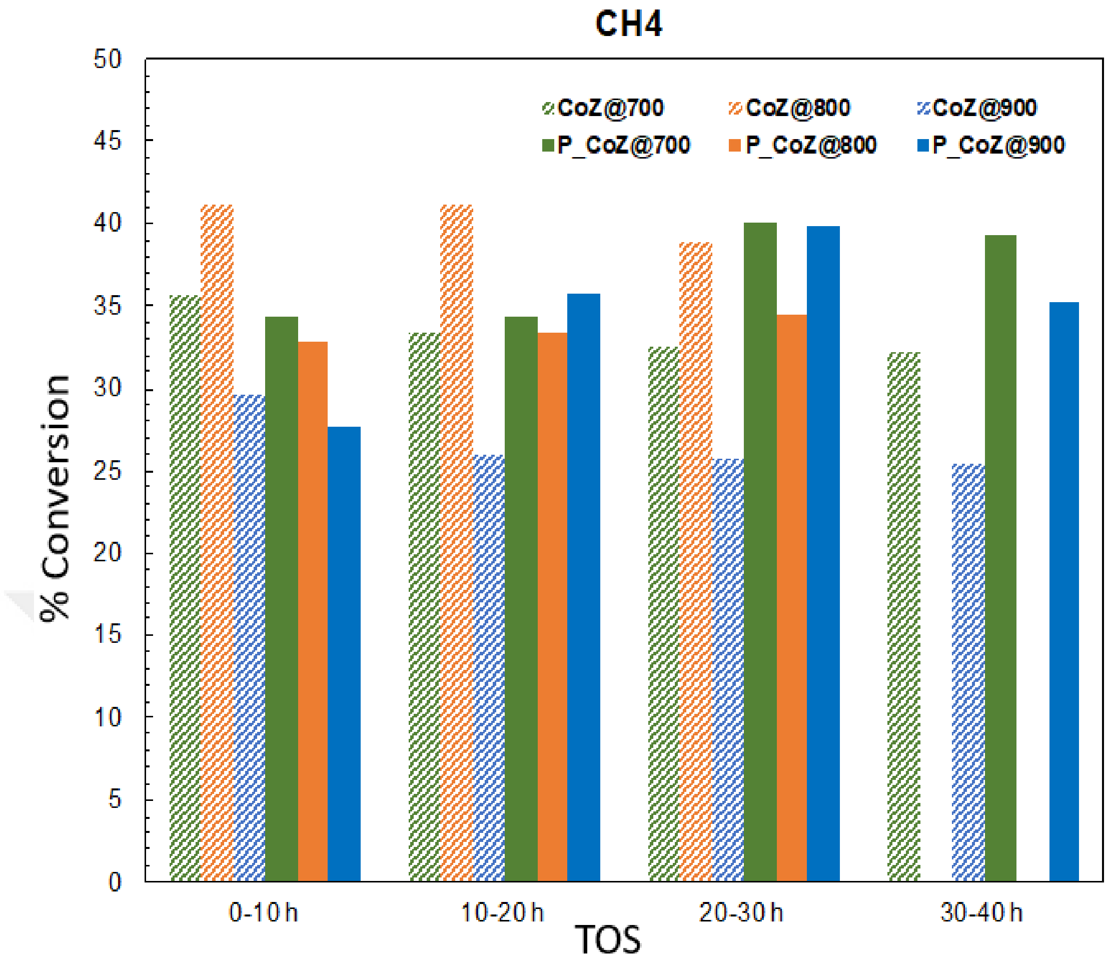

Figure 4.50: Average CH_4 selectivity in every 10 h time on stream for the applied catalysts during Fisher-Tropsch Synthesis.

It is said that in Part 3.2, the reason why only core shell structure was tested on the catalyst which were pyrolyzed at 600°C will be explained. After deductions from not only CO and H_2 conversions but also product selectivity, CoZ@600 gave the most promising results.

So, zinc, manganese and potassium coatings were applied to CoZ@600 as described in Part 3.2, and tested as in Part 3.4.

4.3.3 CO and H_2 conversions over the core and shell catalysts: CoZ@K2O, CoZ@ZnO and CoZ@MnO

Although improved catalytic activity could be expected for nano-sized catalysts thanks to the increased number of actives sites such as edge and corner atoms, deteriorated stability would be another concern depending on reaction conditions.

Nano-sized materials were more prone to sintering due to their high surface energy. In addition, selectivity to target product was the other important issue to be considered in the design of a catalyst.

Various methods have been used to solve the above mentioned problems of nano-catalysts. Constructing core-shell nano-structures through layer by layer synthesis was one of them. In this respect, three sets of catalysts with Co/ZIF-67 core and a metal oxide (K_2O, ZnO or MnO) shell have been prepared and tested.

As seen in the Figure 4.51, 4.52 and 4.53, all three catalysts in core-shell structure have shown improved stability compared to CoZ@600 catalyst. Highest CO and H_2 conversions were recorded over Co core-ZnO shell catalyst (CoZ@ZnO). When the selectivity values of CoZ@ZnO were evaluated, the lowest olefin selectivity with CoZ@ZnO was ascribed to its high hydrogenation activity making mostly CH_4 and C_{5+}.

In case of manganese oxide shell, C_2-C_4 olefin selectivity were the most among all tested catalysts.

Due to the competition between the hydrogenation and oligomerization reactions of the primary hydrocarbon products, methane selectivity might decrease with an increase in olefin selectivity or vice versa. Studies to date on manganese promoted FT catalysts mostly pointed out oligomerization path dominating and leading a shift from paraffinic to olefinic products together with an increased C_{5+} selectivity.

A similar behavior for manganese oxide in the shell structure has been observed and this shows that MnO shell structured cobalt catalysts behave iron-like catalysts. In case of K_2O shell, the lowest C_2-C_4 paraffin selectivity was recorded compared to all tested catalysts. This might be ascribed to the lagged hydrogenation that leads the olefinic intermediates to re-adsorb onto the catalytic surface to grow the hydrocarbon chains beyond C_{5+}.

Probably due to the combined effect of K_2O and altered transport phenomena facilitated the re-adsorption of olefin intermediates over CoZ@K_2O. In terms of conversion and selectivity, namely total C_2-C_4 paraffin and C_{5+} selectivity, CoZ@ZnO has appeared to be the highly active catalyst giving paraffinic and liquid hydrocarbon products with the highest yield. Therefore, zinc-based catalysts have been seen as the best candidate for further activity improvement.

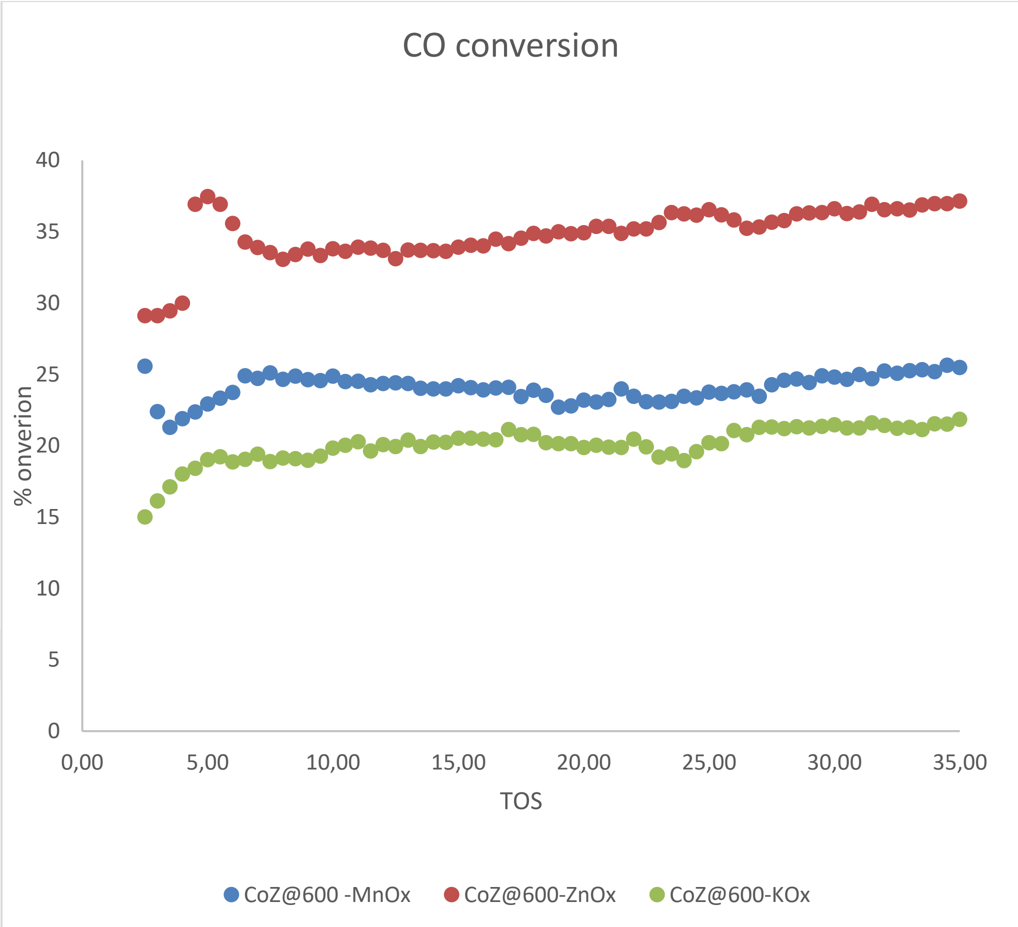

Figure 4.51: CO conversions in 35 h time on stream for the coated catalysts.

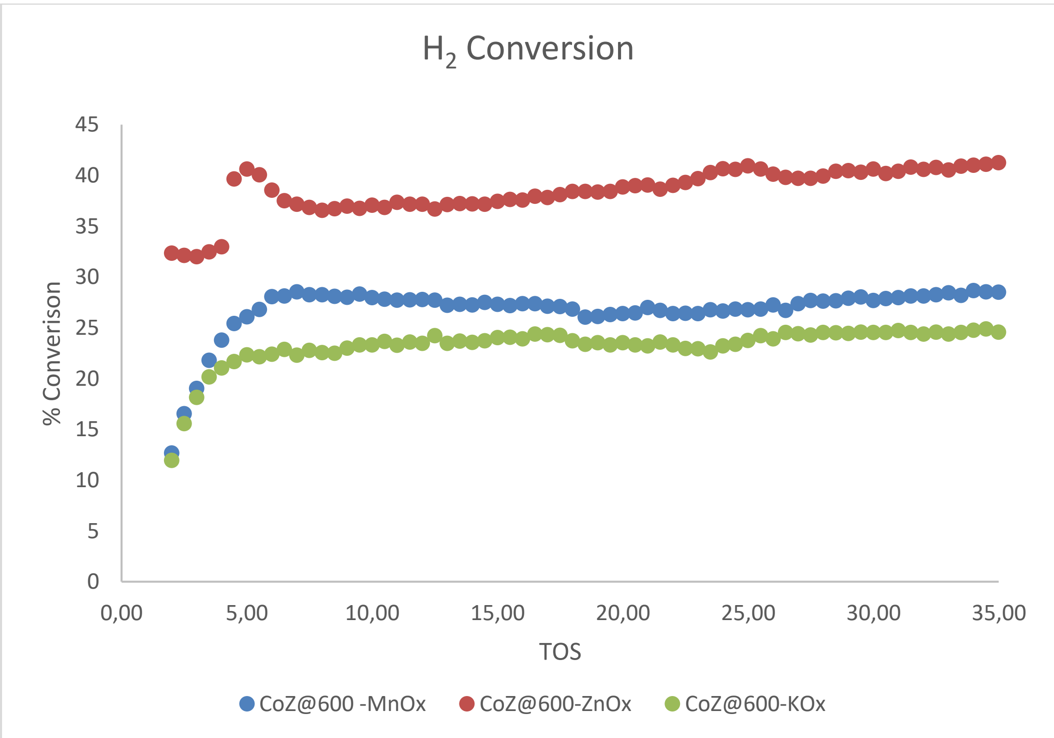

Figure 4.52: H_2 conversions in 35 h time on stream for the coated catalysts.

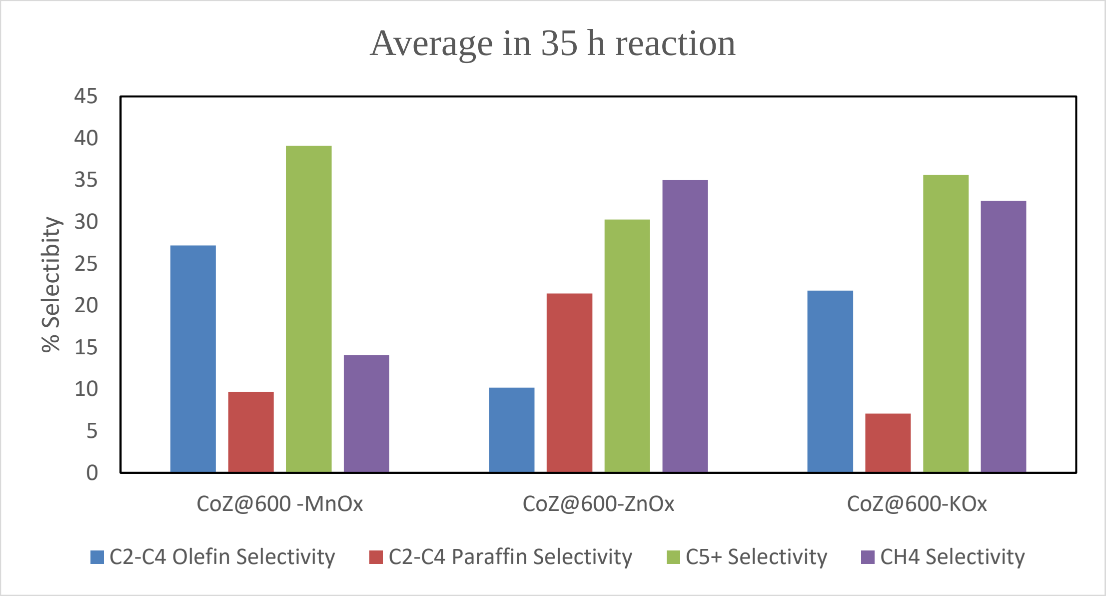

Figure 4.53: Average product selectivities of coated catalysts on 35 h time on stream.

4.4 Elemental Analysis of Spent Catalysts

To investigate any correlation between the hydrogenation activity of FTS catalysts with the formation of a hydrocarbonaceous overlayer, elemental analysis for CHN was applied on the spent catalysts. The analysis results on the degree of carbon and hydrogen retention within the catalyst were given in Table 4.9 and 4.10. As seen in the Table 4.9, higher initial CO conversions were obtained on plasma treated samples. However, plasma treated ones lost their activity fast compared to the ones without plasma treatment. At a first glance, CO activation on the catalytic surfaces were evident from the increased concentration of carbon and hydrogen over the catalytic surfaces but in a less systematic fashion. Initial and average CO conversions may be a way of measure for CO dissociation and hydrocarbon chain growth rates, respectively. Ideally a well balance between the rate of CO dissociation and the rates of chain growth gives highly stable catalysts otherwise coking occurs due to the uncontrolled rate of hydrocarbon chain growth. Low carbon and hydrogen content may be due to either the poor catalytic activity or relatively balanced rates of CO dissociation and chain growth. Regarding this, low temperature pyrolyzed catalysts (group I) were evalueted first. The results on CoZ@400, COZ@500 and CoZ@600 are interesting. Both carbon and hydrogen contents of these catalysts increased from 3.04 and 0.35 to 9.23 and 1.37, respectively. However, whereas CoZ@400 and CoZ@600 catalysts were the ones showing higher catalytic stability and having higher average CO conversions, CoZ@500 was less stable and has shown lower CO conversion. This result can be interpreted as the balance between the CO dissociation and the chain growth rates may not be ensured for the catalyst pyrolyzed at 500 °C. Another point that should be remarked here that P_CoZ@400 with the highest content of C and H gave the highest intial CO conversion but deactivated fast. In general, plasma treated samples, P_CoZ@400, P_CoZ@500 and P_CoZ@600, have shown less catalytic stability compared to the ones without plasma treatment although no systematic change was observed that could be related with the elemental analysis results.

Table 4.3. CNHS analysis on weight basis low temperature.

Sample	**C**	**H**	**C/H**	**CO_i Conv.***	**CO_{avg} Conv.***
CoZ@400	3.04	0.35	8.8	40.2	28.9
P_CoZ@400	10.48	1.60	6.6	60.5	20.5
CoZ@500	5.41	0.74	7.3	25.5	19.2
P_CoZ@500	1.98	1.55	12.8	53.4	20.5
CoZ@600	9.23	1.37	6.7	40.1	31.3
P_CoZ@600	3.81	0.41	9.3	47.4	24.0

*Initial and average CO conversions

For the high temperature pyrolzed samples (group II), the trend on the change of carbon and hydrogen content with the pyrolysis temperature was so clear. In the elemental analyzes of CoZ@700 and CoZ@800 catalysts, elemental hydrogen was not detected while their carbon content was very low, namely below 1%,. Both their initial and average CO conversion values were less than the low temperature pyrolyzed catalysts. On the other hand, CoZ@900 has unexpectedly high carbon and hydrogen content as seen in the Table 4.10. As a result of this, a severe deactivation occurred on it. In line with the results obtained for non-plasma treated samples, plasma treated ones has shown a similar trend. While P_CoZ@700 and P_CoZ@800 were deactivated fast relatively while a high catalytic activity was achieved on P_CoZ@900. This catalyst was also the one with the highest carbon and hydrogen content.

Table 4.4. CNHS analysis on weight basis high temperature.

Sample	C	H	C/H	CO_i Conv.*	CO_{avg} Conv.*
CoZ@700	0.58	<0.1	18.9	33.5	17.3
P_CoZ@700	4.17	0.38	10.9	50.0	14.8
CoZ@800	1.57	<0.1	19.1	28.8	14.2
P_CoZ@800	0.66	<0.1	66	67.8	13.7
CoZ@900	8.23	1.23	6.7	47.6	13.0
P_CoZ@900	13.05	2.0	6.6	58.0	25.6
Fresh CoZ@700*	<0.1**	<0.1	-	-	-

*****It was given for comparison

**The detection levels of the elemental analyzer ~0.1 wt %

4.5 General Evaluation

In brief, Fischer-Tropsch reaction is a surface polymerization reaction including initiation by CO activation into CHx monomers, hydrocarbon chain growth and termination of the growing chain to end up with linear paraffins or 1-olefins. Cobalt (Co) and iron (Fe) have been well proven catalysts for this reaction. Their choice depends on the target product since the selectivity of cobalt and iron catalysts differentiates. Cobalt catalysts have shown high CH_4 and C_{5+} but low olefin selectivity compared to iron catalysts. The activity of cobalt catalysts mainly depends on the reducibility and dispersion of cobalt oxides together with the particle size of the final metallic Co^o sites. (Iglesia, 1997). The main challenge in controlling cobalt crystal size is the cobalt-support interaction. In order to achieve high metal loading with reasonable dispersion and small metallic cobalt crystal size, the use of metal-organic frameworks (MOFs) was the main issue of the thesis study.

Metal organic frameworks (MOFs) are a class of micro porous crystalline materials made up of a metal and an organic ligand with high surface area and porosity. Carbon framework serves as a sacrificial template in the preparation of metal nanoparticles encapsulated by a carbon matrix under controlled pyrolysis-calcination-reduction conditions. The organic linker in the MOF structure partly decomposes to form both graphitic carbon and framework carbon hosting the metallic cobalt. Because of its low cost and easy preparation, MOF derived cobalt catalysts widely proceeds over ZIF67. Zeolitic imidazolate frameworks (ZIFs) is a kind of MOF but with a similar zeolite topology (Bibi et al., 2021). Nitrogen content of the organic linker in ZIF-67 is considered to give N-doped carbon and Co-N moieties contributing to the catalytic performance. Nitrogen content of ZIF-67 may act as an electron donor and induce interaction between cobalt nanoparticles and N-doped carbon towards improving the final textural properties of the catalyst (Otun et al., 2020). Moreover, by applying argon plasma etching as post treatment, surface defects and oxygen vacancies might be created to generate more active sites through lattice distortion and electronic compensation (Li et al., 2019).

Metal-organic frameworks (MOFs) materials have proven to be an ideal sacrifice template for the preparation of metal oxides. In spite of the loss of surface area and porosity upon calcination, morphology of Co_3O_4 is the other main parameter determining the catalytic activity. For example, as reported by Lv and his colleagues, Co_3O_4 nanotubes showed a much higher catalytic activity and stability than the spherical nanoparticles for the catalytic oxidation of CO (Lv et al., 2013).

Ma et al. (2019) synthesized Co_3O_4 catalyst with different morphologies (double-sided nanobrush, rods, hexagonal plates and double-side helianthus discs) for catalytic oxidation of benzene. They found that double-sided nanobrush Co_3O_4 catalyst exhibited superior catalytic activity possibly due to the rich Co^{3+} species on the surface of the Co_3O_4, its reducibility at low temperature, the presence of lattice oxygen defects and highly active oxygen species (Ma et al., 2019). So, pyrolysis as conducted at different temperatures before the calcination can be a way of tuning the morphology and reducibility of the catalysts which might be effective on the catalytic activity and stability (Lv et al., 2013).

5. CONCLUSION

In thesis studies, nano sized cobalt oxide structures upon pyrolysis and calcination have been verified even if high surface area MOF structure has been lost.

In the pyrolysis step, N content of the organic linker in ZIF-67 synthesis might help to have N-doped carbon and creation of Co-N moieties. Proving the efficacy of plasma treatment, structural and compositional changes such as expanded space distance, surface roughness, increased surface nitrogen content and the dominance of octahedral coordinated Co^{3+}-O structure over tetrahedral coordinated Co^{2+}-O structure have been observed. Higher temperatures of TPR peak maxima for plasma-treated samples have been interpreted as having “strong metal surface interaction” (SMSI). Regarding FTS performance of plasma treated catalysts, even the reaction started with high CO conversions, average CO conversions were much lower than those of the catalyst without plasma treatment. Altered surface features and loss of active sites by coking might be the reason of their poor activity. The high olefin and C_{5+} selectivity over plasma treated catalysts might also come from improved CO dissociation and reduced hydrogen transfer rates. So, further encapsulation of highly active nano-sized cobalt oxide particles with a secondary metal oxide shell were considered as a means for the facilitating diffusion of reaction products to suppress coke formation.

For the low temperature pyrolyzed catalysts, pyrolyzed catalysts were more active and stable than the plasma treated ones. Regarding H_2 conversions, H_2 conversions were lower than CO conversions. This difference was more noticable for plasma treated samples. However, no CO_2 be detected in the product stream indicating the absence of water gas shift activity as expected from cobalt based catalysts.

Moreover, the catalysts without plasma treatment were found to be more selective towards C_2-C_4 paraffins. Since it was widely accepted that inhibited re-adsorption of olefinic intermediates and relatively low hydrogen transfer rates were in responsible for high olefin selectivity, it had been argued that plasma treated catalysts might have an altered catalytic surface feature promoting olefinic products. Finally, high methane selectivity was observed for all cases with or without plasma treatment.

For the high temperature pyrolyzed catalysts (group II), olefin products may favourably form possibly due to the less extended growth of hydrocarbon chain under the effect of low CO conversion except for P_CoZ@900. One reason of the lower olefin selectivity on P_CoZ@900 may be due the highest CO and H_2 conversions among all high temperature pyrolyzed catalysts. A systematic change in C_{5+} selectivity values were not observed for high temperature pyrolyzed catalysts. A stable C_{5+} selectivity was noticed for all samples in category II. In general, plasma treated samples gave lower C_{5+} selectivity compared to the non-plasma treated ones. In general, methane selectivity was high for all cases.

The expected outcomes of core-shell catalysts can be summarized as enhanced catalytic activity and improved selectivity to alkenes and higher hydrocarbons via changing surface electronic features as given by transition metal oxides such as manganese or cerium oxides, improved stability with decreased CH_4 selectivity by tuning the competing hydrogenation and oligomerization reactions of the primary hydrocarbon products and finally enhanced reducibility of the cobalt and to scavenge poisoning sulfur compounds.

All three catalysts in core-shell structure have shown improved stability compared to CoZ@600 catalyst. Highest CO and H_2 conversions were recorded over Co core-ZnO shell catalyst (CoZ@ZnO). When the selectivity values of CoZ@ZnO were evaluated, the lowest olefin selectivity with CoZ@ZnO was ascribed to its high hydrogenation activity making mostly CH_4 and C_{5+}. In case of manganese oxide shell, C_2-C_4 olefin selectivity were the most among all tested catalysts. Due to the competition between the hydrogenation and oligomerization reactions of the primary hydrocarbon products, methane selectivity might decrease with an increase in olefin selectivity or vice versa. In case of K_2O shell, the lowest C_2-C_4 paraffin selectivity was recorded compared to all tested catalysts. This might be ascribed to the lagged hydrogenation that leads the olefinic intermediates to re-adsorb onto the catalytic surface to grow the hydrocarbon chains beyond C_{5+}. Probably due to the combined effect of K_2O and altered transport phenomena facilitated the re-adsorption of olefin intermediates over CoZ@K_2O. In terms of conversion and selectivity, namely total C_2-C_4 paraffin and C_{5+} selectivity, CoZ@ZnO has appeared to be the highly active catalyst giving paraffinic and liquid hydrocarbon products with the highest yield.

Last of all, further studies can focus on advanced characterization techniques for the evaluation and better understanding of morpholgy&structure of the coated catalysts. And also, Core-Shell structure can be modified by changing coating metal oxides.

REFERENCES

Bai, S., Huang, C., Lv, J., & Li, Z. (2012). Performance of cobalt-based Fischer-Tropsch synthesis catalysts using dielectric-barrier discharge plasma as an alternative to thermal calcination. *Plasma Science and Technology*, *14*(1), 54–57. https://doi.org/10.1088/1009-0630/14/1/12

Bartholomew, C. H., & Farrauto, R. J. (2006). Fundamentals Of Industrıal Catalytıc Processes.

Bibi, S., Pervaiz, E., & Ali, M. (2021). Synthesis and applications of metal oxide derivatives of ZIF-67: a mini-review. *Chemical Papers*, *75*(6), 2253–2275. https://doi.org/10.1007/s11696-020-01473-y

Chen, K., Bai, S., Li, H., Xue, Y., Zhang, X., Liu, M., & Jia, J. (2020). The Co3O4 catalyst derived from ZIF-67 and their catalytic performance of toluene. *Applied Catalysis A: General*, *599*, 117614. https://doi.org/10.1016/j.apcata.2020.117614

Chen, Y., Li, X., Nisa, M. U., Lv, J., & Li, Z. (2019). ZIF-67 as precursor to prepare high loading and dispersion catalysts for Fischer-Tropsch synthesis: Particle size effect. *Fuel*, 802–812. https://doi.org/10.1016/j.fuel.2018.12.085

Chen, Y., Wei, J., Duyar, M. S., Ordomsky, V. V., Khodakov, A. Y., & Liu, J. (2021). Carbon-based catalysts for Fischer-Tropsch synthesis. *Chemical Society Reviews*, *50*(4), 2337–2366. https://doi.org/10.1039/d0cs00905a

Cheng, K., Kang, J., King, D. L., Subramanian, V., Zhou, C., Zhang, Q., & Wang, Y. (2017). Advances in Catalysis for Syngas Conversion to Hydrocarbons. *In Advances in Catalysis.* https://doi.org/10.1016/bs.acat.2017.09.003

Chu, W., Wang, L. N., Chernavskii, P. A., & Khodakov, A. Y. (2008). Glow-discharge plasma-assisted design of cobalt catalysts for Fischer-Tropsch synthesis. *Angewandte Chemie - International Edition*, *47*(27), 5052–5055. https://doi.org/10.1002/anie.200800657

Davis, S. C., & Boundy, R. G. (2021). *Transportation energy data book: Edition 39* (No. ORNL/TM-2020/1770).

Dembicki, Jr., H. (2017). Practical Petroleum Geochemistry for Exploration and Production. *Practical Petroleum Geochemistry for Exploration and Production*, 1–17. https://doi.org/10.1016/b978-0-12-803350-0.00001-5

Dry, M. E. (2004). FT catalysts. *Studies in Surface Science and Catalysis*, *152,* 533–600. https://doi.org/10.1016/s0167-2991(04)80464-6

Eliseev, O. L., Savost'yanov, A. P., Sulima, S. I., & Lapidus, A. L. (2018). Recent development in heavy paraffin synthesis from CO and H2. *Mendeleev*

Communications, *28*(4), 345–351.

Energy Institute. (2022). The Energy Institute Statistical Review of World Energy. < Retrieved from https://ycharts.com/indicators/world_oil_consumption>

Enerji Piyasası Düzenleme Kurumu. (2023). Petrol Piyasası Sektör Raporu. Retrieved from https://www.epdk.gov.tr/Detay/Icerik/3-0-104/petrolaylik-sektor-raporu

Freund, M., Csikos, R., Keszthelyi, S., & Mózes, G. Y. (1982). Applications of paraffin waxes and liquid paraffins. *Paraffin products: properties, technologies, applications.* Elsevier Scientific, 240-329.

Fu, T., Huang, C., Lv, J., & Li, Z. (2014). Fuel production through Fischer-Tropsch synthesis on carbon nanotubes supported Co catalyst prepared by plasma. *Fuel*, *121*, 225–231. https://doi.org/10.1016/j.fuel.2013.12.049

Galvis, H. M. T., Bitter, J. H., Khare, C. B., Ruitenbeek, M., Dugulan, A. I., & Jong, K. P. de. (2012). Supported Iron Nanoparticles as Catalysts for Sustainable Production of Lower Olefins. *ChemCatChem*, *4*(6), 751–752. https://doi.org/10.1002/cctc.201200178

Galvis, H.M.T. (2013). Direct Production Of Lower Olefins From Synthesis Gas Using Supported Iron Catalysts.

Gholami, Z., Asmawati Mohd ZabiDi, N., Gholami, F., Ayodele, O. B., & Vakili, M. (2017). The influence of catalyst factors for sustainable production of hydrocarbons via Fischer-Tropsch synthesis. *Reviews in Chemical Engineering*, *33*(4), 337–358. https://doi.org/10.1515/revce-2016-0009

Gholami, Z., Tišler, Z., & Rubáš, V. (2020). Recent advances in Fischer-Tropsch synthesis using cobalt-based catalysts : a review on supports , promoters , and reactors Recent advances in Fischer-Tropsch synthesis using. *Catalysis Reviews*, *00*(00), 1–84. https://doi.org/10.1080/01614940.2020.1762367

Gioria, E., Duarte-Correa, L., Bashiri, N., Hetaba, W., Schomaecker, R., & Thomas, A. (2021). Rational design of tandem catalysts using a core-shell structure approach. *Nanoscale Advances*, *3*(12), 3454–3459. https://doi.org/10.1039/d1na00310k

Gokulakrishnan, P., & Richard, M.S. (2007). Autoignition of Aviation Fuels: Experimental and Modeling Study. Collection of Technical Papers - 43rd Joint Propulsion Conference. 7. 10.2514/6.2007-5701.

Gommes, C. J. (2019). Ostwald ripening of confined nanoparticles: Chemomechanical coupling in nanopores. *Nanoscale*, *11*(15), 7386–7393. https://doi.org/10.1039/c9nr01349k

Iglesia, E. (1997). Design, synthesis, and use of cobalt-based Fischer-Tropsch synthesis catalysts. *Applied Catalysis A: General*, *161*(1–2), 59–78. https://doi.org/10.1016/S0926-860X(97)00186-5

Jahangiri, H., Bennett, J., Mahjoubi, P., Wilson, K., & Gu, S. (2014). A review of advanced catalyst development for Fischer-Tropsch synthesis of hydrocarbons from biomass derived syn-gas. *Catalysis Science and Technology*, *4*(8), 2210–2229. https://doi.org/10.1039/c4cy00327f

Khodakov, A. Y., Chu, W., & Fongarland, P. (2007). Advances in the development of novel cobalt Fischer − Tropsch catalysts for synthesis of long-chain hydrocarbons and clean fuels. *Chemical reviews*, *107*(5), 1692-1744.

Kuo, G. (2019). When Fossil Fuels Run Out, What Then? Retrieved from https://mahb.stanford.edu/library-item/fossil-fuels-run/

Lappas, A., & Heracleous, E. (2016). Production of biofuels via Fischer–Tropsch synthesis: biomass-to-liquids. *Handbook of biofuels production* (pp. 549-593). Woodhead Publishing.

Leckel, D. (2009). Diesel production from fischer - Tropsch: The past, the present, and new concepts. *Energy and Fuels*, *23*(5), 2342–2358. https://doi.org/10.1021/ef900064c

Li, G., & Tang, Z. (2014). Noble metal nanoparticle@metal oxide core/yolk-shell nanostructures as catalysts: Recent progress and perspective. *Nanoscale*, *6*(8), 3995–4011. https://doi.org/10.1039/c3nr06787d

Li, J., Ma, C., Zhu, S., Yu, F., Dai, B., & Yang, D. (2019). A review of recent advances of dielectric barrier discharge plasma in catalysis. *Nanomaterials*, *9*(10), 1–34. https://doi.org/10.3390/nano9101428

Li, X., Almkhelfe, H., Bedford, N. M., Back, T. C., Hohn, K. L., & Amama, P. B. (2019). Characterization and catalytic behavior of Fischer–Tropsch catalysts derived from different cobalt precursors. *Catalysis Today*, *338*, 40–51. https://doi.org/10.1016/j.cattod.2019.05.023

Li, M., Bian, Z., Kathiraser, Y., & Kawi, S. (2016). Design of highly stable and selective core/yolk-shell nanocatalysts-review. *Applied Catalysis B: Environmental*, *188*, 324–341. https://doi.org/10.1016/j.apcatb.2016.01.067

Luo, Q. X., Guo, L. P., Yao, S. Y., Bao, J., Liu, Z. T., & Liu, Z. W. (2019). Cobalt nanoparticles confined in carbon matrix for probing the size dependence in Fischer-Tropsch synthesis. *Journal of Catalysis*, *369*, 143–156. https://doi.org/10.1016/j.jcat.2018.11.002

Lv, Y., Li, Y., & Shen, W. (2013). Synthesis of Co3O4 nanotubes and their catalytic applications in CO oxidation. *Catalysis Communications*, *42*, 116–120. https://doi.org/10.1016/j.catcom.2013.08.017

Ma, X., Yu, X., Yang, X., Lin, M., & Ge, M. (2019). Hydrothermal Synthesis of a Novel Double-Sided Nanobrush Co 3 O 4 Catalyst and Its Catalytic Performance for Benzene Oxidation. *ChemCatChem*, *11*(4), 1214–1221. https://doi.org/10.1002/cctc.201801539

Mahmoudi, H., Mahmoudi, M., Doustdar, O., Jahangiri, H., Tsolakis, A., Gu, S., & LechWyszynski, M. (2017). A review of Fischer Tropsch synthesis process, mechanism, surface chemistry and catalyst formulation. *Biofuels Engineering*, *2*(1), 11–31. https://doi.org/10.1515/bfuel-2017-0002

Makhlouf, S. A., Bakr, Z. H., Aly, K. I., & Moustafa, M. S. (2013). Structural, electrical and optical properties of Co3O 4 nanoparticles. *Superlattices and Microstructures*, *64*, 107–117. https://doi.org/10.1016/j.spmi.2013.09.023

Otun, K. O., Liu, X., & Hildebrandt, D. (2020). Metal-organic framework (MOF)-derived catalysts for Fischer-Tropsch synthesis: Recent progress and future perspectives. *Journal of Energy Chemistry*, *51*, 230-245.

Qiu, B., Yang, C., Guo, W., Xu, Y., Liang, Z., Ma, D., & Zou, R. (2017). Highly dispersed Co-based Fischer-Tropsch synthesis catalysts from metal-organic frameworks. *Journal of Materials Chemistry A, 5(17),* 8081–8086.

Semih Eser. (2011). *Petroleum Processing, Paraffins*. Retrieved from https://www.e-education.psu.edu/fsc432/content/paraffins

Speight, J. G. (2020). Hydrocarbons from crude oil. *Handbook of Industrial Hydrocarbon Processes*. https://doi.org/10.1016/b978-0-12-809923-0.00003-5

Stratiev, D., & Bourgas, L. N. (2015). Effect of gasoline hydrocarbon composition on the properties of the blend gasoline / bioethanol. *Oxidation Communications 34* , No 1 , 183-192, 183–192.

Suaria, G., Aliani, S., Merlino, S., & Abbate, M. (2018). The occurrence of paraffin and other petroleum waxes in the marine environment: a review of the current legislative framework and shipping operational practices. *Frontiers in Marine Science*, *5*, 94.

Sun, X., Suarez, A. I. O., Meijerink, M., Van Deelen, T., Ould-Chikh, S., Zečević, J., & Gascon, J. (2017). Manufacture of highly loaded silica-supported cobalt Fischer–Tropsch catalysts from a metal organic framework. *Nature communications*, *8*(1), 1680.

Tao, X., Sun, C., Han, Y., Huang, L., & Xu, D. (2019). The plasma assisted preparation of Fe-MOFs with high adsorption capacity. *CrystEngComm*, *21*(15), 2541–2550. https://doi.org/10.1039/C9CE00015A

U.S. Energy Information Administration. (2022). Oil and petroleum products explained. Retrieved from https://www.eia.gov/energyexplained/oil-and-petroleum-products/use-of-oil.php

Wang, L., Liu, X., Wang, X., Yang, X., & Lu, L. (2010). Preparation and electrochemical properties of mesoporous Co 3O4 crater-like microspheres as supercapacitor electrode materials. *Current Applied Physics*, *10*(6), 1422–1426.

Wang, Z., Zhang, Y., Neyts, E. C., Cao, X., Zhang, X., Jang, B. W. L., & Liu, C. J. (2018). Catalyst Preparation with Plasmas: How Does It Work? *ACS Catalysis*, *8*(3), 2093–2110. https://doi.org/10.1021/acscatal.7b03723

Xie, J., Paalanen, P. P., van Deelen, T. W., Weckhuysen, B. M., Louwerse, M. J., & de Jong, K. P. (2019). Promoted cobalt metal catalysts suitable for the production of lower olefins from natural gas. *Nature Communications*, *10*(1), 1–10. https://doi.org/10.1038/s41467-018-08019-7

Xu, L., Jiang, Q., Xiao, Z., Li, X., Huo, J., Wang, S., & Dai, L. (2016). Plasma-Engraved Co3O4 Nanosheets with Oxygen Vacancies and High Surface Area for the Oxygen Evolution Reaction. *Angewandte Chemie - International Edition*, *55*(17), 5277–5281. https://doi.org/10.1002/anie.201600687

Yao, Y., Liu, X., Gorimbo, J., Xiong, H., Fox, J., Glasser, D., & Hildebrandt, D. (2020). Fischer-Tropsch synthesis: A long term comparative study of the product selectivity and paraffin to olefin ratios over an iron-based catalyst activated by syngas or H2. *Applied Catalysis A: General*, *602*, 117700.

CURRICULUM VITAE

PERSONAL INFORMATION

Name: Yavuz Aydemir

WORK EXPERIENCES

Product Development Engineer - Oils&Lubricants

VITOL-PETROL OFİSİ A.Ş.
01/10/2022 – Current ISTANBUL , Türkiye

Production Intern

SOCAR Türkiye
01/06/2019 – 01/07/2019 IZMIR , Türkiye

R&D Project Engineer

Istanbul Technical University - SENTEK
01/09/2021 – 01/09/2022

EDUCATION

B.Sc.Metallurgical and Materials Engineering
Istanbul Technical University
01/09/2018 – 01/09/2022

B.Sc.Chemical Engineering
Istanbul Technical University
01/09/2016 – 01/09/2020

Master of Science - Chemical Engineering
Istanbul Technical University
01/09/2021 – 01/06/2023

LANGUAGES

Turkish
English
German

SKILLS

Microsoft Office
Power BI
MatLab